Progress with the Colliding Shock Lens

by

Andrew Conrad Khoro Mahlase

August 2013

Submitted in fulfilment of the academic

requirements for the degree of

Master of Science in the

School of Physics

University of KwaZulu-Natal

Durban

Abstract

The Colliding Shock Lens (CSL) exploits the interference of shock waves in a gas to form a region in which high pressure, temperature and density change the refractive index of the gas, making it possible to focus laser light. They are real optical elements, sometimes have very good optical qualities and can be made out of air. CSL's are dynamic lenses, which last for a few microseconds and are always evolving. As gas structures, they can be applied to focus high power laser light when solid lenses would be damaged. The shocks are generated by spark gaps or exploding wires.

In the former case, ignitrons were used to trigger the CSL circuit but are unreliable and have become obsolete. In this thesis an alternative, more reliable and cheaper trigger mechanism is investigated, using needle pins.

The CSL's that were tested previously were too small for any practical use and in this thesis a continuation into the feasibility of scaling the optical aperture of the CSL is investigated.

Another application of colliding shocks is the formation of virtual capillaries, which are a series of spark gaps set out on the surface of a cylinder, forming a cylindrical lens. In this thesis a set of exploding wires on a circumference are investigated.

The limitations with the above experiments is that physical probes positioned at points of interest would interfere with the experiment, hence making it impractical to determine the parameters of interest as mentioned above. Computational Fluid Dynamics (CFD) is employed in this thesis to try and alleviate the above problem.

Preface

The experimental work described in this dissertation was carried out in the School of Physics, University of KwaZulu-Natal, Durban, from January 1996 to February 1999, under the supervision of Professor Max M. Michaelis. The modelling and simulation work was carried out in the Aeronautics Systems Competency, Defence Peace Safety and Security, Council of Scientific and Industrial Research, Pretoria, from May 2003 to December 2007, under the supervision of Doctor Irvy (Igle) Gledhill.

These studies represent original work by the author and have not otherwise been submitted in any form for any degree or diploma to any tertiary institution. Where use has been made of the work of others it is duly acknowledged in the text.

Declaration

I, Conrad Mahlase declare that

1. The research reported in this thesis, except where otherwise indicated, is my original research.

2. This thesis has not been submitted for any degree or examination at any other university.

3. This thesis does not contain other persons' data, pictures, graphs or other information, unless specifically acknowledged as being sourced from other persons.

4. This thesis does not contain other persons' writing, unless specifically acknowledged as being sourced from other researchers. Where other written sources have been quoted, then:

   a) Their words have been re-written but the general information attributed to them has been referenced

   b) Where their exact words have been used, then their writing has been placed in italics and inside quotation marks, and referenced.

5. This thesis does not contain text, graphics or tables copied and pasted from the Internet, unless specifically acknowledged, and the source being detailed in the thesis and in the References sections.

Signed: .....

On this 15 day of AUGUST 2013

As the candidate's Supervisors we hereby certify that this statement is correct and that we agree with the submission of this thesis

Prof. Max Michaelis Dr. Igle Gledhill

(SUPERVISOR) (CO-SUPERVISOR)

Acknowledgments

First and foremost I would like to thank my supervisor, Prof. Max Michaelis, for his dedication, patience, advice and resourcefulness. Not forgetting his history lessons and humour.

My co-supervisor, Dr. Igle Gledhill, for her perpetual belief, assistance and mentorship. She has truly helped me with a whole lot of things.

Dr. Arnold Prause for quickly getting me started and showing me the ropes.

Dr. Aldo Conti for being a pleasant co-worker and friend.

The staff of the then UND Physics department and the workshop, for making the experimental part of the thesis a success and helping with the initial understanding of the task and goal.

UND for their financial support.

The staff of ASC at the CSIR for making the CFD and the write-up of the thesis achievable. Giving advice and support at difficult times.

The CSIR for allowing me the opportunity to use the expensive CFD code and time to write the thesis up.

My friends for encouraging me to get going even when the path was tough.

And lastly to my family for giving me the emotional support and being patient with me when I spent lengthy times away from them, even when they did not agree with me.

Contents

List of Figures

List of Tables

1. Introduction

With the advent of high powered lasers in research and in industry there is an inherent difficulty in using conventional solid state lenses to propagate the laser beam. The high powered laser beams tend to cause damage to the lenses and subsequently alter the optical properties of the lens. This leads to undesirable consequences for the design specifications of the lasers.

A survey of alternative lenses, to address the problems and possible solutions, is provided in this chapter. A comparison of the advantages and disadvantages between solid state and gas lenses is also presented. The literature covering the research done on the Colliding Shock Lens (CSL) is summarised in this chapter.

The primary aim of the research was to determine if the CSL can be scaled to bigger optical apertures, so that it could be used in industry. Secondary sub-tasks were investigated to help achieve the primary goal.

A more reliable alternative triggering mechanism is investigated and the previous experiments performed by Bucellato *etal.* [1] were redone with the new mechanism.

The CSL that was investigated by Buccelato *etal.* [1] was 11 mm in diameter and had an opening of 7.5 mm though which the laser light could propagate. This optical aperture was too small for practical industrial laser focusing applications. The CSL was scaled to bigger apertures to demonstrate that it could be scaled.

A subsidiary purpose was to develop "virtual capillaries" which could be useful for future high repetition rate "laser accelerators". Another application of colliding shocks is the formation of "virtual capillaries" (VC) as first performed by Kuppen

[2]. Kuppen employed a series of spark gaps set out on the surface of a cylinder and in line. The virtual capillaries are also produced with cylindrical colliding shocks in air. In this thesis this copper wire was exploded to create cylindrical shocks that resemble Kuppen's experiments.

Computational Fluid Dynamics (CFD) was exploited to give insight into the physics of the CSL, as putting diagnostic probes in the path of the shock waves would result in them interfering and interacting with the shock waves. The CSL was simulated as a 2D, Euler, inviscid, compressible, perfect gas model.

1.1. Problems with Solid State Lenses

Some of the documented problems with solid state lenses are discussed below.

1.1.1. Thermal Lensing

This is a lensing effect induced by temperature gradients which can occur both in the gain medium inside the laser cavity and also in the lens medium [4]. The heating of the lens causes changes in the refractive index through the following mechanisms:

- The lens medium is hotter on the beam axis, compared to the outer regions, causing a transverse gradient of the refractive index.
- Thermally induced mechanical stress causes further refractive index changes.
- Mechanical stress can also lead to bulging of the surfaces of the lens.

1.1.2. Coating Damage

The two most common sources of catastrophic coating damage for high energy pulsed lasers operating in the visible and near infrared are external contamination and "hot spots" in the beam structure [4, 3]. External contamination can be further subdivided into

1. discrete absorption site such as lint, dust or a material nodule and

2. diffuse contamination due to gaseous or molecular contaminants.

For a discrete absorption site, high fluence (energy per unit area per pulse) generates a large amount of heat in a very small volume near the surface of the component. If the absorption is sufficient a small explosion is produced that ablates part of the coating, producing a catastrophic failure. However, the absorber is also ablated, and what remains is a scattering site with the subsurface damage but no absorption. Hence, subsequent pulses cause no further growth of the damage site. Discrete damage sites are usually microscopic ($<$ 50 to 100 μm), whereas diffuse contaminants tend to produce relatively uniform damage over the beam diameter. When such diffuse contamination is low enough, it is not uncommon to see a noticeable "beam print" that is characteristic of the distribution of energy within the beam.

"Hot spots" in the beam structure occur when a region of the beam possesses a considerably higher fluence than the nominal value. Most solid-state laser cavities are a "thermodynamic nightmare" that, under the right conditions, can produce high order transverse modes with very high local fluence. The short pulse duration, high repetition rate and dynamic thermal environment inside the laser can make it particularly difficult to identify when and where this has occurred. Frequently, the peak fluence in a hot spot, which may last for only a pulse or two, can exceed the specified output of the laser by a few orders of magnitude, leading to catastrophic failure of the component [3].

1.1.3. External Contamination

Water vapour which is present in the atmosphere is one of the threats that cause contamination on solid state lenses [4]. At idle times of a laser system the water vapour deposits itself on optical equipment and carries with it airborne contaminants that stay on the optics even when the vapour has evaporated. These will then be

ablated when the laser beam strikes the optical elements. Damage unavoidable when working with high power lasers [4].

1.2. Recent Research on Solid State Lenses

To remedy some of the problems stated above some considerable research has gone into adaptive optics. Adaptive optics works by measuring the distortion and rapidly compensating for it either using deformable optics or material with variable refractive properties.

1.3. Comparison of the Colliding Shock Lens with Solid State Lenses

Solid state lenses are used conventionally and have been for many years. They are available in many sizes and shapes and can be easily handled. They are however brittle and need safe handling. They can be damaged as discussed above in Section 1.1 on page 12.

CSL's on the other hand are made of air (or gas) and hence cannot be destroyed. The lenses have a very long focal length in comparison to their small diameter. This can be desirable for instance in laser drilling for good quality holes. This was demonstrated by Michaelis *etal.* [5]. However, the CSL produces electromagnetic and acoustic noise as it uses sparks. Michaelis *etal.* [6] discuss the applications of gas lenses and the possibility of pulsed gas lenses as a solution to high laser fluence and radiation damage to lenses in post-break-even fusion experiments.

1.4. CSL literature

Interest in the field had been stimulated by the early observation by Michaelis that it was possible to focus laser beams through flames [7, 8]. The idea that shocks might produce denser, hotter regions, which would function better as lenses, led to the invention of the Colliding Shock lens [1, 9]. In succeeding years, the work has been carried out primarily by the UKZN group, and as a result there is very little literature beyond that cited here.

The use of refractive fringe diagnostics to determine electron densities in laser-produced plasmas at the time was resulting in estimates that were an order of magnitude too large [10, 11, 12]. This led to investigations of the propagation of laser light in regions of varying gas density, and improvements to spark-generated colliding shock lenses [10]. Interest in the applications of gas lenses rose, due to their ability to solve the problems associated with high laser fluence and radiation damage [6], and laser drilling was demonstrated [5]. A simple gas lens telescope was constructed and used to image the sun and moon [13].

In Chapter 2, a detailed account of the development of the gas lenses produced by spherical shocks from spark gaps [1], and the scale-up of the spark gap lenses [2, 14, 15, 16], will be given. In 1995, the use of a gas lens as a Q-switching element in a laser cavity was demonstrated [17].

Interest in the mechanism by which the lens is formed then turned the investigations towards models of shock wave by using surface waves in water [18]. The production of a lens by colliding cylindrical shocks generated by exploding wires was demonstrated by Conti [19], and improvement of the electronics for obtaining accurate reproducible delay times between the lens generation and the laser firing was undertaken [20].

Since gas lenses showed promise as non-solid, non-rigid optical elements, the UKZN group reviewed a variety of mechanisms for their production, including compressed air gas lenses, drawn-air gas lenses, spinning pipe gas lenses, gas dynamic

lenses generated by air from nozzles, and laser-produced plasmas [21]. Of these, the gas lens produced by a heated spinning metal pipe has proved the most promising [22]. Optical quality has been characterised [23, 24]. Recent Computational Fluid Dynamics investigations have been undertaken [25] to confirm the structure of the lens itself with experimental measurements. The drilling of holes in metal plates with laser beams focussed by this type of continuous lens has been demonstrated [26].

It should be noted that some work has been performed on lensing effects by the plasmas produced when intense beams are foucssed on planar carbon targets [27], on pulsed gas lenses [28], and on phase conjugation using both a gas lens and stimulated Brillouin scattering [29].

The limitations of the colliding shock lens work up to 1998 [30] led to the intention in this thesis to improve and scale the lenses, and investigate the exploding wire experiment.

1.5. The structure of the thesis

The operating principles of the spark gap CSL are described in Chapter 2, with a detailed account of progress on this configuration by previous authors. Modifications to the electronics and optics were necessary.

Scaling experiments were conducted on the exploding wire system, and these are covered in Chapter 3. The image acquisition system is described. Experimental results are shown.

Exploding wires were investigated in Chapter to compare the shock formation with that of the spark gaps.

A Computational Fluid Dynamics (CFD) model was constructed as described in Chapter 5. The results show the formation of a high density, high temperature lens region as expected. Conclusions regarding the experimental modifications required

for scaling are discussed in Chapter 6. The CFD results are shown to be qualitatively similar to the experimental results, but high speed cameras are required for a quantitative comparison. Recommendations for future work are provided.

2. Colliding Shock Lens (CSL)

The novel CSL invented and patented [9] at the University of Kwa-Zulu Natal (UKZN) consists of pairs of opposing electrodes (needles) on a circumference placed symmetrically with equidistant spacing. These electrodes act as arc gaps that are driven by a bank of capacitors. The bank of capacitors discharges across the spark gaps or exploding wires (as will be discussed in Chapter 4), thereby creating converging spherical or cylindrical shock waves, respectively. The shock waves interact with each other to form a region of air with high density, temperature and pressure at the centre of the device. This alters the refractive index of air and hence enables this formed region to refract light.

CSL's are gradually becoming one of the better known applications of gas structures [6, 21, 15]. Throughout this thesis air is the only gas that will be used. They are dynamic lenses, which last for a few microseconds during which they evolve. The CSL has different foci depending on the delay set for the approaching pulse of light. The relatively small lifetime does not seem to pose problems as they are intended only to be used with pulsed lasers. Most modern pulsed lasers have pulse durations of around or below 1 μs. These CSL devices of course cannot be damaged or destroyed by the laser, as is the case with most solid state lenses. The damage caused on ordinary solid state lenses changes the optical specifications of the lens as described on Section 1.1 on page 12. The damage produces undesirable effects on spot size, beam profile, beam position, etc.

2.1. CSL's Operational Principle

Consider two spherical shocks that collide. The nature of their interaction is dependent on their relative strengths, as suggested by Bucellato [1]. The different conditions can be described:

- When weak shocks at low Mach number collide, they pass through each other unmodified
- When weak shocks of intermediate strength collide, they also pass through each other with their profiles unmodified, but experience some temporal retardation
- When several stronger spherical shock waves collide with each other, they merge to form a very high density region before moving apart, having lost all information about their pre-collision structure
- Finally, when very strong shocks collide they produce a turbulent region at the point of impact.

Bucellato *etal.* [1] argue that when several spherical shocks expand from points equidistant on a circumference, they generate a spherically symmetric converging shock front. Converging spherical symmetric shock waves produce a region of high temperature, pressure and density in the region of implosion. After the spherical shocks converge to a point, a regular and stable axi-symmetric cigar shaped expanding density structure forms as shown in Figure 2.1.1. It is in this region that the graded lens is expected.

The term "Mach addition" has been applied to the constructive interference at the centreline [1, 18]. To a good approximation, once the maximum density has been reached, and the ellipsoidal or cigar shaped region has been formed, waves propagating outward thereafter can be regarded as originating in the high density region. The original shock structure has been lost in the interference.

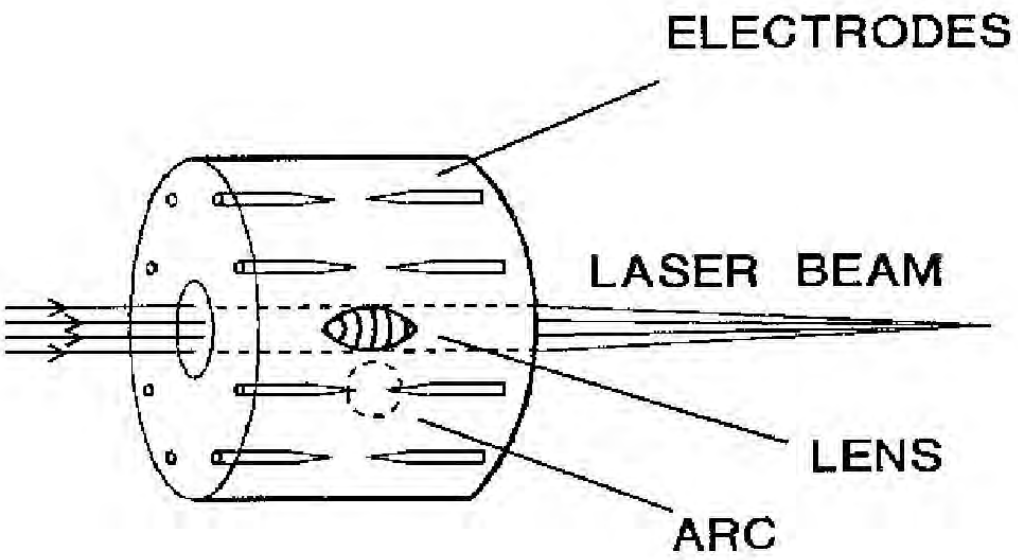

Figure 2.1.1.: Schematic of the CSL's Operational Principle taken from [1].

The reflections of shocks from solid surfaces or symmetry planes has been described by Courant and Friedrichs [32]. It is beyond the scope of this work to provide the theory, but a summary is given in Appendix A for future reference.

The very first CSL designed and constructed at the Laser Physics Group of UKZN consisted of four pairs of opposing electrodes equi-spaced on the circumference of a circle 11 mm in diameter.

This was quickly replaced by eight pairs of electrodes as described by Buccellato *et al.* [1].

2.2. Description of the first CSL's Experimental Setup

The Figure 2.2.1 shows a schematic representation of the entire setup as described in Buccellato's thesis [10]. The charging capacitor C was connected in series with the gaps of the CSL. The value of C determines the input of the energy of the shocks. At breakdown the 10 H coil acts as an open circuit and hence all the current will flow to the CSL.

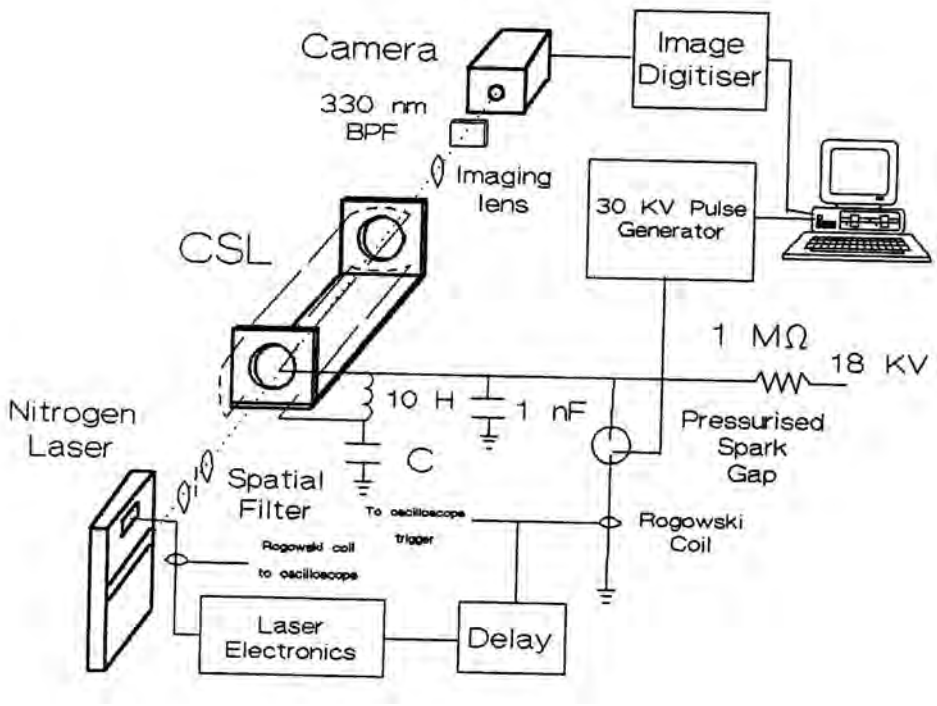

Figure 2.2.1.: Schematic representation of the CSL's Experimental Setup, [10].

A spatially filtered nitrogen laser beam of FWHM (Full width at half maximum) 1 ns was used. The beam was directed through the centre of the CSL, through an imaging lens, through a filter (330 nm, bandwidth 10 nm) and onto a CCD (charge coupled device) camera. The image from this was then sent onto an oculus card (image digitizer) in a computer and stored as an image file on the computer. The laser was a device made in the university workshop, consisting of a circuit board which had been etched in the middle of one side to create a gap. Nitrogen gas flowed

through the gap encased in a plexiglass housing with aluminum electrodes. The two sides were charged up to 20 kV. One side was pulled to ground with the aid of a pressurized spark gap creating a potential difference between the two sides. Current then flowed through the gap and excited the nitrogen gas which then lased. The laser pulse length was less than 1ns. The energy, 1 mJ, was surprisingly large for such a simple and affordable device. These N_2 lasers were developed at the CSIR (Council for Scientific and Industrial Research) by H. von Bergman and V. Hasson [31].

The Rogowski coil in the discharge circuit triggered the nitrogen laser via a variable delay box. The coil detects the electromagnetic radiation produced by the noisy breakdown of the CSL and sends the signal to the delay box which in turn triggers the laser. The signal was also sent to an oscilloscope for diagnostic purposes.

The electrodes of the CSL were mounted on two opposite plexiglass plates with a circular hole in the centre of diameter 7.5 mm allowing a laser beam to be directed along the axis of the CSL. The electrodes were made up of needles of diameter 0.85 mm with an arc gap spacing of 1 mm. The gaps were connected in series in order to have approximately simultaneous breakdown.

A review of the refractive fringe diagnostic was done by Waltham *etal.* [11]. Prior to investigating the interference of spherical shock waves Michaelis *etal.* [12] applied the refractive fringe diagnostic to these shocks, in air, generated by an arc discharge. Buccellato *etal.* [1] investigated the properties of the interacting shock waves by recording a succession of images at different time delays. The time sequence images are given in Figure 2.2.2 on the next page. The images were obtained with shock speeds of approximately Mach 1.5 [1].

Forbes [18] also simulated the CSL using shallow water waves and he showed that there were very strong similarities between the properties of the CSL and the colliding water waves on a sloping bottom.

The first picture A shows the shocks just after breakdown, still moving inwards

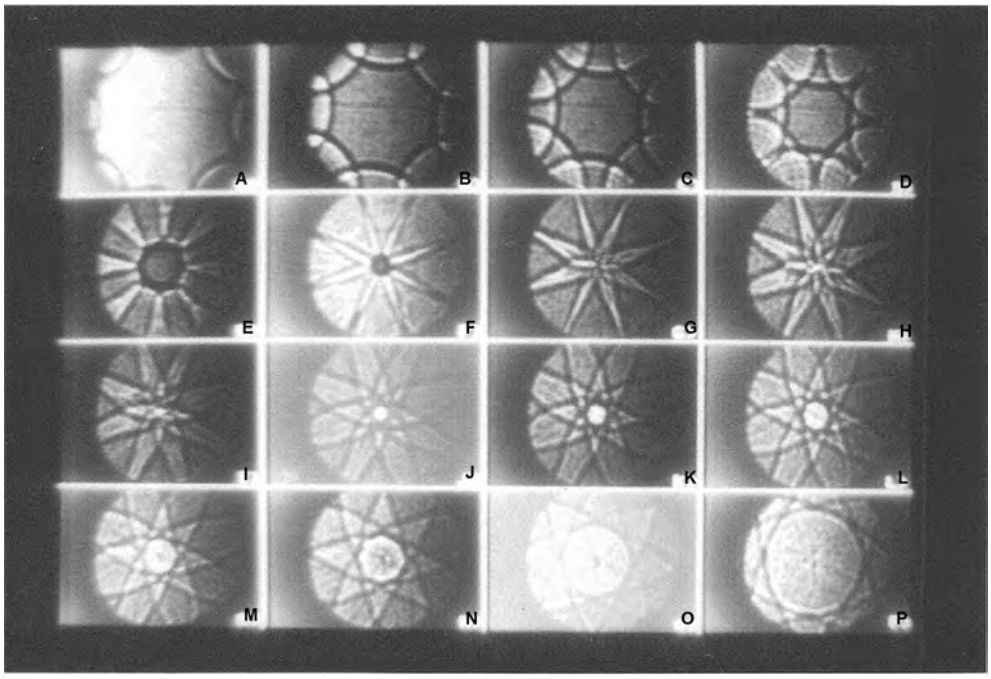

Figure 2.2.2.: Time sequence of an eight arc CSL from Bucellato *etal.* [1]

and not having interacted. Images D to E show the shocks interfering with each other as they travel towards the centre of the circumference. On images F to I all the shocks meet at the implosion point. Images J to M show the lens forming diffraction patterns when focusing is achieved closer to the CCD camera. Images N to P show the colliding shock waves moving away from the centre.

A high density expanding region of air is created after the shocks have collided (images F and G). Images H and I show the formation of a small centre region through which the beam is focussed. In subsequent images this region expands and the focus is lost.

It was also found with this device that the laser beam could be focused down to a spot size of 100 μm (FWHM). This was the first demonstration that a CSL might find research or industrial uses. A hole with a diameter less than 1 mm was drilled with a CSL and a ruby laser [5] .

2.3. Trigger Modifications

The ignitron is a mercury vapour rectifier. The ignitron-driven driven CSL trigger circuit employed by Buccellato *et al.* [10] became unreliable for a variety of reasons. Transportation, shaking or disuse are some of the factors that rendered ignitrons unreliable in holding off high voltages. One of the reasons that may cause the unreliability is that the mercury vapour may splutter and be deposited on the anode. There may be small bumps on the anode, where the electric field may be high, leading to breakdown. If the mercury wets the carbon electrode then the trigger will not fire the ignitron.

One of the significant reasons to investigate alternative triggering methods was that much larger CSL's were required, as is discussed in chapter 3 on page 26, requiring higher voltages.

In the initial circuit, as shown in Section 2.2.1 on page 21 and discussed in Section 2.2 on page 21, the ignitron trigger failed repeatedly at high voltage. It was decided to investigate an alternative triggering method employing a master spark gap. Several circuits were tested and eventually the one shown in Figure 2.3.1 was connected.

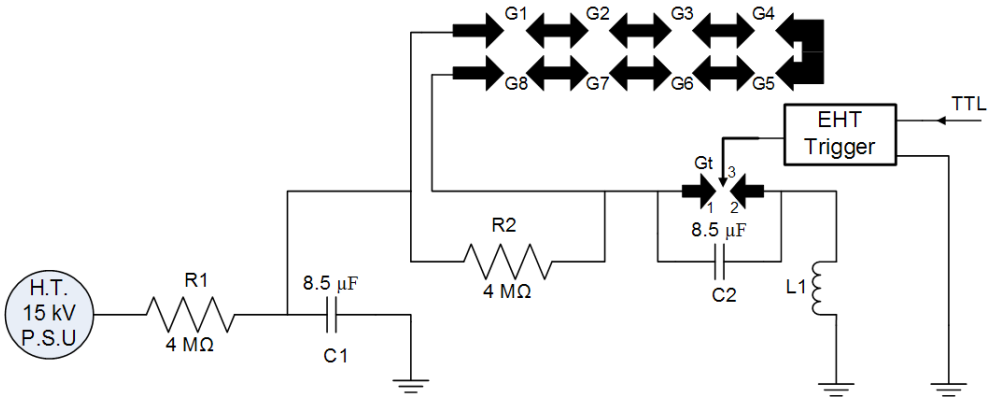

Figure 2.3.1.: Spark gap and trigger circuit.

This is a simplified electrical circuit in which all eight spark gaps are shown in series with the trigger spark gap.

The circuit consists of eight spark gaps (G1 - G8) making up the part of the

colliding shock lens together with a third spark (Gt), which is the trigger spark gap. The trigger spark gap contains three electrodes : pins 1 and 2 are the main electrodes which face each other and pin 3 is the third electrode lying in between. Pins 1 and 2 are charged continuously by a 15 kV power supply. The charging of these capacitors occurs via two 4 MΩ resistors as shown in the diagram. The 15 kV power supply can only supply a few milli-amps of current and is therefore not responsible for firing of the spark gap directly.

Assuming that the capacitors are fully charged, the spark gaps G1 - G8 are initiated to break down simultaneously as follows : a second high voltage power supply driven by a TTL (transistor-transistor logic) pulse from a computer, supplies a high voltage (20 kV) pulse to the trigger pin (pin3) relative to the ground pin (pin 2) of the trigger spark gap. This causes a spark to occur between pins 2 and 3. Since C2 is fully charged this spark initiates a breakdown between pin 1 and 2 causing C2 to discharge through the trigger spark gap.

The moment Gt breaks down, the right hand pin of spark gap G8 is now effectively at the ground potential and the full voltage across C1 is applied across the series combination G1 - G8, causing all of them to break down simultaneously. With all the spark gaps arranged cylindrically, simultaneous breakdown generates shock waves. The 15 kV power supply cannot maintain the conduction through the spark gaps due to the high resistance of R1. Thus once G1 - G8 have discharged, the spark gaps revert back to the non-conducting state.

The purpose of the inductor L1 is to form a resonant circuit together with C1. The current will thus decay once conduction through the spark gap occurs. Due to the dissipative nature of the breakdown in the spark gaps the sinusoid decays within one or two cycles. This results in a single narrow pulse of current that passes through the spark gaps.

3. Scaling the CSL

3.1. Introduction

It had been noted in Buccellato's [10], Lisi's [14] and Kuppen's [2] work that for the conventional CSL's thus far developed, the optical apertures were too small to have any application in industry or even research. The optical apertures were of the order of millimeters. It became apparent that a lens that would deliver a bigger optical aperture, of the order of centimeters, should be designed and tested. This approach would demonstrate that the CSL could in principle be scaled up.

Several CSL's were designed by Kuppen [2], but were not fully tested. In the current work, their different properties were investigated as discussed in this chapter. The limitations to these CSL's will also be mentioned.

3.2. Scaling Experiments

Five different CSL's were constructed [2] including the initial CSL to study the five physical characteristics, namely shock strength, electrical diameter, number of electrodes, the presence of an enclosure, different gas types and gas pressures.

The shock strength was varied in two ways, viz. by changing the charging voltage applied to the charging capacitor, and by changing the capacitance of the charging capacitor whilst keeping the charging voltage constant.

The electrical diameter (d_0 as shown in Figure 3.2.1) is the radial spacing of the

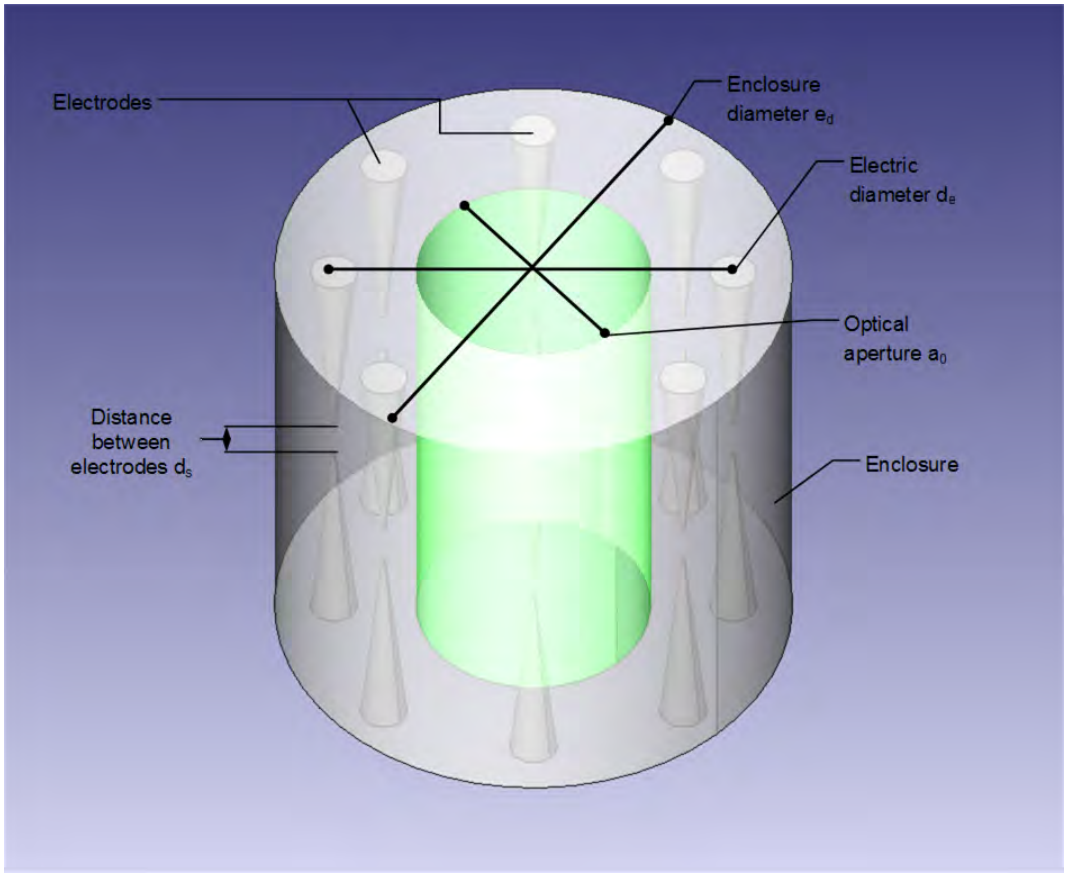

Figure 3.2.1.: Labels of the different parameters of the CSL.

electrodes. In these experiments the "electrical diameter" was changed using different CSL's. The electrical diameters ranged from 11 mm to 160 mm for the devices.

The "optical aperture" (a_0 as shown in Figure 3.2.1) is the aperture of the gas lens produced and varies from 1 mm to 1 cm.

The number of electrodes were also varied to study the effects these numbers have on the lens region.

"Enclosed CSL's", with enclosure diameter e_d as shown in Figure 3.2.1, have walls which confine the shock waves.

The distance between the electrodes is shown as d_s in Figure 3.2.1.

3.3. Experimental Setup

The experimental setup described in Section 2.2 on page 21 and as shown in Figure 2.2.1 on page 21 was modified as follows.

3.3.1. Optical Setup

For the smallest CSL, a single lens was used to expand the beam, as shown in Figure 3.3.1. The magnification of the system is adjusted by changing the distance between the lens and the photographic paper. Because the CSL device was small the beam does not diverge much while going through it. To obtain images at the far field, a small telescope was set up to collimate the beam. Because of the weakness of the CSL it was important to obtain a parallel beam. One advantage of the spark gap CSL is that it does not require a very precise alignment (as in the case with the exploding wire experiment described later in Chapter 4 on page 58.)

A shutter was used in front of the laser that was operated by an electromagnet. The nitrogen laser often fired spuriously and the shutter played a significant role in protecting the photographic paper from being exposed by unintentional shots.

Figure 3.3.1 shows the optical path of the laser beam as it traverses the optical equipment. The collimator consisted of two lenses with focal lengths of 500 mm and 50 mm respectively, (Figure 3.3.1). The lens at the filter had a 100 mm focal length.

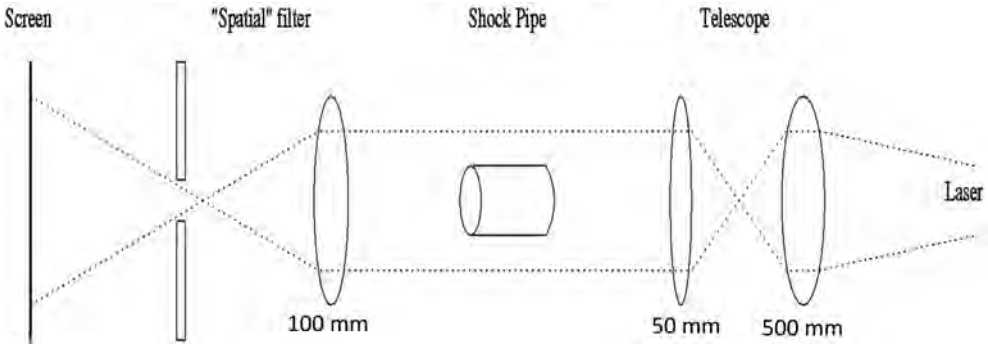

Figure 3.3.1.: The optic circuit of the experiment.

3.3.2. The Electrical Circuit

The electric and electronic part of the experiment can be divided into two well-defined separated sections: an electronic circuit that controls the triggering and diagnostics, and the high voltage circuit that produces the spherical shock.

3.3.2.1. Electronic Circuit

The electronic circuit is shown on Figure 3.3.2. The main signal to run the experiment comes from the main trigger, which is a small box that delivers a 5 V square pulse, which was designed at UKZN (formerly UND) by G. Turner as part of a Masters thesis [20]. The pulse is sent both to the high voltage trigger of the spark gap and to the oscilloscope. Once the spark gap opens and the BCSL (Big Colliding Shock Lens) breaks down, an optical trigger picks up the light and sends a signal to the delay box. The delay box then triggers the laser with the appropriate delay, in accordance with the requirements of the experiment. A Rogowski coil in the high voltage room, which is screened with a Faraday cage (chicken wire) to protect the electronics from electromagnetic radiation, then picks up the electromagnetic noise both from the main experiment and from the laser, allowing the precise measurement of the delay, without relying on the value set on the delay box.

3.3.2.2. High Voltage Circuit

Figure 3.3.3 shows the high voltage circuit used for the BCSL. The coil is connected in parallel with the BCSL. The pins form an open circuit and the coil is necessary to charge the BCSL spark gaps to the same voltage as that of the capacitor. The coil is a good conductor but behaves almost as an open circuit at the high frequencies of the discharge.

The high voltage power supply is controlled from the control room as described in Section 3.3.2.1. For safety reasons the operator may not be in the vicinity of the dangerous high voltage equipment. Between the power supply and the experiment

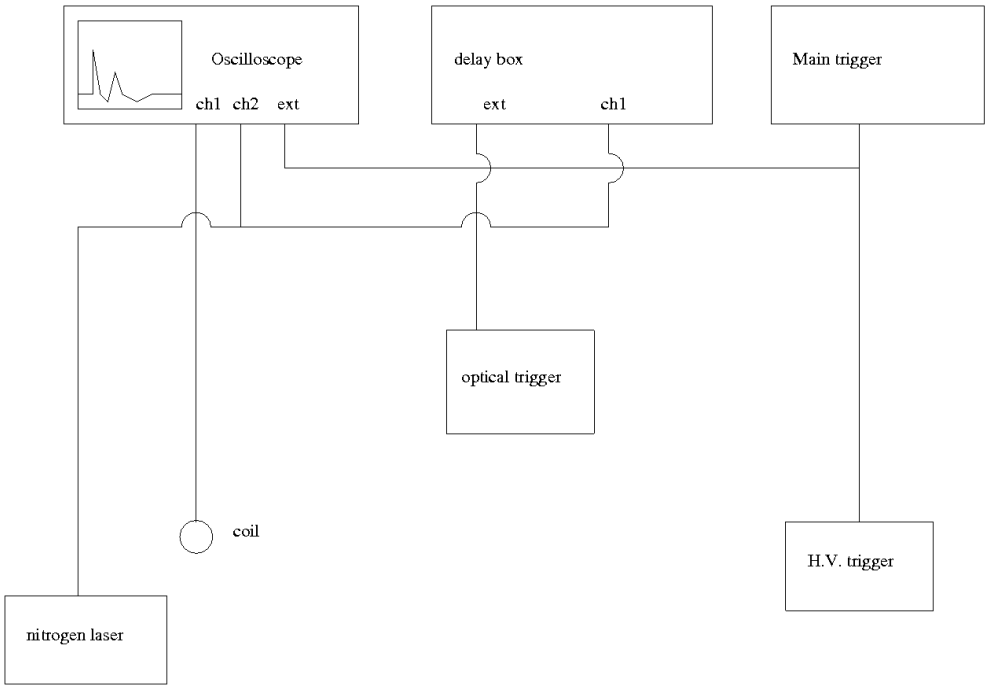

Figure 3.3.2.: The electronic circuit in the experiment.

there is a resistor (400 Ω) and an inductor. These protect the power supply from voltage spikes during the main discharge. The voltage across the capacitor is measured with a multimeter connected to a 1:1000 high voltage probe. The capacitance of the capacitor was varied using 1, 4 or 8 μF capacitors.

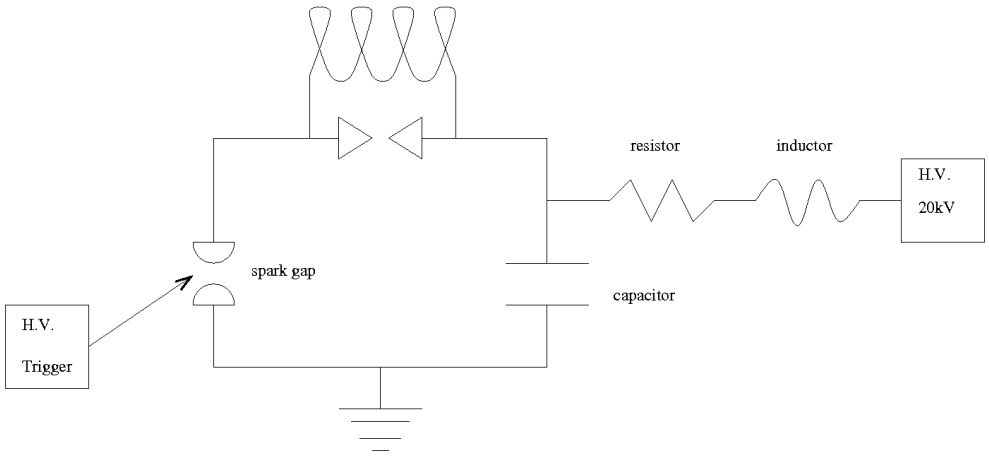

Figure 3.3.3.: The high voltage circuit of the BCSL experiment.

3.3.3. Spherical Shocks

Spherical shocks were used in most of the experiments. These are shocks that are produced when air is ionized between two pins that are some distance apart as in Figure 3.3.4.

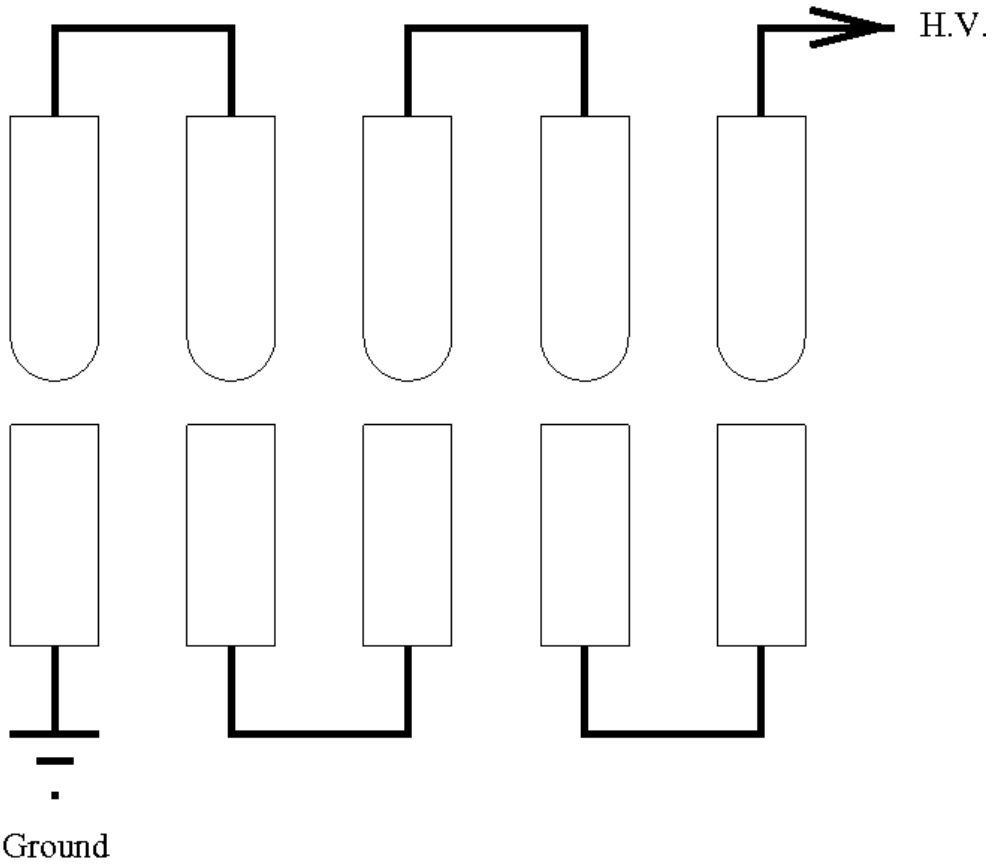

Figure 3.3.4.: Hemispherical and flat electrodes used to produce spherical shock waves.

One set of 16 electrodes is rounded and the other set of 16 electrodes is flat (3.3.4) to facilitate aligning of the anodes and cathodes. It is more difficult to align two pointed objects with exactly the same spacing for 16 pairs of electrodes. Misalignment makes the shock generation uneven, with some electrodes discharging before others, delaying the generation of the shocks with respect to each other. After a few discharges the electrodes erode unevenly and must be machined again.

3.3.4. Image Acquisition System

At the beginning of the experiment, the acquisition system consisted of a CCD camera connected with a computer through a digitizing board (Figure 2.2.1 on page 21). Unfortunately, these cameras are very sensitive to the electromagnetic noise produced in the experiments. Much of the image was lost because of the noise. For this reason, despite the many advantages offered by the CCD camera, a much simpler imaging system, namely photographic paper, was used instead. Photographic paper is very sensitive to the ultraviolet light emitted by the nitrogen laser and is easy to develop. However photographic paper has many disadvantages. Firstly the image obtained is a negative. Secondly, and most importantly, it saturates quickly and does not allow a quantitative comparison of the laser intensity in different parts of the image.

A more pertinent problem with the paper is a safety issue. Paper needs to be protected from light, and working with high voltages in darkness is a safety risk. A red light was installed in the laboratory. However, attention was still required to avoid touching high voltage electrodes.

3.3.5. The big CSL

The CSL's described above have optical apertures of up to 5 mm, too small for reasonable application. The next aim was enlarge the optical aperture, to at least 10 mm. Therefore a bigger electrical diameter is required, to allow the shocks to meet in the center with a larger radius of curvature, to obtain the necessary Mach addition. Since the shock waves travel a longer distance, the energy was increased, to allow Mach addition to take place and to avoid a broadening of the shocks.

A diameter of 300 mm was used with sixteen pairs of pins, in order to increase the optical quality of the lens by generating a smooth circle. At the beginning, an attempt was made to operate the lens with the pins connected in parallel, usually in couples. The voltage across the capacitors can then be reduced, allowing the use

of a cheaper and simpler power supply and reducing the dangers in the laboratory. However, it was observed that this configuration leads to a large difference in the breakdown time of different pairs of pins, which yields an unacceptably distorted lens.

The electrodes used were made out of steel. The electrodes for the discharge are a flat surface and a sphere as in Figure 3.3.4. Two spherical pins would alleviate breakdown, but are more difficult to align. The distance between electrodes (d_s as shown in Figure 3.2.1) was approximately 0.1 mm, for a safe breakdown at the required voltage to operate the lens. The separation of the electrodes is important as the breakdown voltage was approximately 20 kV.

3.4. Results and Discussion

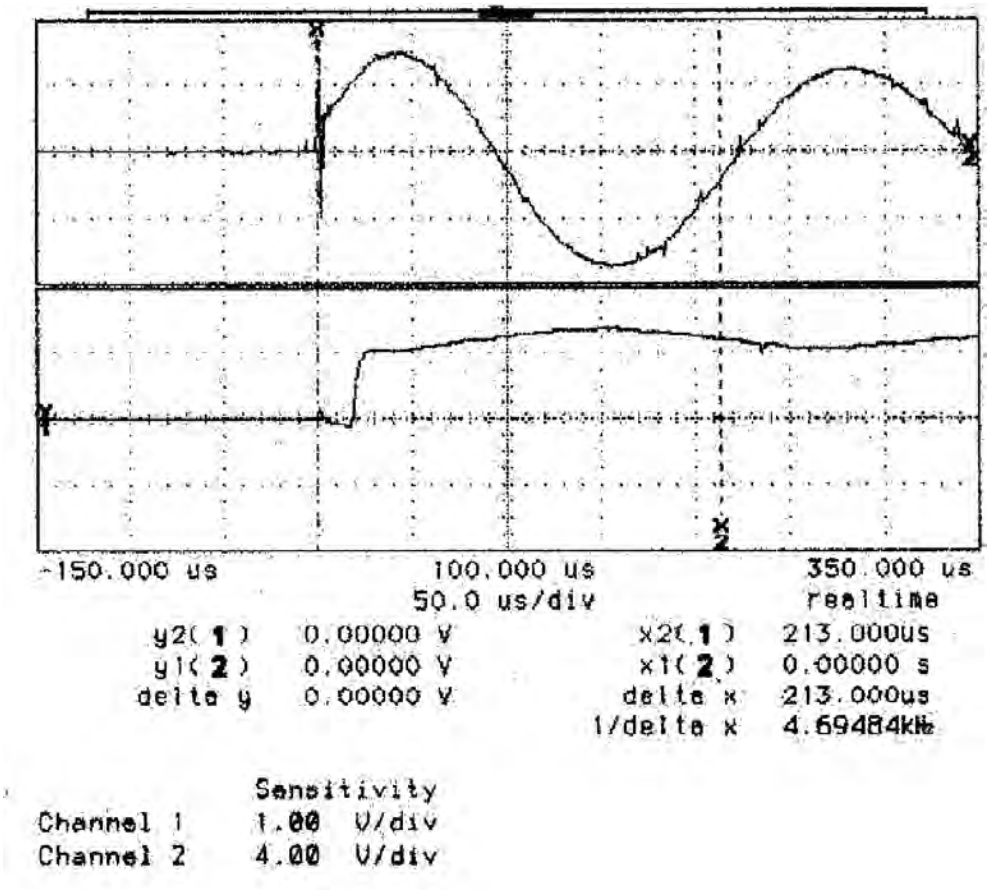

Figure 3.4.1.: Oscilloscope trace: no breakdown at electrodes .

Figure 3.4.2 shows an oscilloscope trace of the experiment under normal operation, for comparison with Figure 3.4.1 where no breakdown occurred. The first high peak from the left of the top trace is the electromagnetic noise coming from the breakdown of the electrodes and the second peak is that produced by the laser. The bottom trace shows the signal produced by the optical trigger.

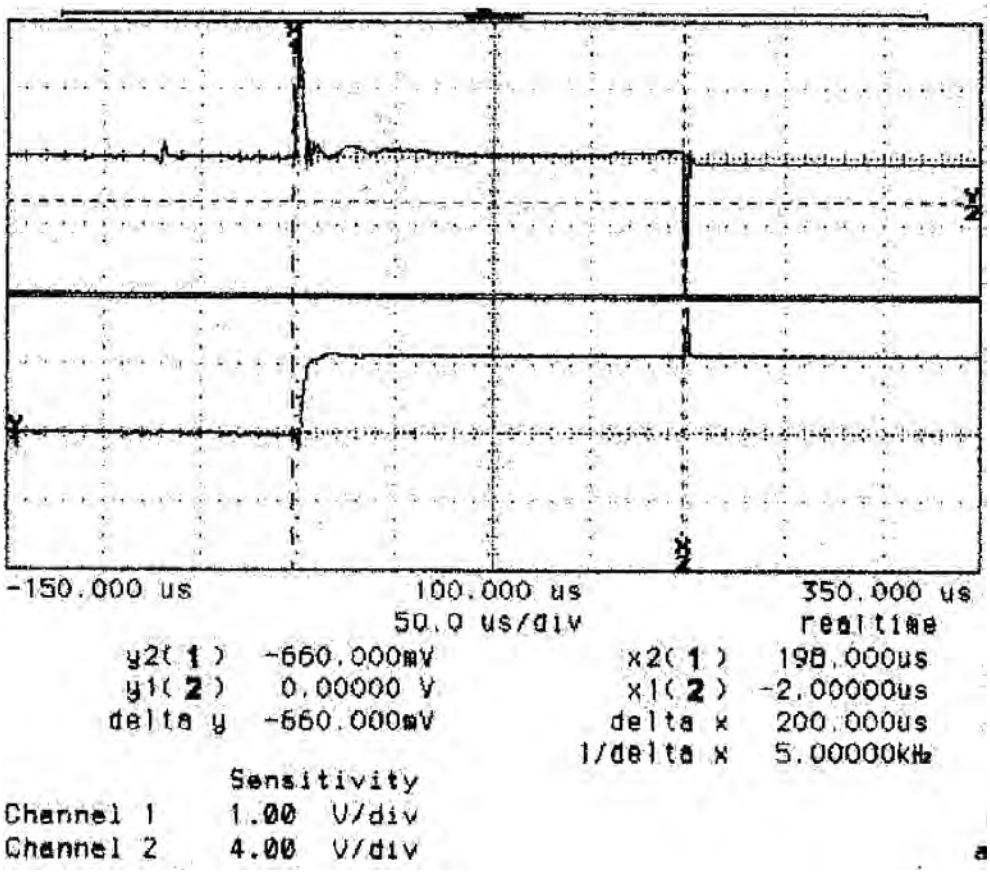

Figure 3.4.2.: Oscilloscope trace: normal breakdown of electrodes.

The second problem experienced with the BCSL was that the electrodes are eroded by the arc discharge. To make the alignment of the electrodes easier, a flat electrode was used adjacent to the spherical electrode. After several BCSL breakdowns the flat electrode develops a concave shape and the gap has to be decreased to obtain the same conditions for breakdown. This adjustment changed the geometry of the position of the electrodes and also changed the voltage at which the breakdown occurred.

3.4.1. Speed Measurement

The size of the lens corresponding to every chosen delay was calculated from the measured speed of the shock waves. This was done by measuring the diameter for two known delays, after checking the reliability of the system over a few shots. A reference object with a 6 mm gap was used to obtain the scale of the image (Figure 3.4.3). The shocks propagate with a approximately circular front. The diameter of the shock front was measured for two cases at different delays. The radii are approximately 1.95 mm and 4.10 mm respectively, and the delay time between them is 5.0 μs. The resulting speed, with a voltage of 20 kV, and an energy of about 800 J from the capacitor was calculated to be approximately 1.25 Mach as shown below in Equation 3.4.1.

$$M = \frac{\triangle x}{c \triangle t} \tag{3.4.1}$$

where M is the Mach number, $\triangle x$ is the difference in radii of the two shock formations, $\triangle t$ is the delay time between them and c is the speed of sound at sea level at standard temperature and pressure ($c \approx$343.3 m/s).

3.5. Results

It should be noted that the pictures following in Chapter 3 have negative greyscales, i.e. the highest light intensity corresponds to the darkest part of the image.

The first results on the BCSL were obtained using an energy of 300 J from the capacitor. In the result very regular shock propagating fronts up to 12 mm were observed. However it was observed that the lens did not form for diameters larger than 6 mm, and the laser pulse was not focused. In these cases the energy was not high enough to obtain Mach addition. The shocks pass through each other

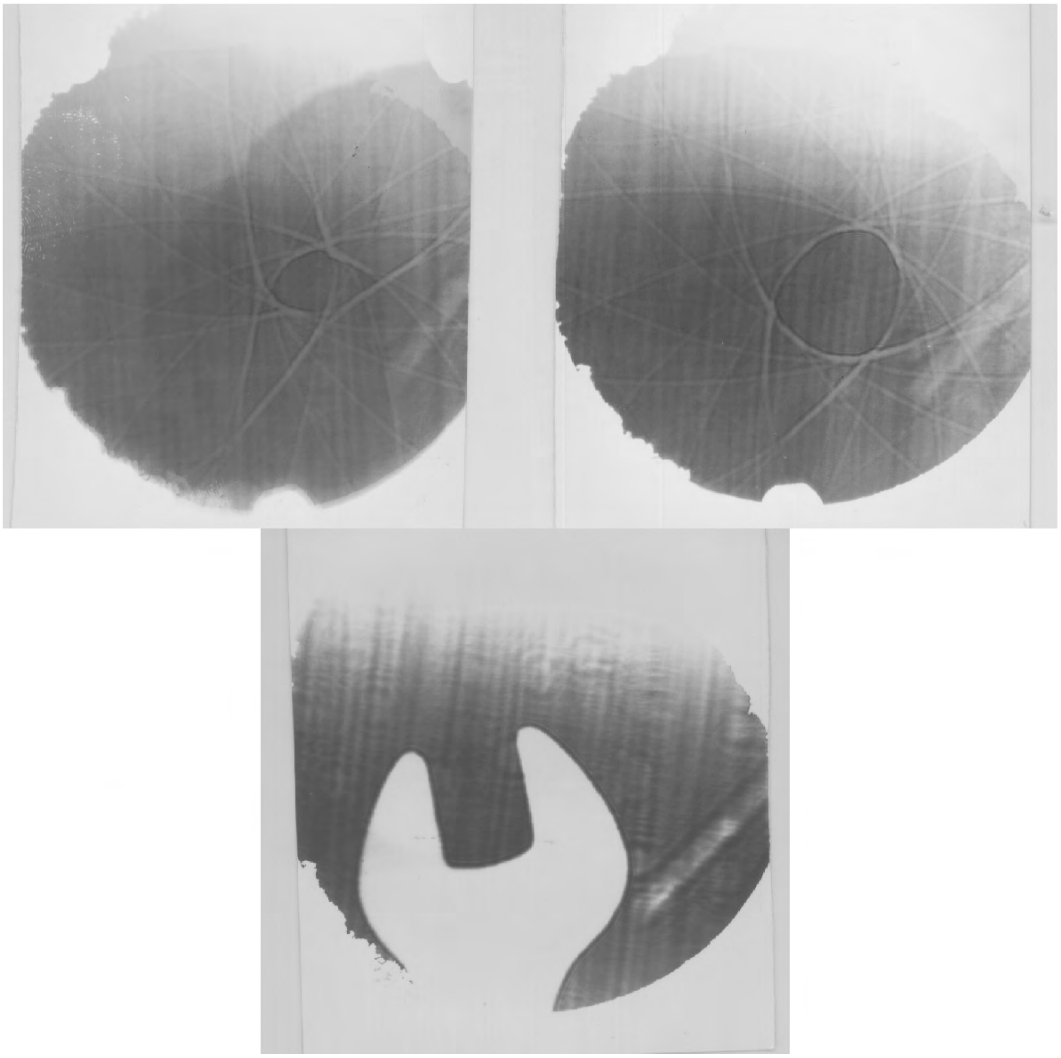

Figure 3.4.3.: The three pictures used to measure the speed of the shock waves

unmodified and do not create the cigar of hot dense air that forms the gas lens.

Subsequently, a series of focused images was obtained with an energy of 800 J from the capacitor and the results are shown in Figures 3.5.1 to 3.5.6. Note that the photographic paper is exposed to obtain the radius of the lens and the image of the focus in two subsequent experiments. Graph paper with lines at 1 mm intervals is included for scale.

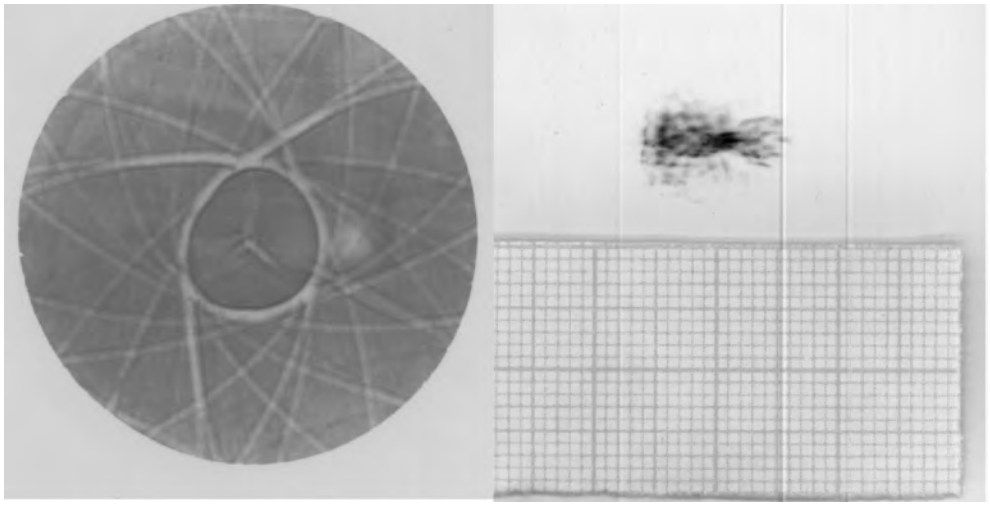

Figure 3.5.1.: An image of the lens and of the corresponding focus. The diameter of the lens is 7.2 mm.

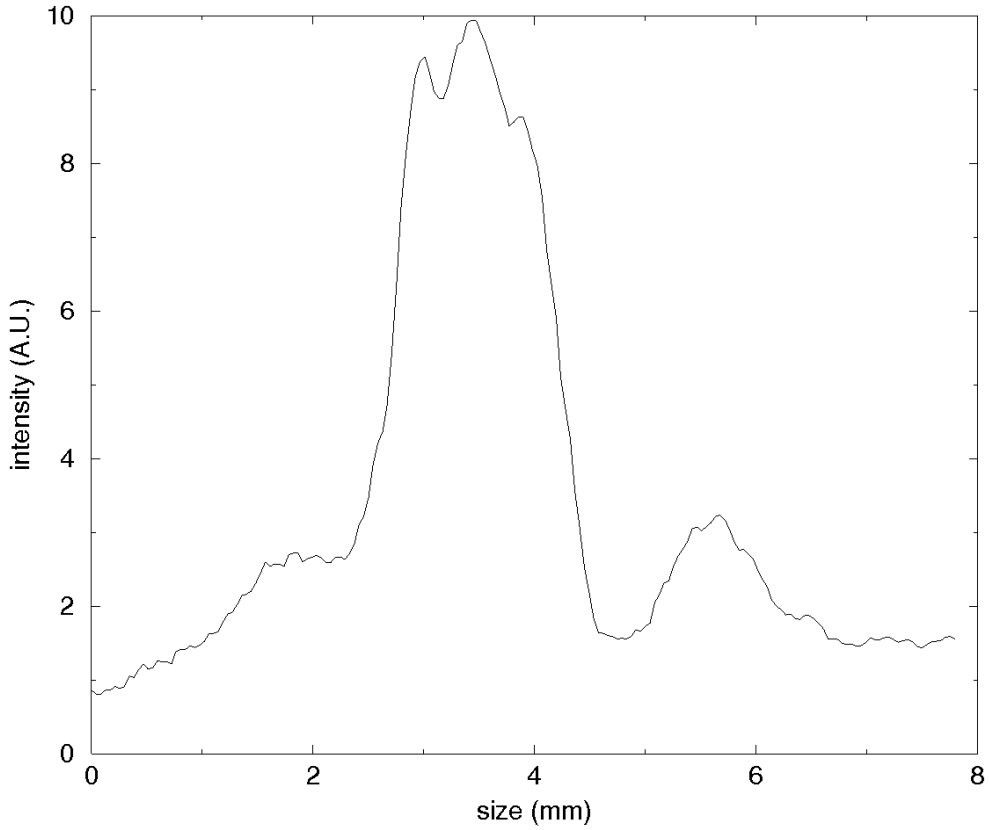

Figure 3.5.2.: Densitometry of Figure 3.5.1. It can be seen that the actual size of the focus is approximately 2 mm. The intensity of the absorbance is approximately 10 A.U. (Absorbance Units)

Densitometry is the measurement of optical density in light-sensitive material, such as photographic paper or photographic film, due to the exposure to light.

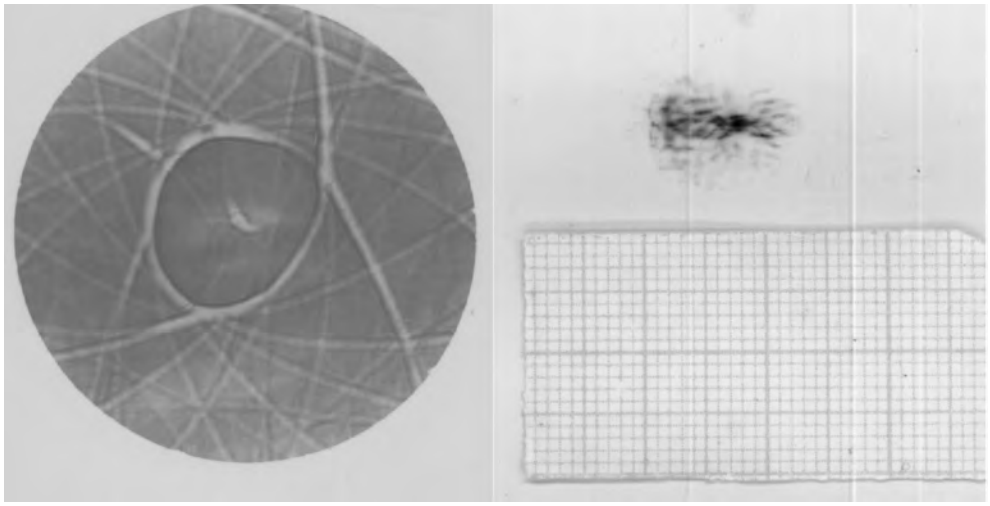

Figure 3.5.3.: An image of a 9.0 mm lens and the corresponding focus.

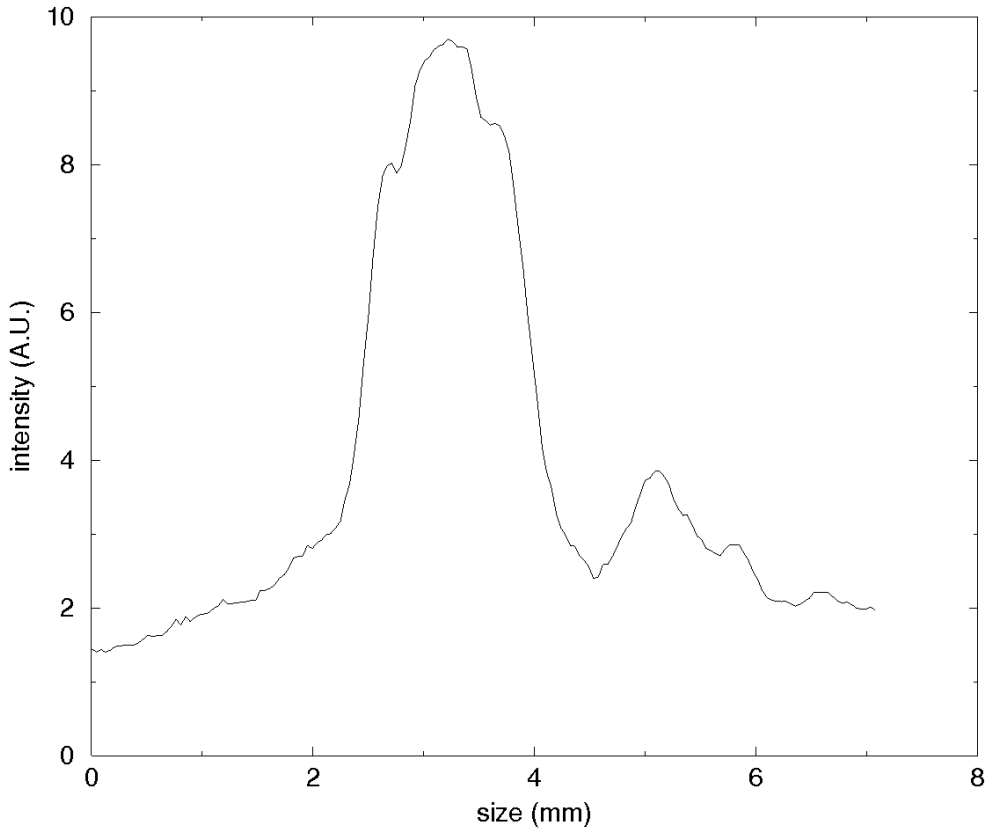

Figure 3.5.4.: Densitometry of Figure 3.5.3. The focus size is less than 2 mm.

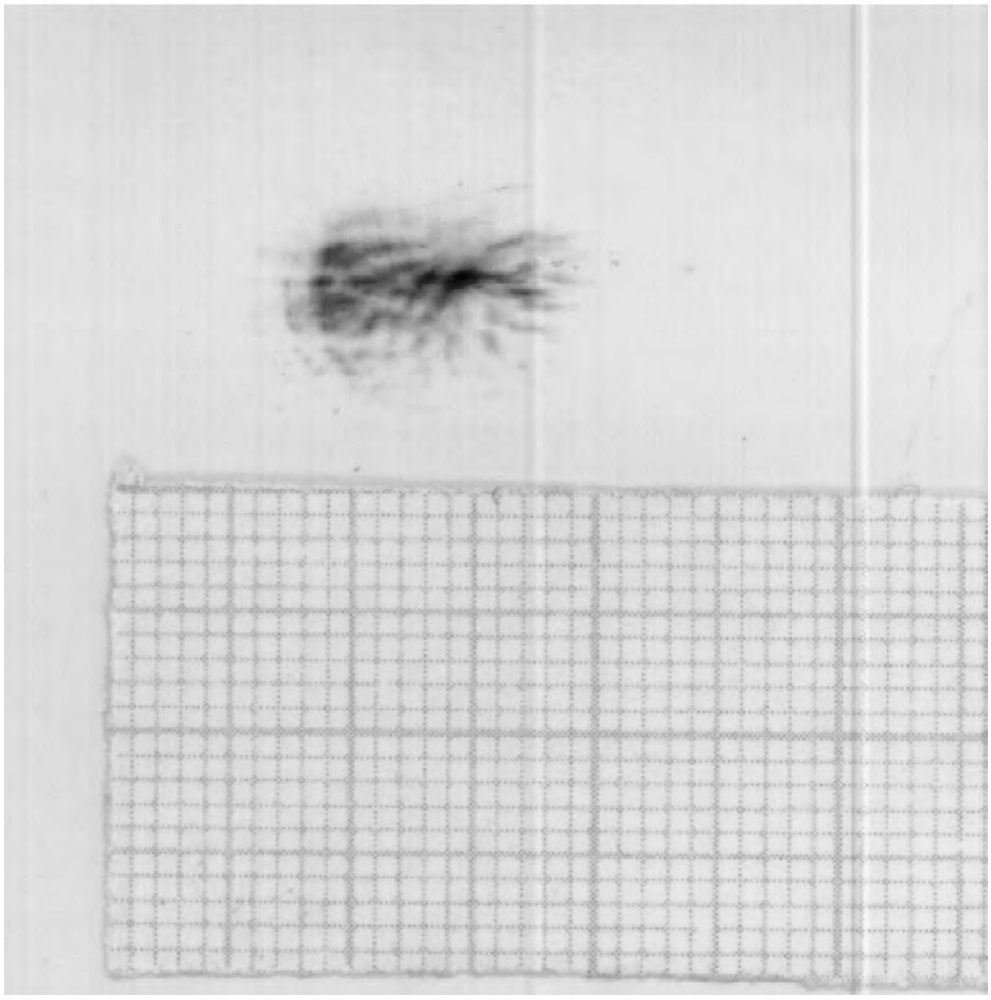

Figure 3.5.5.: One of the best foci obtained during the experiment. The diameter of the lens was in this case 10 mm. The focus is smaller than 1 mm.

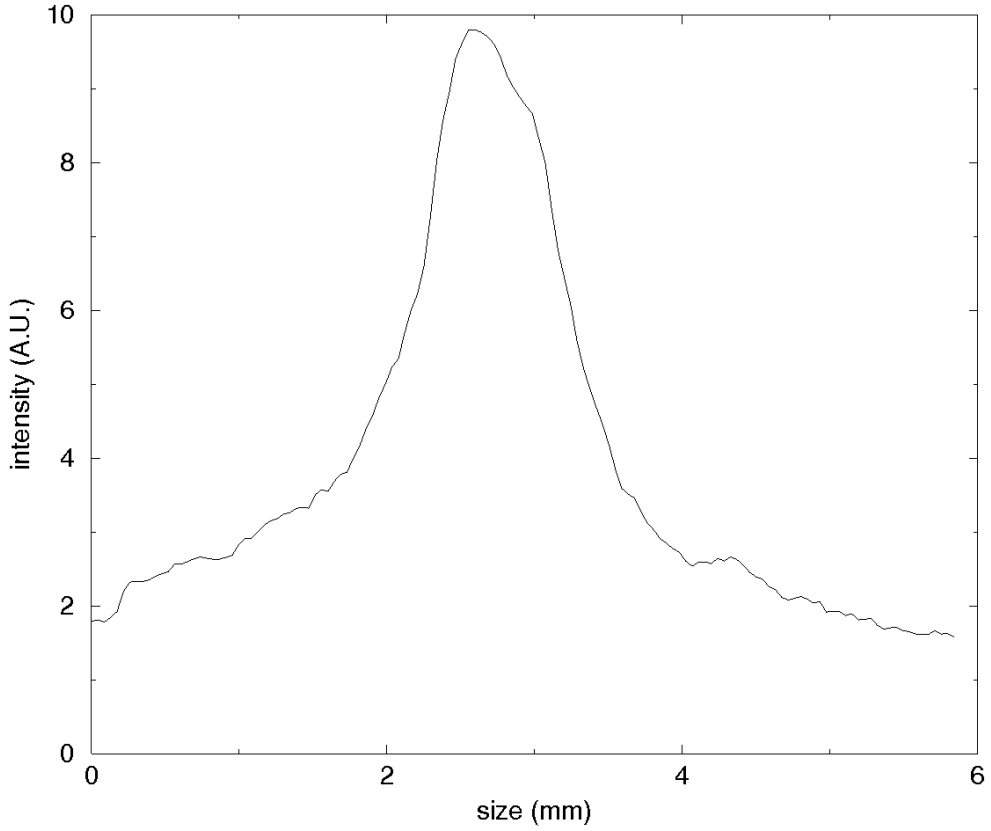

Figure 3.5.6.: Densitometry of Figure 3.5.5.

Mach addition (section 2.1) is the effect that constructive interference on the centre line acts as a source of outgoing waves. The effect of Mach addition may be observed by comparing Figure 3.5.7, obtained before the collision of the shocks, with those obtained later, Figures 3.5.7 and 3.5.9. All the pictures obtained before collision show a very irregular shape, which, in most of the BCSL breakdowns, is more regular after the collision.

Another series of results is shown in Figures 3.5.9 to 3.5.23. In this case, the telescope was adjusted to have a parallel beam and focus it only with the CSL, without the aid of any additional lens.

Figures 3.5.8 on page 42 and 3.5.9 on page 43 show lenses of good quality, i.e. small focus diameter, obtained with an energy of 600 J. In this case the lens has a more regular circular shape. Many refraction fringes may be noted downstream of the shocks.

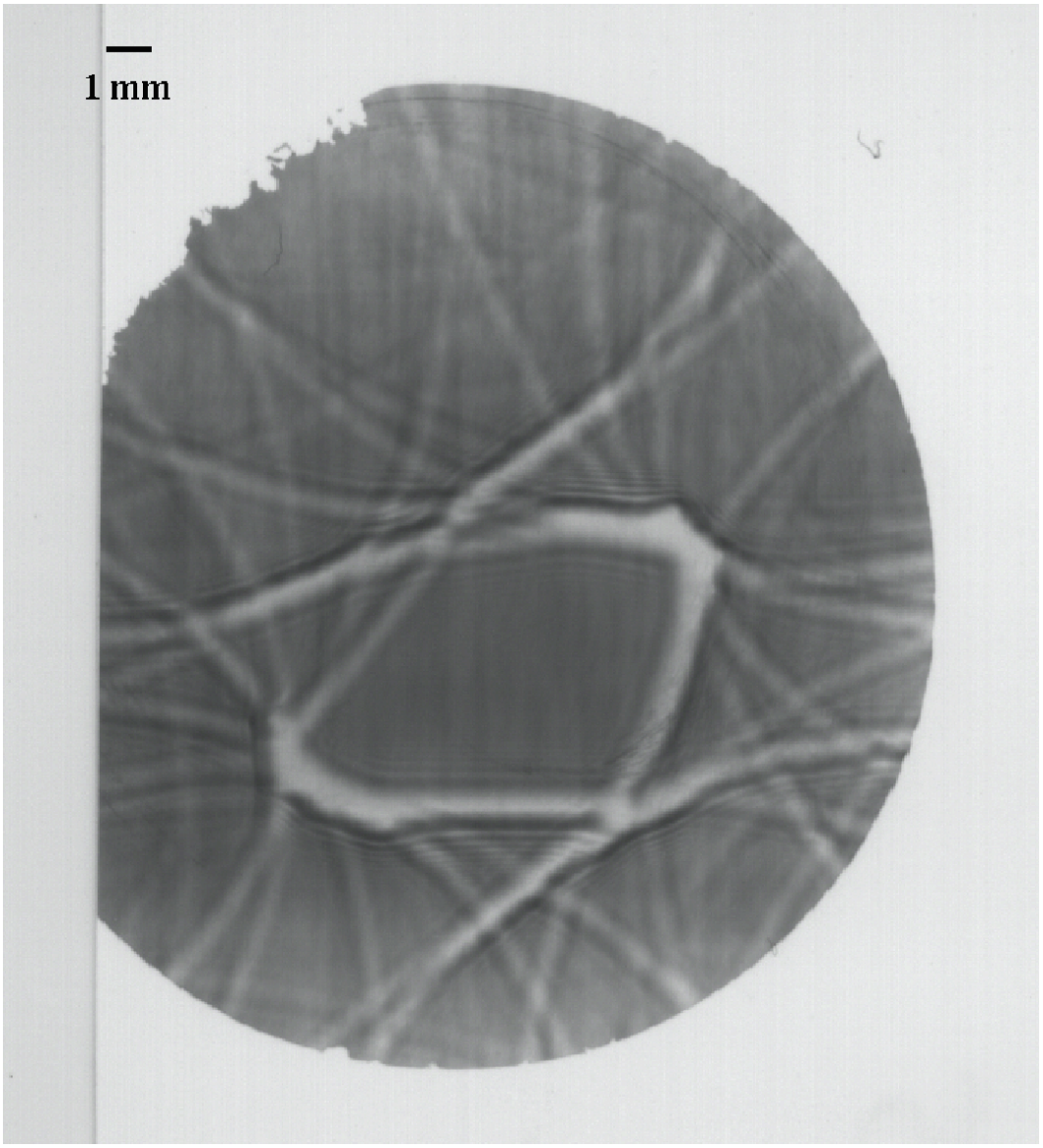

Figure 3.5.7.: An image of the shock obtained before collision in the center.

It can be noted that for small delays after the collision of the shock in the center, a strong small lens can be observed with a focal length shorter than 2 m (see Figure 3.5.11 on page 45).

Figures 3.5.10 on page 44 and 3.5.11 on page 45 show a strong focus at short focal lengths obtained immediately after collision, when the lens has still a diameter of approximately 1 mm. The lens has a much shorter focal length, but its size does not make it interesting for any practical application.

The two pictures 3.5.13 on page 47 and 3.5.15 on page 49 show the size of the lens

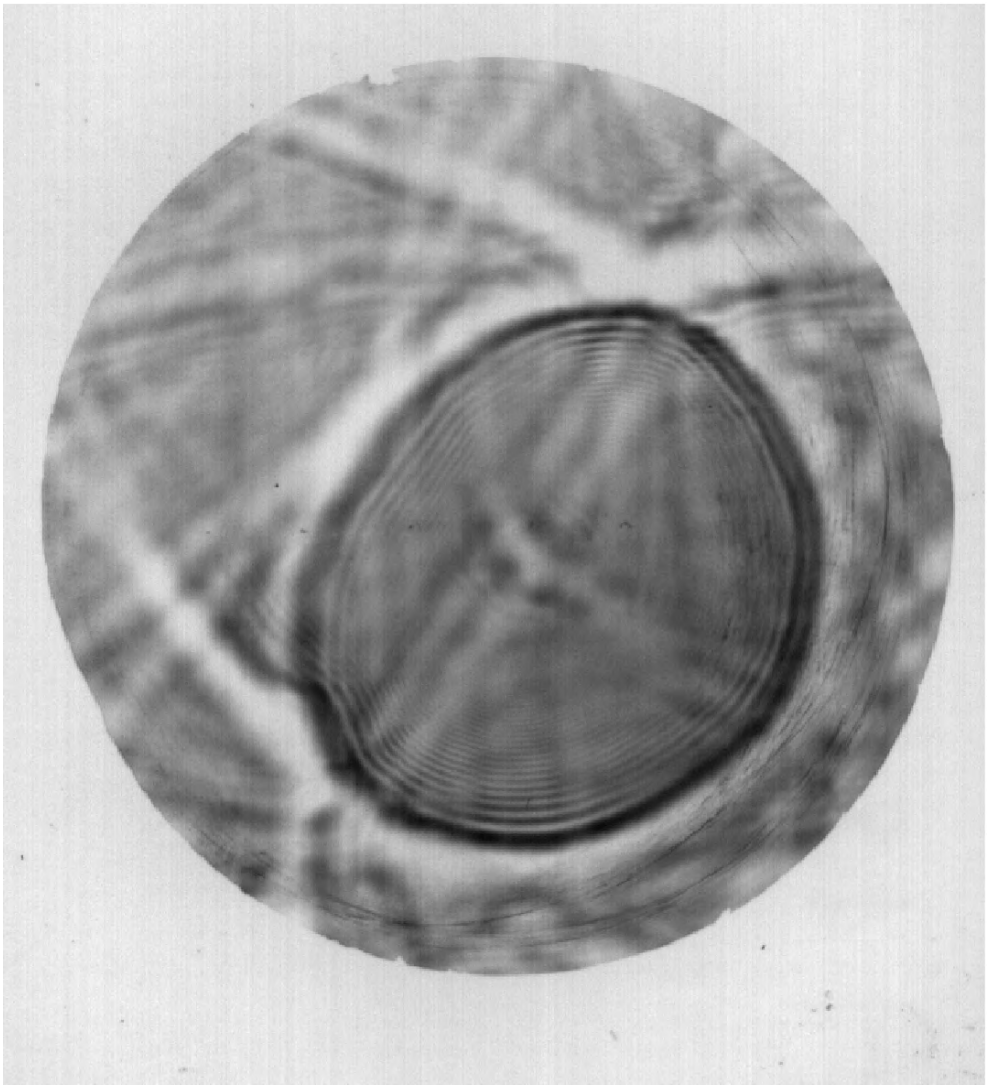

Figure 3.5.8.: An image of a good quality lens, obtained with an energy of 600 J.

in the near field. It is interesting to notice that the two images were obtained with the same delay between the laser and the CSL. Despite the fact that the delay was the same, the two images show a difference in size of more that 10%. If this yields a corresponding difference in focal length, the fluctuation in the focus position could be as high as 2 m. This implies that the diameter of the focus could be actually smaller than that measured. Unfortunately, images of the near and far fields cannot be obtained at the same time, and the size of the lens in every BCSL breakdown is not known. This can in principle be done using a beam splitter placed immediately after the device, but it requires a higher laser energy than that available.

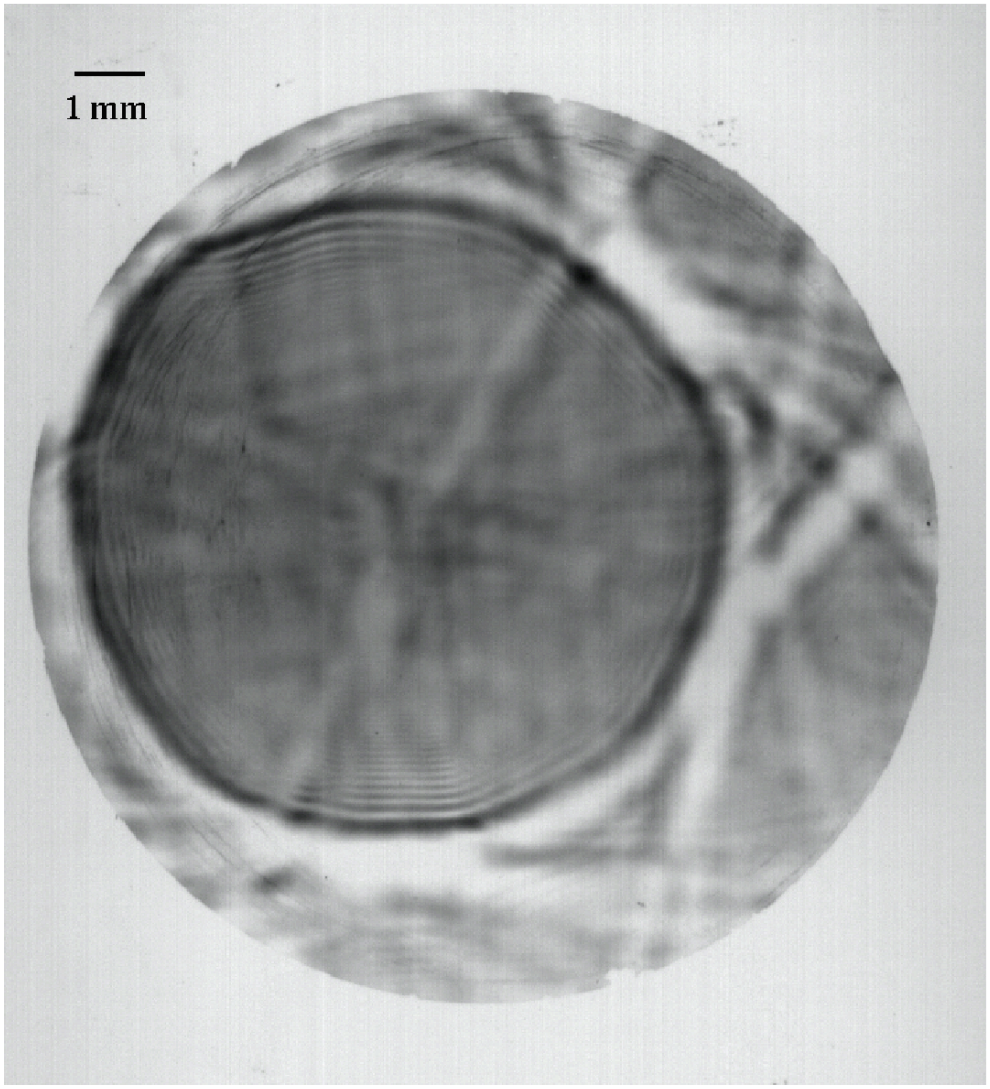

Figure 3.5.9.: An image of a good quality lens, obtained with an energy of 600 J.

In Figures 3.5.12 on page 46 and 3.5.14 on page 48 the telescope was adjusted in order to have a parallel laser beam. Their corresponding oscilloscope traces are shown on Figures 3.5.13 on page 47 and 3.5.15 on page 49 respectively.

The image in Figure 3.5.16 on page 50 was obtained very close to the CSL, only 3.3 m away. It is clear that the lens is focusing, but the focus is further from the lens than 3.3 m. Images taken at distances in the range between 5 m and 10 m show similar results.

The images from Figure 3.5.17 on page 51 to 3.5.23 on page 57 show the results obtained with the lens at a distance of 15 m. The size of the focus is relatively

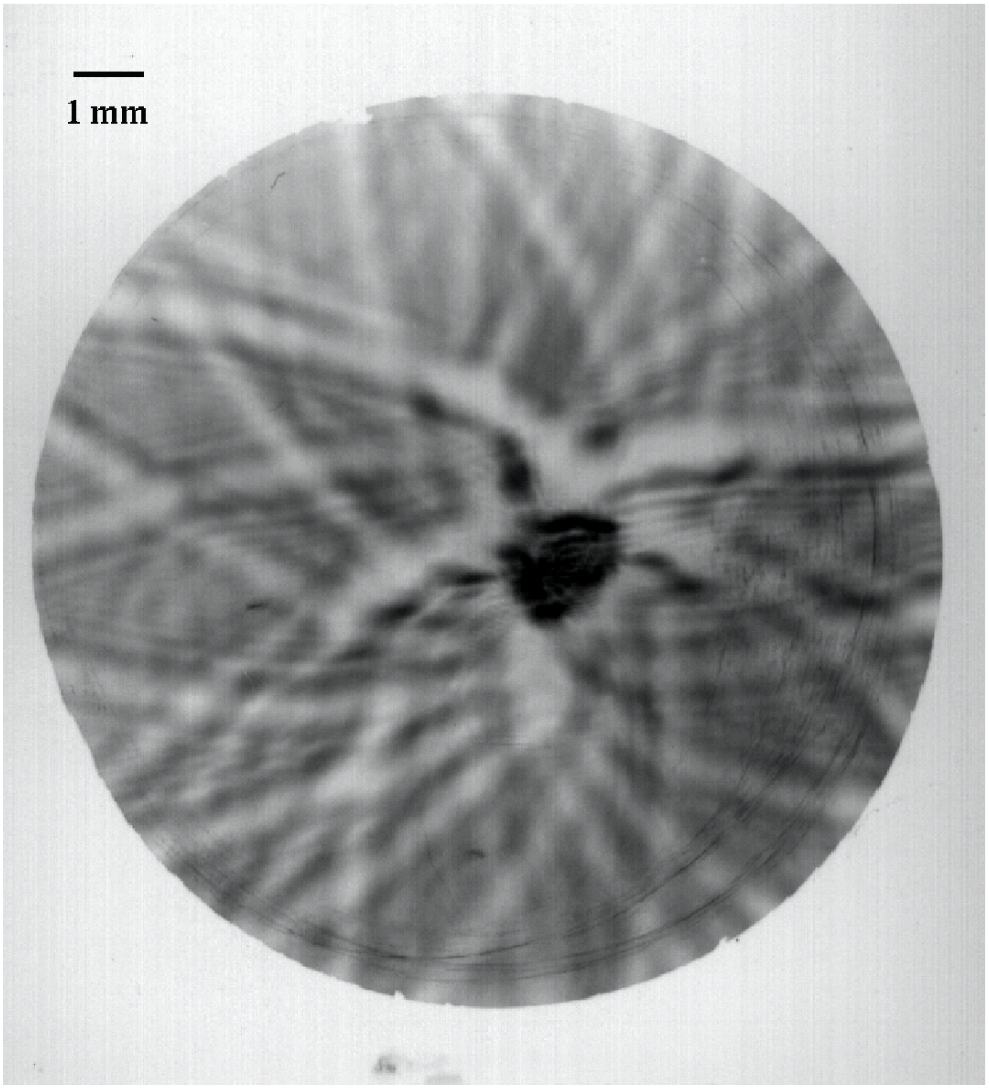

Figure 3.5.10.: Image of a strong and short focus.

big, but Airy rings can be seen around it. Airy rings or disks are descriptions of the best focused spot of light that a perfect lens with a circular aperture can make. The Airy pattern is the diffraction pattern formed at the focus of a beam passing through a circular aperture. It is characterised by a bright central disc and fainter concentric rings, and can be used to indicate that the best diffraction-limited focus of the beam has been found. All the images were taken with the same delay, but the actual diameter of the lens could not be measured in all cases and there was uncertainty that the lens was really always the same diameter. Therefore the results must be considered as a lower limit of the quality of the lens.

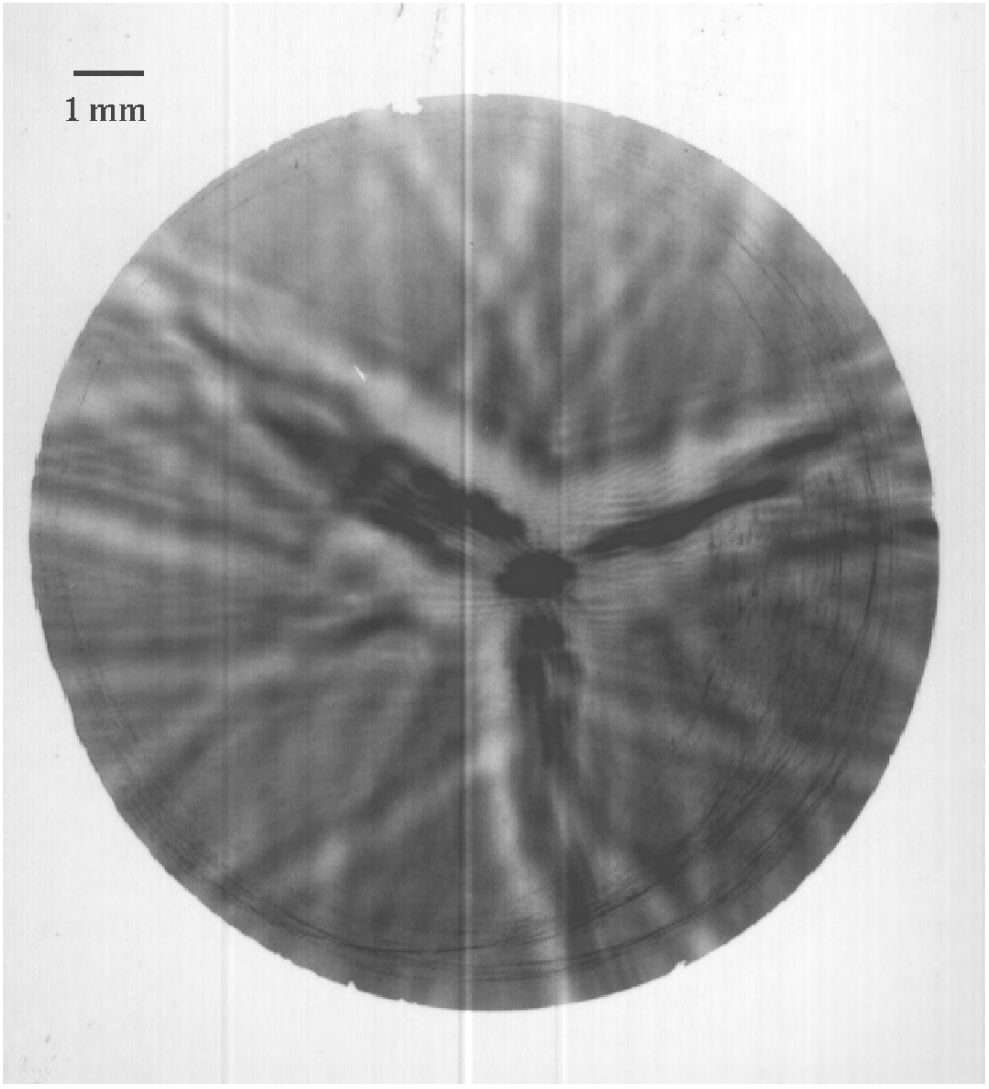

Figure 3.5.11.: A second example of a strong focus at a short focal length.

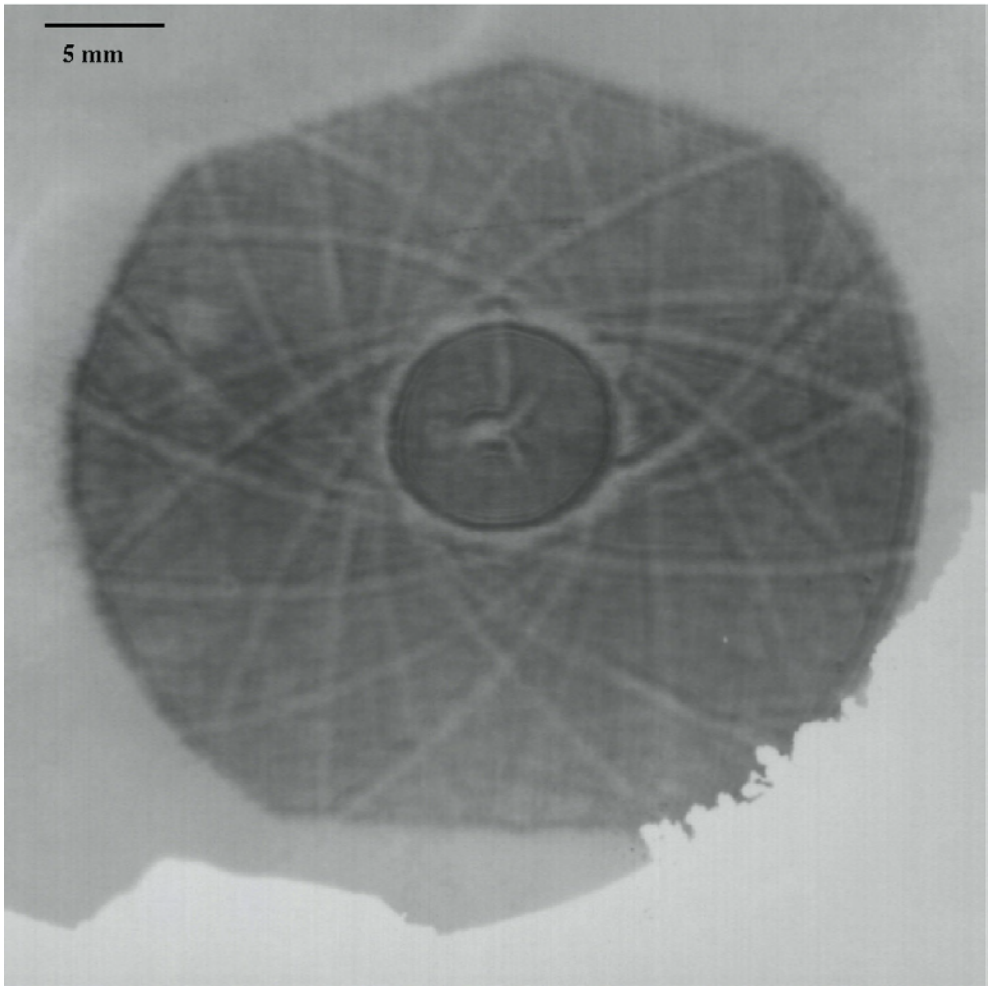

Figure 3.5.12.: Image of a lens obtained in the near field, 910 mm away from the device. The diameter of the lens is approximately 9.0 mm.

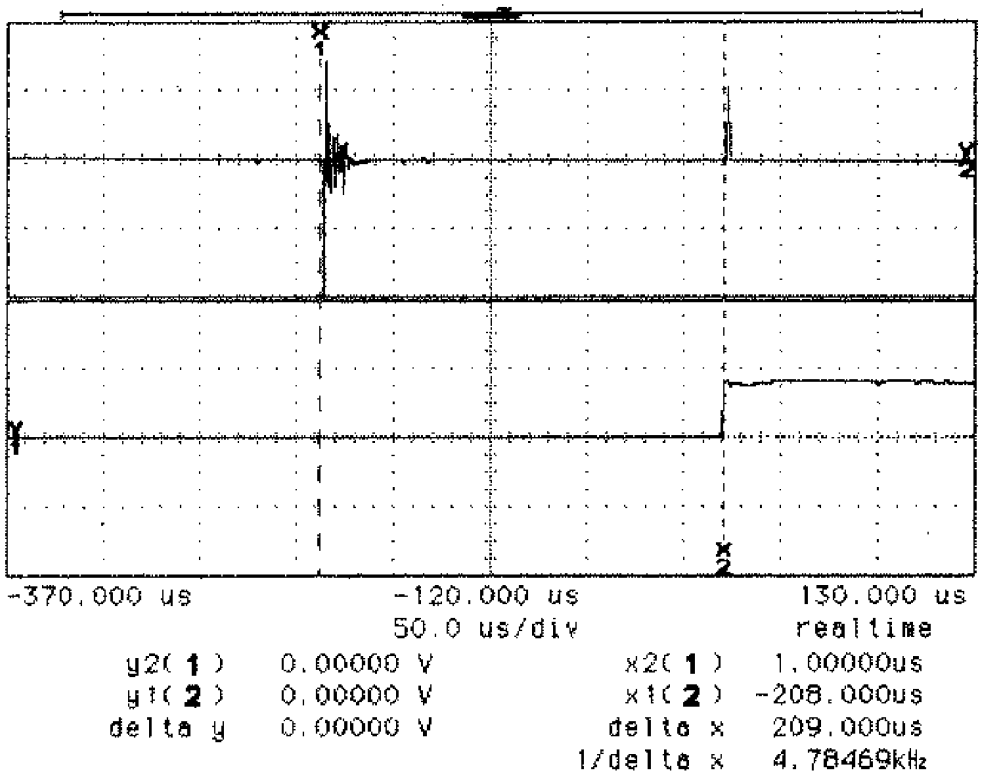

Figure 3.5.13.: The oscilloscope trace corresponding to Figure 3.5.12 on the previous page.

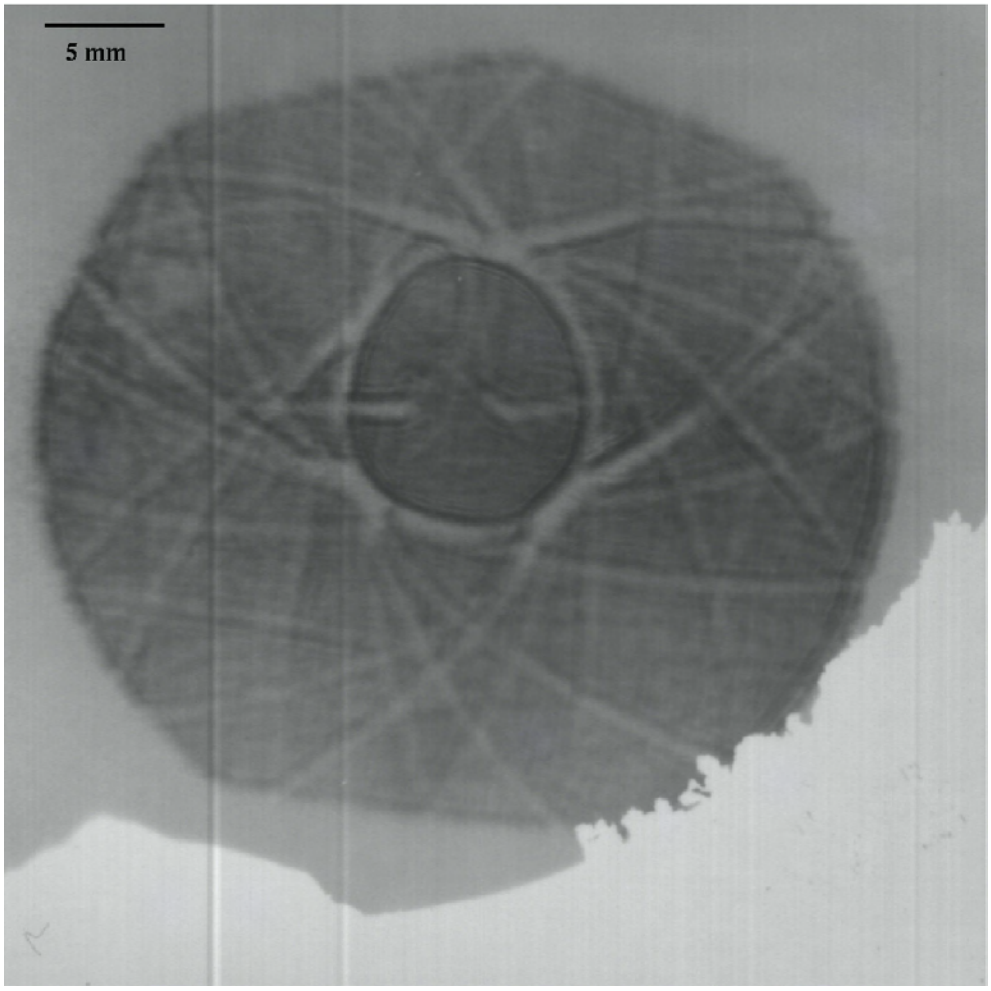

Figure 3.5.14.: A second example of the lens obtained in the near field, 910 mm away from the device. The diameter of the lens is approximately 10.3 mm.

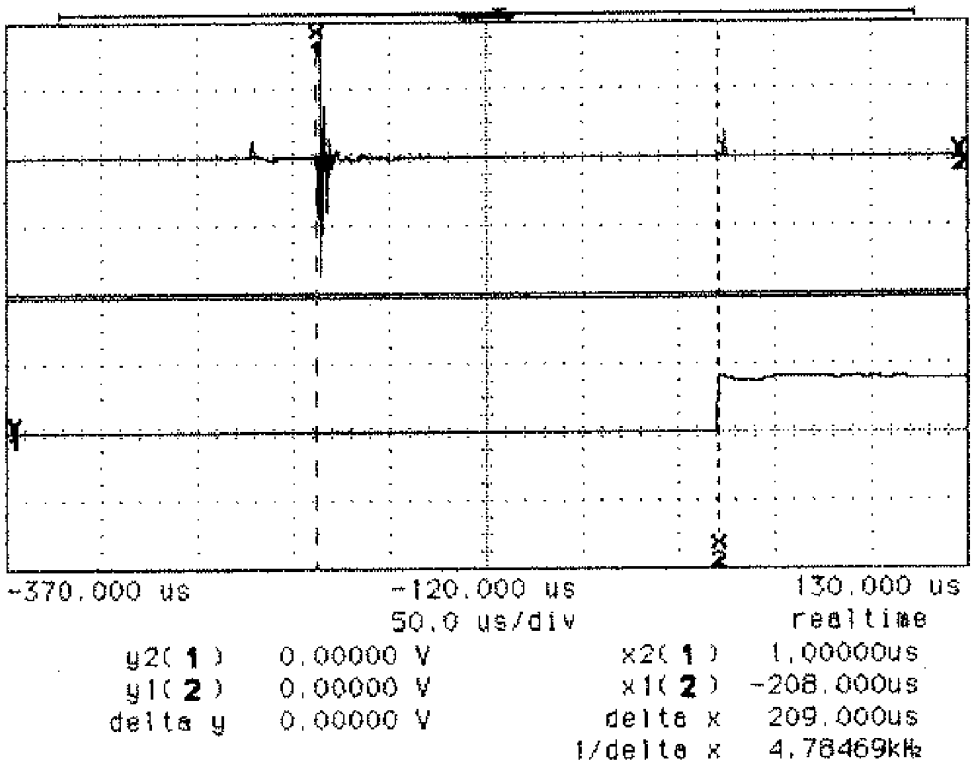

Figure 3.5.15.: The oscilloscope trace corresponding to Figure 3.5.14 on the previous page.

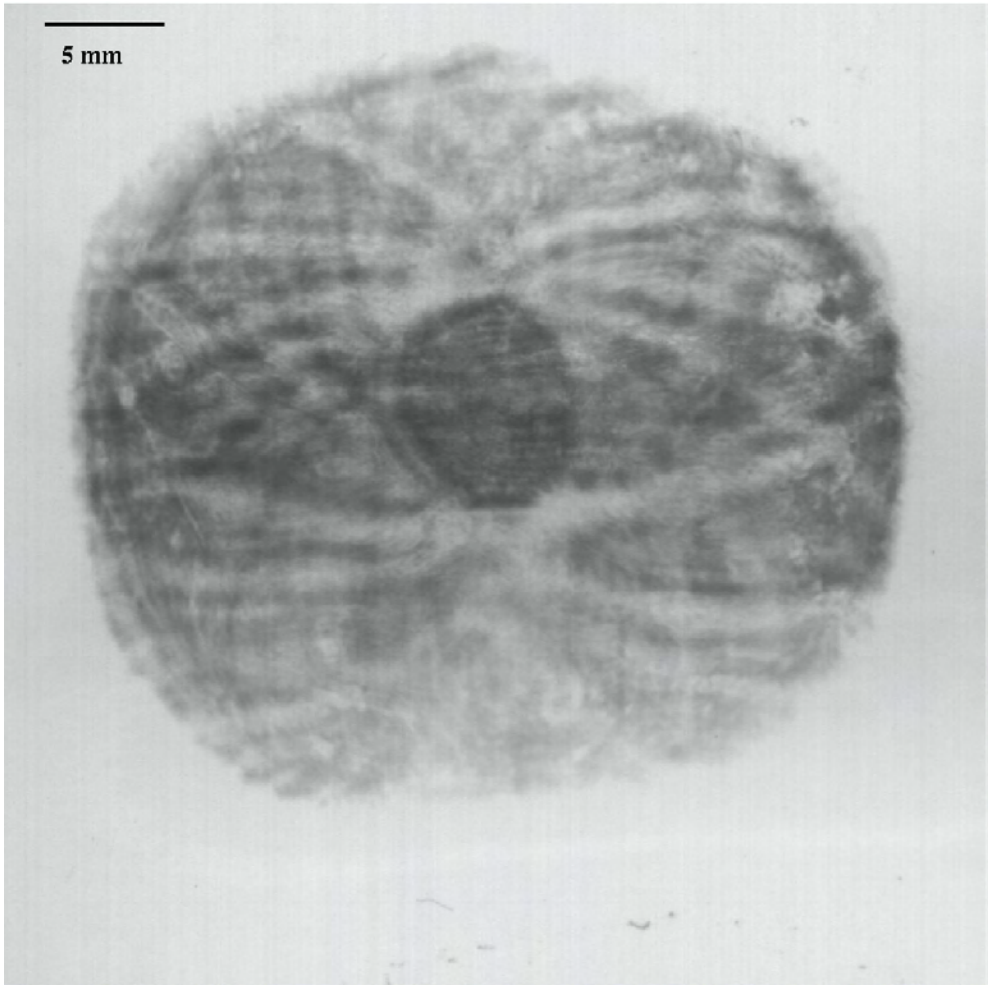

Figure 3.5.16.: Image of the converging beam of a 10 mm CSL at a distance of 3.3 m. The darker circle in the center indicates that the light is actually converging in focus.

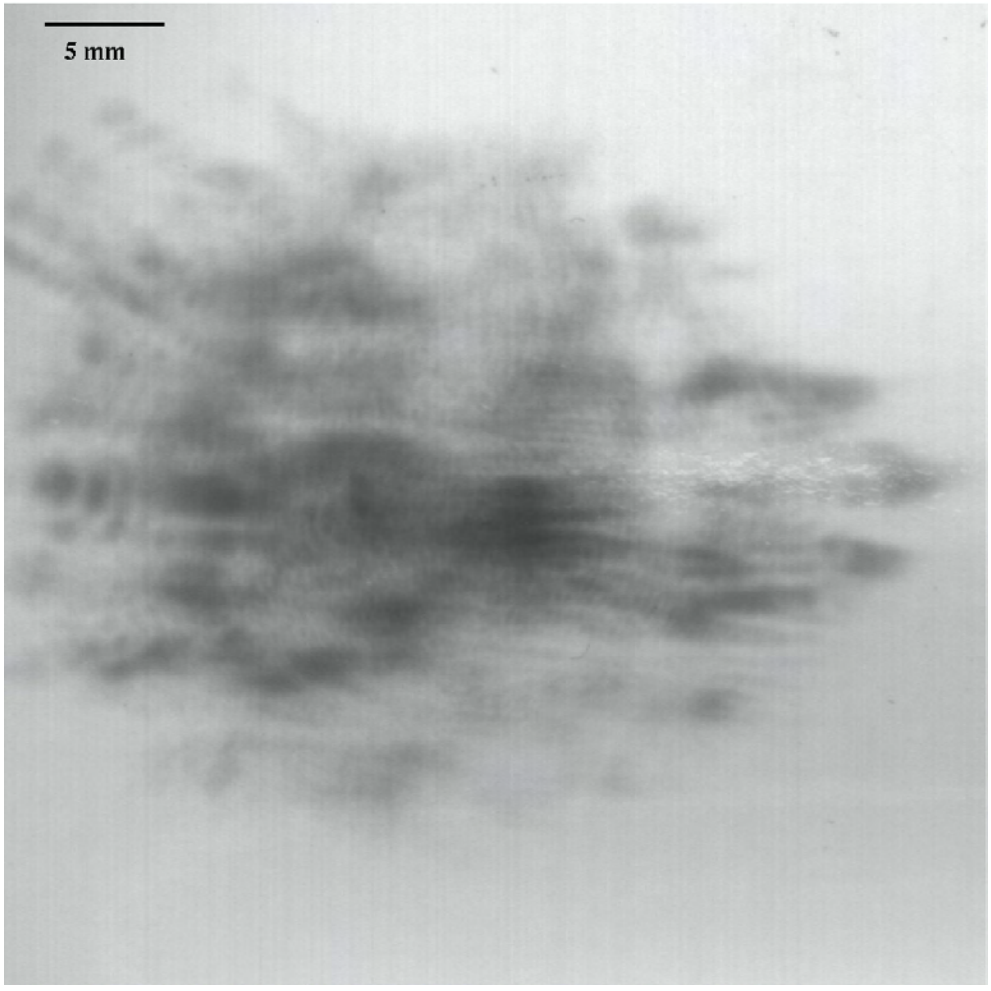

Figure 3.5.17.: An image of the focus obtained on the far field at more than 10 m from the lens. The size of the focus is about 2 mm, comparable with a diffraction limited beam.

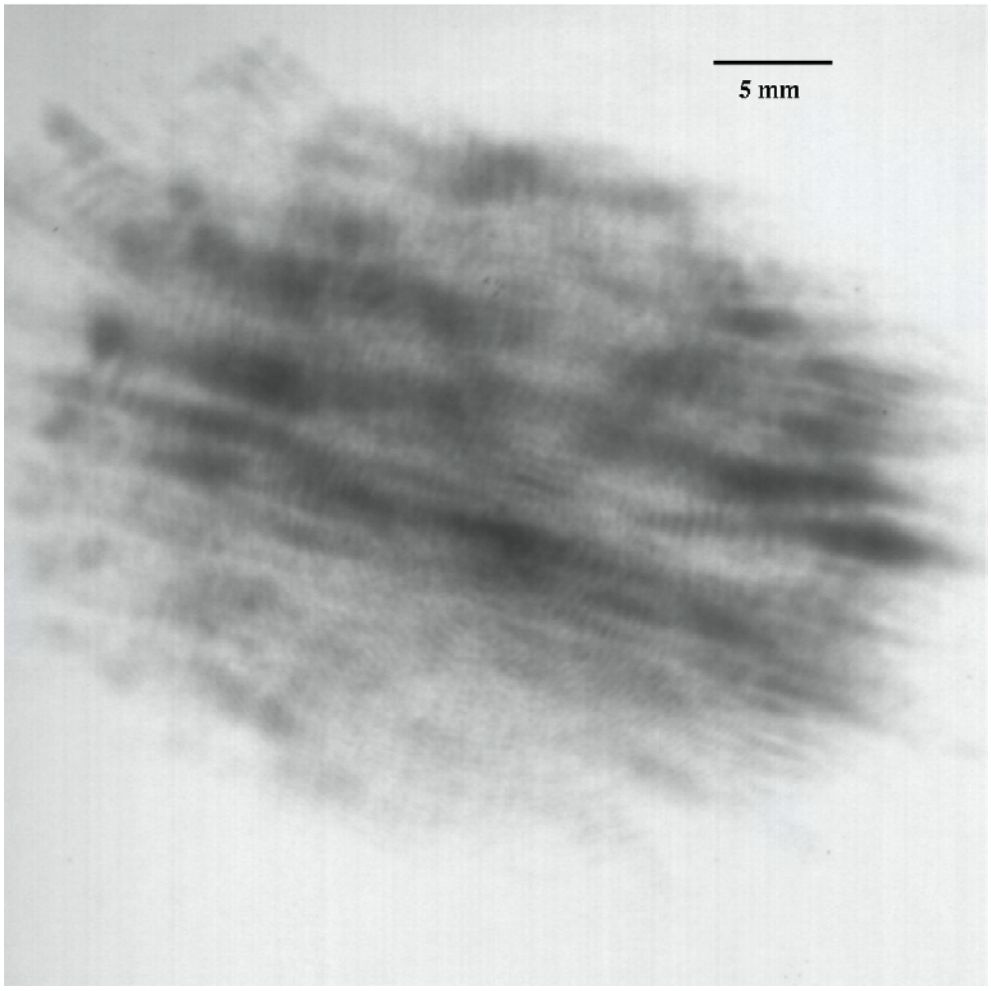

Figure 3.5.18.: Image of the focus obtained in the far field, approximately 15 m away from the lens. Part of the poor quality of the focus derives from the fact that our lab was not long enough and we had to use two mirrors to be able to take images at large distances from the lens.

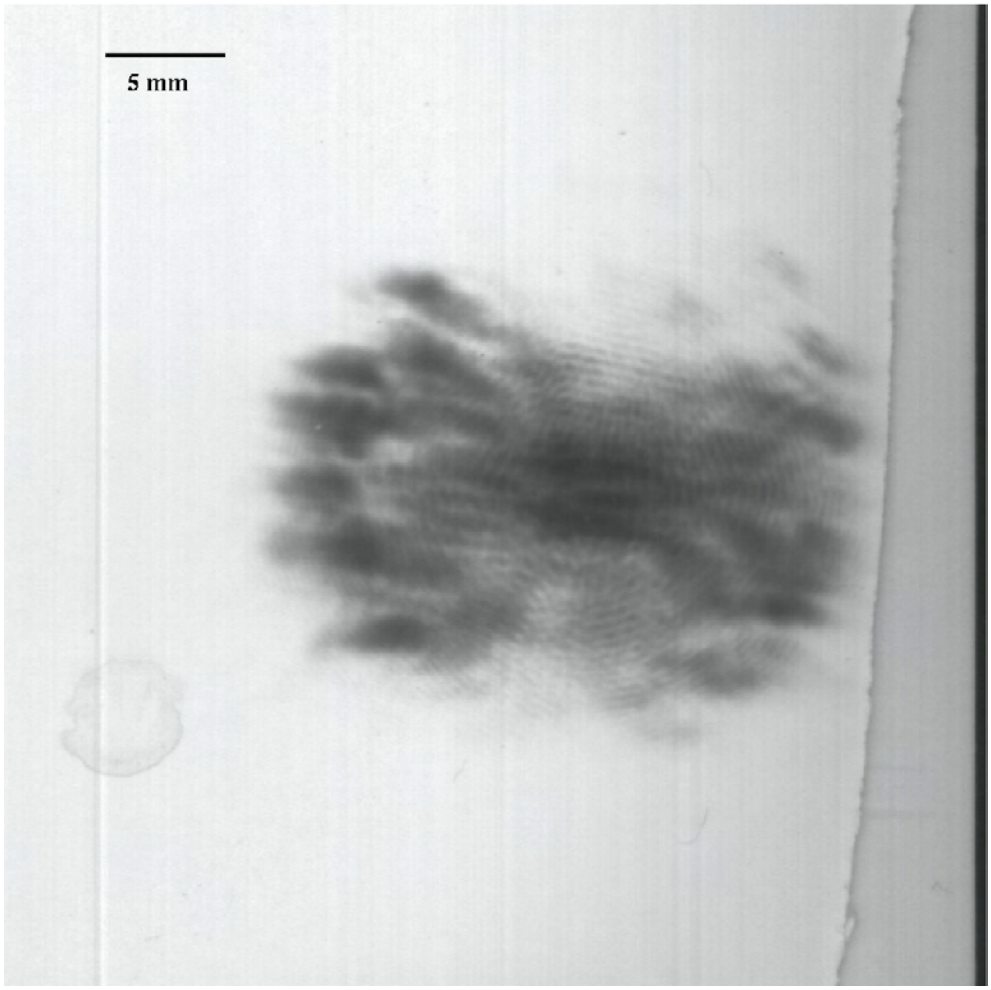

Figure 3.5.19.: Image of the focus for Figure 3.5.20.

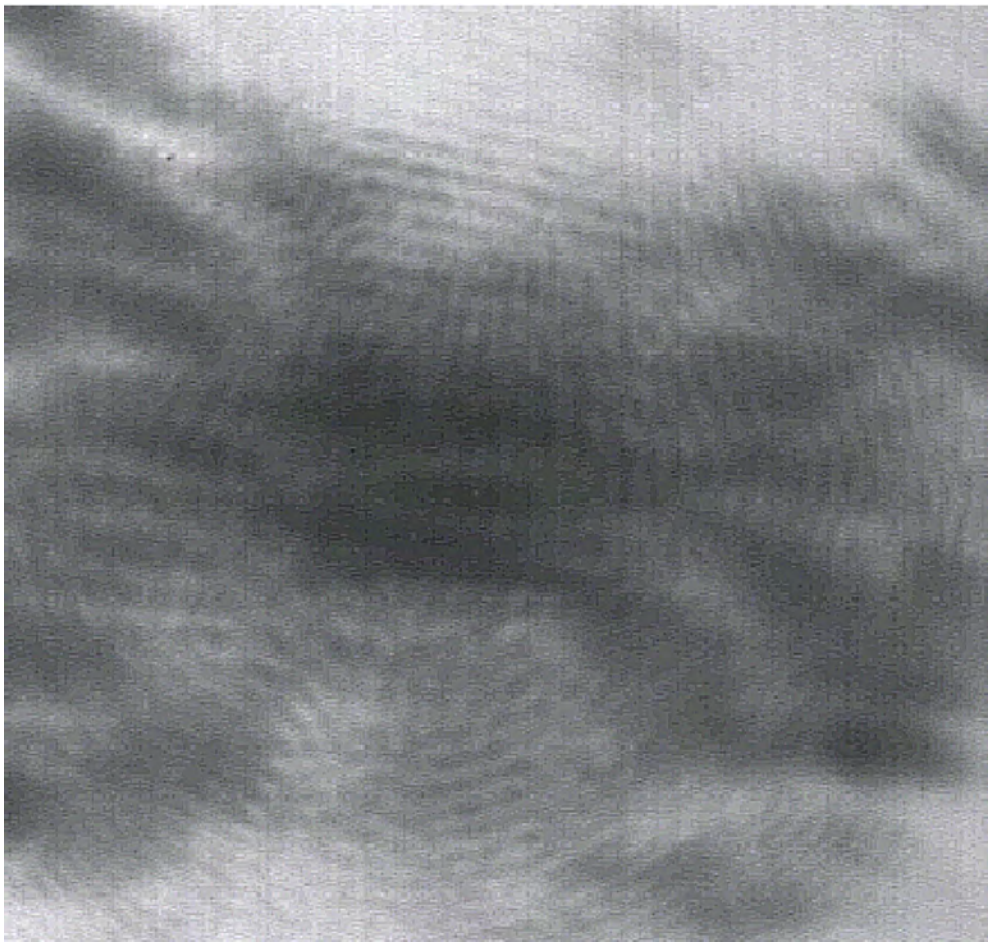

Figure 3.5.20.: Detail of the center of the focal spot of Figure 3.5.19, processed in order to make visible the Airy rings.

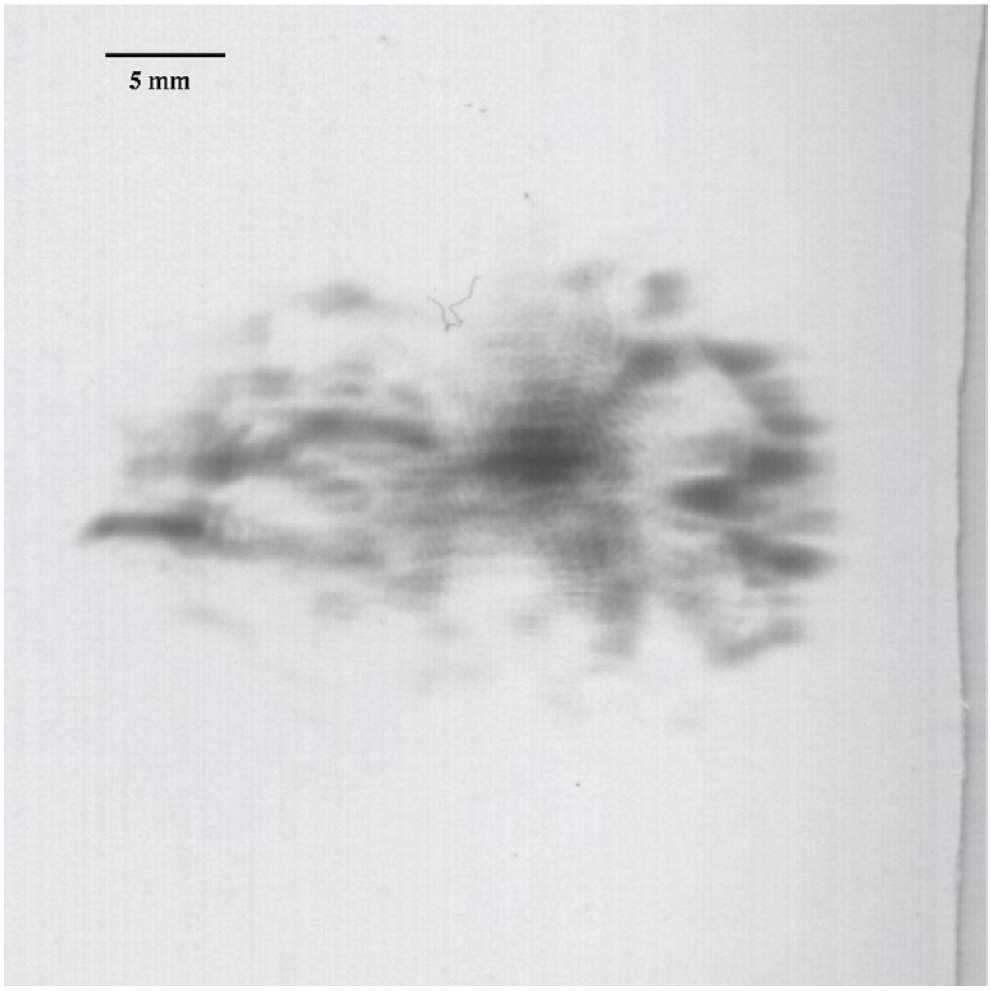

Figure 3.5.21.: Image of the focus at the same conditions as 3.5.19. Despite the fact that the delay and all the other parameters of the experiment were the same as in the previous one, the focus has a larger diameter.

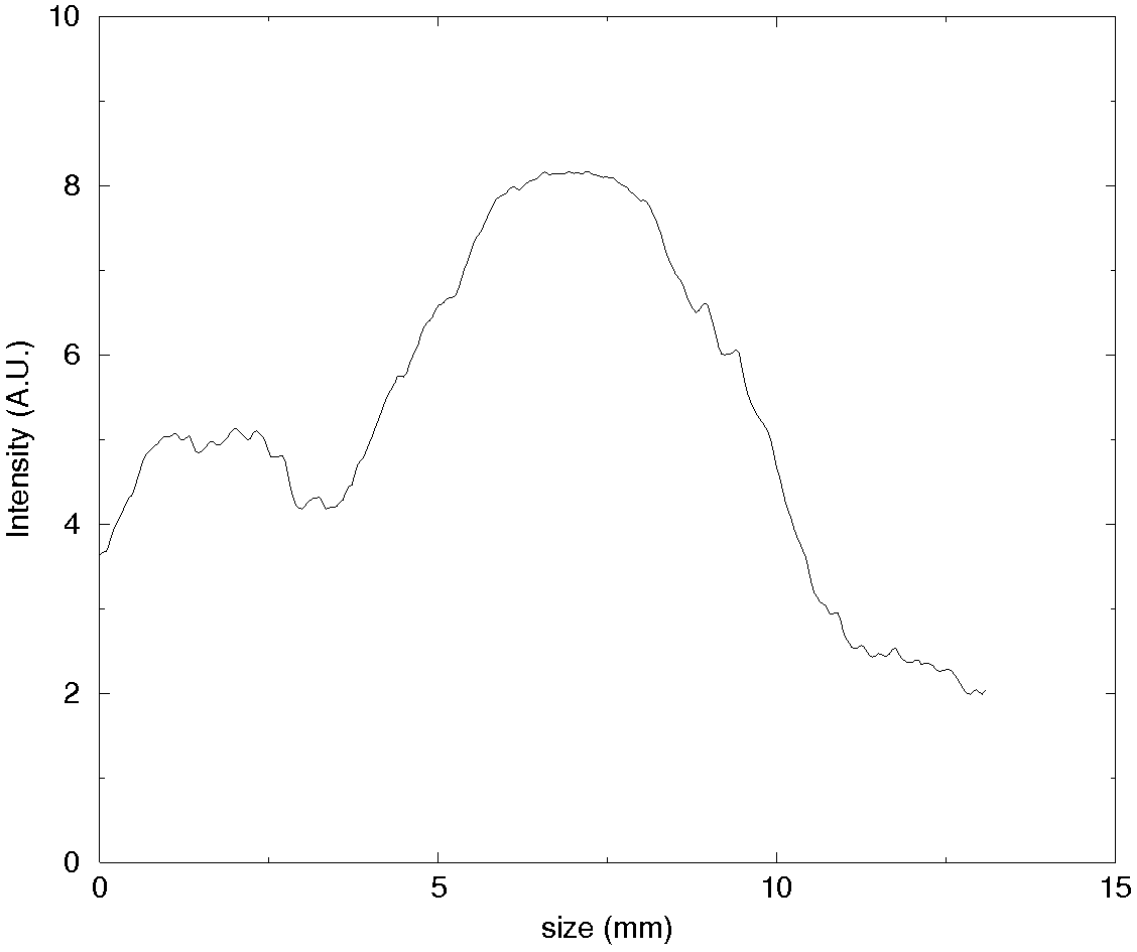

Figure 3.5.22.: Densitometry of image 3.5.21. The focus is larger than 5 mm.

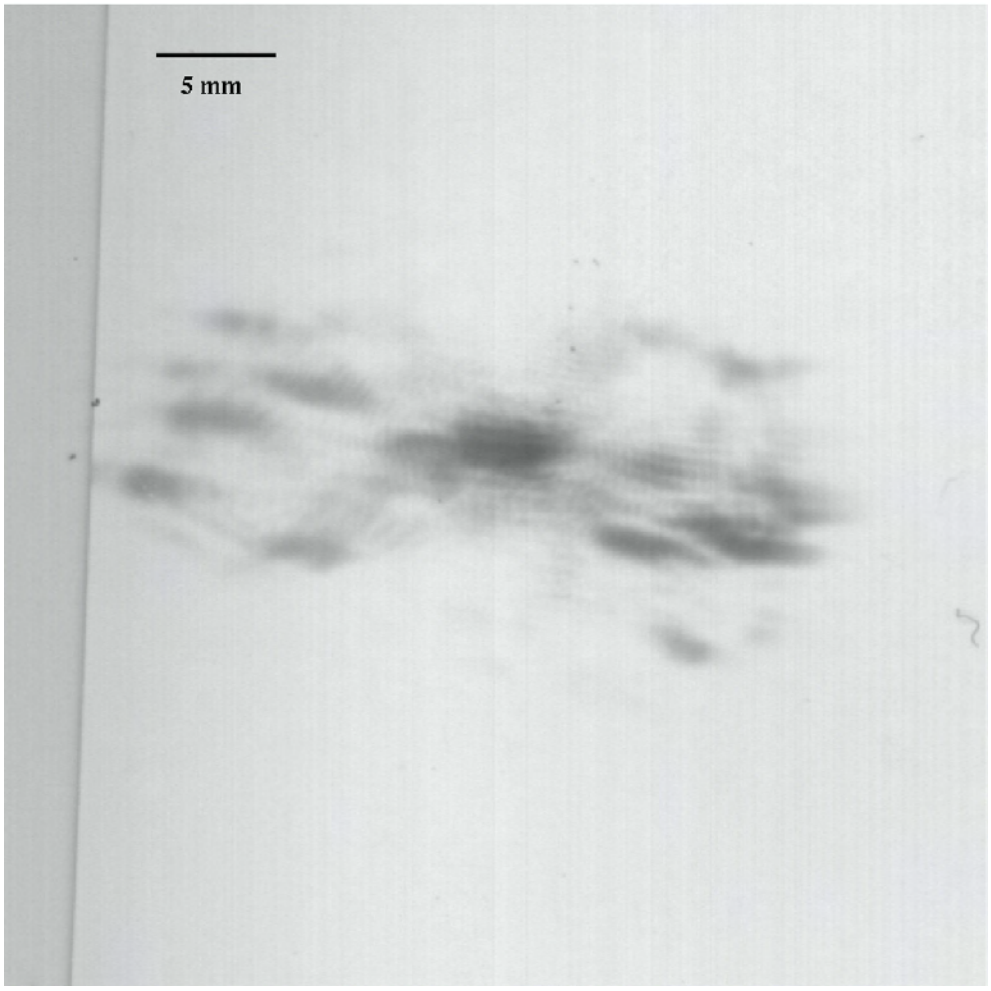

Figure 3.5.23.: Image of a good focus, obtained with the same conditions of the previous images.

4. Exploding Wire Experiments

Colliding shocks can be formed by "virtual capillaries" (VC) as first demonstrated by Kuppen [2]. Kuppen employed a series of spark gaps set out on the surface of a cylinder and in line (Figure 4.1.1). Unfortunately, because these were only four lines of spark gaps the shocks failed to demonstrate Mach addition. Kuppen did however utilize the device to obtain a "cylindrical lens".

In a subsequent experiment a set of exploding wires were utilized to generate the VC. Such VC could be of interest to laser acceleration schemes and for UV lasers in which the solid state capillaries erode after a small number of shots. The objective in this chapter is to compare the mechanisms of the cylindrical shocks generated by the VC to that of the spherical shocks generated by the spark gaps in Chapter 3. Because the VC experiment is based on cylindrical shocks it is amenable to numerical simulation in two dimensions, if end effects are neglected. This simplifies CFD considerably.

In the case of the VC experiment, a 1 μF capacitor was used and the voltage was in the range between 16 kV and 20 kV. This particular experiment is very sensitive to the energy stored in the capacitor. If the voltage is too low, the explosion is weak and almost no shock production is observed. If the voltage is too high, after the collision of the shocks there is turbulence and no pipe is observed.

4.1. Cylindrical Shocks

Two different systems can be used to produce the cylindrical shocks, depending on the needs of the experiment. If a high repetition rate is required or the experiment is performed in a closed environment, the best way is to use a row of small spark gaps connected in series as in Figure 4.1.1 on the next page.

Figure 4.1.1.: Cylindrical shock generator by a series of spark gaps in series from Kuppen [2]

Due to Mach addition, the individual shocks would then merge into a cylindrical

one.

A cylindrical shock can be obtained in a second way: by discharging a big capacitor through a very thin wire it is possible to explode the wire producing a high quality cylindrical shock. The time needed to replace the wire makes this system unsuitable for experiments which must be operated in repetition mode. In this case, the thickness of the wire is the most critical factor for the quality of the shock. A thin wire has a higher resistance and drains the energy from the capacitor quicker. When the wire is thinner there would be less material, hence less debris, and the amount of energy to explode it is smaller. The risk of significant amounts of debris would be that the beam might interact with it and the debris might also be deposited on undesirable places in the apparatus.

The use of a triggerable spark gap, or a Thyratron, to discharge the energy stored in a big capacitor through the wire fast would produce a good cylindrical shock. This circuit is simpler than in the case of the CSL (Figure 3.3.3 on page 30), as it does not require any coil as in Figure 4.1.2. The wire, not the spark, carries the current. The electromagnetic noise is greatly reduced by the removal of the coil.

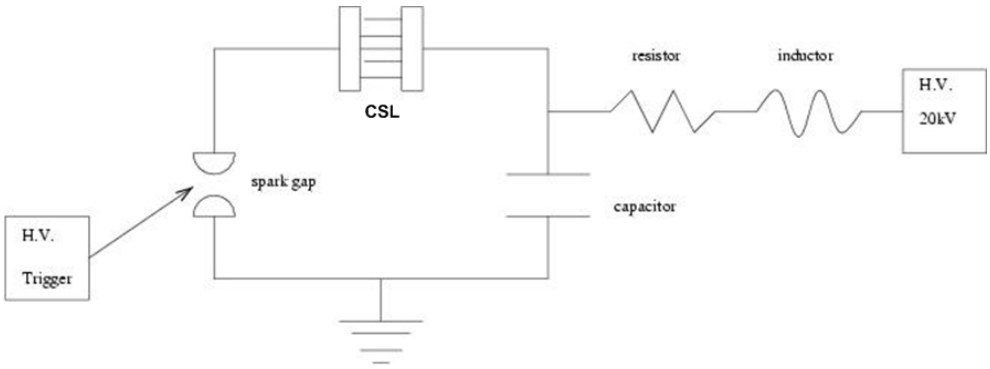

Figure 4.1.2.: The High Voltage circuit of the experiment.

One critical factor for this experiment is the resistance of the wire. If the resistance is too small, the plasma forms very quickly, and the capacitor is partly discharged. In this case, once the plasma has formed the resistance drops to almost zero and the circuit oscillates, radiating away a significant fraction of the energy. The optimal resistance is that which allows the circuit to dissipate most of the energy. The energy

is dissipated into the wire during the first cycle of the oscillation. The resistance of the wire depends on the material and on the thickness. If the wire is very thin, the resistance can be too high and but the amount of debris is reduced.

The wire used in the experiment has a thickness of 130 μm as shown on Figure 4.1.3 which was obtained using a scanning electron microscope (SEM). For the eight shock experiment described in Section 4.2 on page 65, the wire was 50 cm long, with a total resistance of 8 Ω.

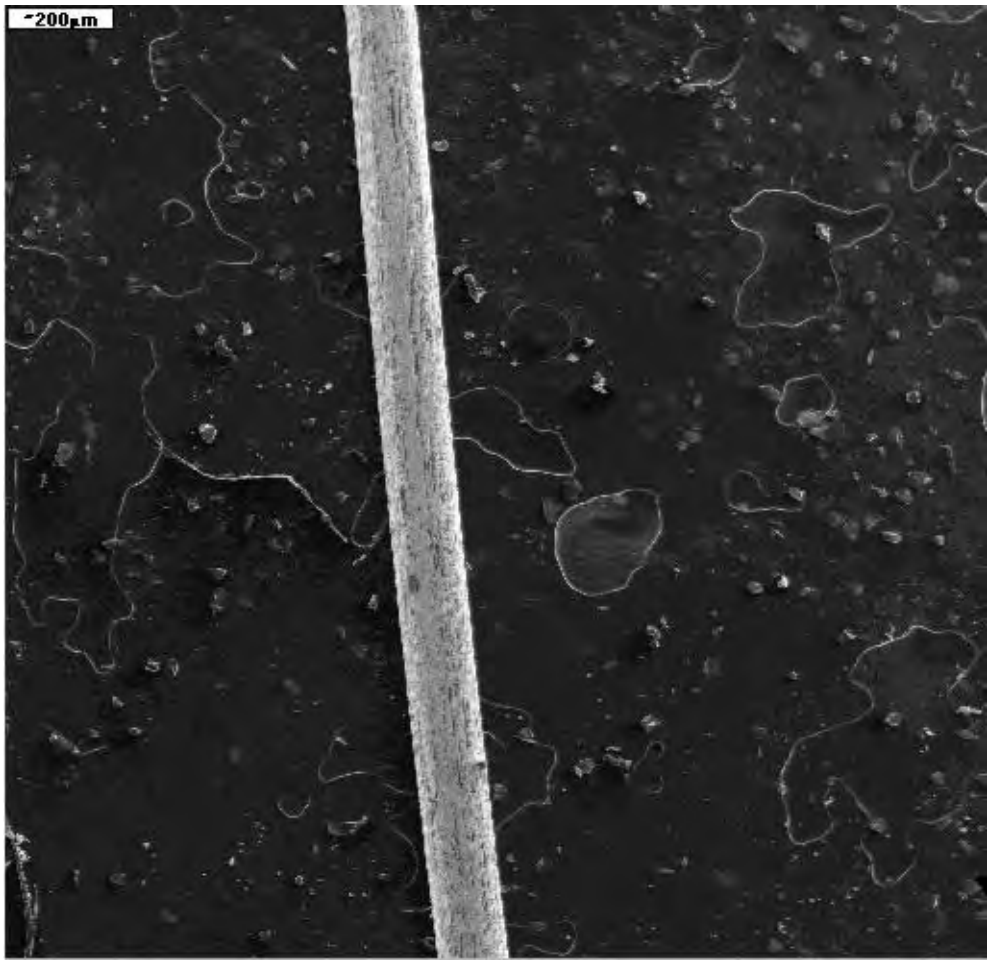

Figure 4.1.3.: A SEM image of a piece of the wire used during the experiment. The wire has a thickness of approximately 130 μm. In order to be sure that the thickness of the wire was uniform, several images of different pieces of wire were taken.

For the diagnostics of the shock waves a nitrogen laser was used. The laser beam is directed through the pipe and produces shadow-grams of the shock waves. The

refractive index of the shocks is so high that they refract the light out of the collecting optics, so no light reaches the film.

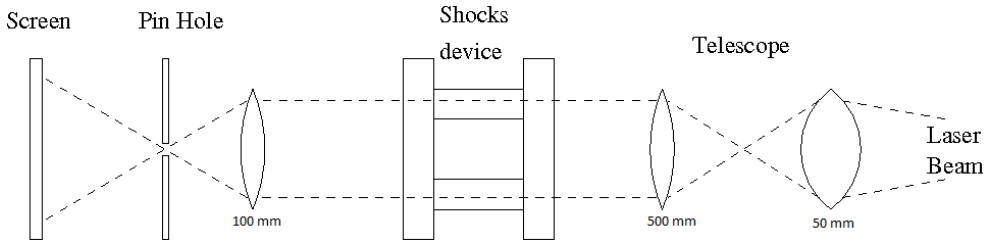

Figure 4.1.4.: The diagnostic setup for the pipe experiment.

The set-up of the experiment is shown in Figure 4.1.4. From the right, the two lenses used for the telescope have a focal length of 50 mm and 500 mm. The lens used for the "spatial filter" has a focal length of 100 mm. The small telescope on the right is necessary to compensate for the divergence of the laser beam. In this experiment, unlike the CSL, the beam has to be parallel and aligned with the pipe. The "spatial filter" on the left was used to eliminate the light of the breakdown, which was very bright. In addition to that, when the photographic paper was very close to the device, a UV filter was used to let through only the light of the laser. The single lens detector also offers the possibility of changing the magnification of the image only by moving the detector, i.e., the photographic paper. The magnification itself was measured by imaging an object of known size as shown in Figure 3.4.3 on page 36.

The first unsuccessful attempt to create a pipe-shaped lens was made by exploding a coil of wire. Unfortunately, the wire is so thin that it needs to be supported. A cylinder of very thin paper, on which the wire was wound, was used. It was hoped that the paper would be blown away by the explosion without affecting the shock waves. However the first experiments showed only one very strong shock propagating, Figure 4.1.5 on the next page. This indicated that the discharge jumped across the coils, instead of flowing through the whole wire, probably helped by a skin effect due to the paper. The shock is traveling toward the top of the picture. The turbulence at the downstream side of the shock is a clear sign that the energy

is too high. The white circle is the cylinder of paper used to hold the wire, and was usually blown away by the explosion.

Figure 4.1.5.: The single strong shock coming from the coil, probably due to the jumping of the arc across the coils.

The second attempt was made using six short pieces of wire connected in parallel. The wires were held between two metal discs, to which the high voltage was applied. With this approach, all the wires exploded, but not simultaneously. In this case, the formation of the pipe does not take place because the shock waves arrive at different times. This system would be improved if the wires are strictly identical in length

and thickness. In this case, there were no means to tighten the wires, which had therefore slightly different lengths and even small kinks.

The third approach provided reasonable results. The separate wires were replaced by one long piece, wound up and down between two insulating holders. In this case, the explosion occurred everywhere at the same time. With this technique some good quality pipes as long as 2.5 cm were obtained. In principle, given enough energy, there is no limit to the length of the pipe. The main problem, in this case, was that the particular holder was not built with enough precision, leading to some differences in the arrival time of the shocks.

4.2. Different Foci

Two wires were used in the first experiment, in order to check that the shocks were really arriving in the center at the same time, in as far as it was allowed by the precision of the holder. The experiment was very successful and led to the production of a lenticular light guide, which focused the light in the center, producing a line focus as shown on Figure 4.2.1 on page 69. According to Courant and Friedrichs [32] this could be as a result of a regular reflection.

However, two shocks are not enough to produce a proper pipe. Moreover, in this case a number of secondary shocks was observed, sometimes strong enough to produce additional foci. Considering that the wire is short and had a very small resistance, the secondary shock came probably from the oscillations of the capacitor into the plasma. The low resistance of the wire does not in fact allow the energy to be dumped into just one cycle, as could be seen in the oscilloscope traces as shown on Figure 4.2.2 on page 70.

In the following experiment, the same technique was used as with the single wire case, but this time producing four shocks instead of two. Even in this case the experiment was successful and led to the formation of a channel, but with a square

shape. This happens because the angle at which the shock waves collide is too wide to allow sufficient constructive interference or Mach addition to take place. In some cases, the square pipe worked as a very strong gas lens, producing a bright spot. The pictures of the square pipe are shown in Figure 4.2.3 on page 71. Unfortunately, the photographic paper is not a good detector. The paper saturates quite quickly and does not show contrast between different areas of the picture. While developing the pictures in the dark room is it possible to see a dark spot (the images are negative) forming in the center much earlier than the rest of the picture. Attempts were made to stop the development at an early stage, but without any good results. For this experiment the delays were unknown. It is suggested that the experiment should be repeated to ascertain the delay times.

The square pipe is not yet useful, but it is an interesting proof of the versatility of gas structures produced in this way. Given the right geometry of the experiment, many different shapes may be produced.

For instance a curved VC could be used for the "optical cyclotron" described in Michaelis [21]. Such a solid state optical cyclotron would suffer from the same problems as linear laser accelerators.

4.3. The successful VC Pipe

A more approximate circular cross section VC was eventually obtained using eight wires, in the usual configuration of one wire wound across the holder. The first results of this experiment are shown in the Figures 4.3.1a and 4.3.1b on page 72.

Experiments were conducted with different voltages ranging from 16 to 23 kV. With the lowest voltage, the explosion is very weak and there is no shock formation. With some experience, the quality of the shocks can be judged by the noise in the lab. With the lowest voltage, almost no noise can be heard. With the highest voltage, a good channel can be observed before collision, but after collision only

strong turbulence is observed. Even if the quality of the pipe is good the final lens pipe is disrupted by turbulence.

The images in Figure 4.3.1 were obtained with a capacitor of 1 μF charged to a voltage of 23 kV, which corresponds to an energy of 260 J (see graph 4.3.2 on page 73 for the 1 μF capacitor). The images taken after the collision of the shocks show only turbulence. As shown in Figure 4.3.2 on page 73, the spark gap can only be operated at limited voltages and that the 4 μF and 8 μF are rated only up to 20 kV, it is clear that there are some energies at which it is impossible to operate.

The energy was therefore too high. Nevertheless, before collision a channel as small as 500 μm could be obtained as shown in Figure 4.3.1b on page 72. The final channel was even smaller, but the holder moved every time a new wire was inserted and this prevented a good alignment of the laser.

The wire holder, as shown in Figure 4.3.3, allows us to use three different distances from the wire to the center of the holder, respectively 10, 20 and 30 mm. The experiment showed that the larger distance is unusable, because the shocks become too broad and too weak, before they reach the center, and the pipe has a poor quality, i.e., a small gradient of the density is observed. The air does not become dense enough to alter the refractive index sufficiently to form a lens. The smaller diameter is unusable as well, because the ends of the wire are too close to each other and there is an arc between them, instead of exploding the wire. In subsequent experiments, the distance between the wire and the center was fixed at 20 mm.

It was observed that after different breakdowns the final voltage across the capacitor after the explosion was different, and in two different ranges. Fast shots were isolated, in which the final voltage was lower than 300 V, and so more energy was sent through the wire, producing faster shocks. In the case of the slow shots the final voltage across the capacitor was approximately 1 kV.

A result of a breakdown of the VC in the experiment is shown in Figure 4.3.4. In this case, the voltage was decreased to 19 kV, and therefore the energy to 180 J.

This voltage reduction allowed the turbulence to be reduced as well. For the first time a channel after the collision was observed, with an acceptable density profile.

In Figure 4.3.5 the circle is not perfect, probably because of small errors in the position of the wire. It can be observed that there is no turbulence behind the shocks. On the left the effect of Mach reflection can be noted as a flattening of the shock. This could be explained by Mach reflection as described by Courant and Friedrichs [32].

As described in Chapter 1 and in Appendix A, two types of shock wave reflections are encountered. At low shock interaction angles, regular reflection, identified with Buccellato's weak shock collision, is expected. When the angle between the shocks is larger, the formation of a Mach stem is expected. It is possible that this phenomenon is visible in Figure 4.3.5. Further work on this aspect is recommended.

The circular nature of the pipe is improved in Figure 4.3.6. Figure 4.3.7 shows small distortions that are smoothed by Mach addition after collision. The images after collision tend to show more regular shapes.

Figure 4.3.8 shows a breakdown at a higher speed. The variation in shock speed is attributed to variations in the energy delivered by the capacitor, and therefore in the speed of the shocks.

Figure 4.3.9 on page 80 to 4.3.16 on page 90 all have been taken with the energy in the capacitor being 180 J.

Figure 4.3.10 on page 81 was taken with a time delay of 57.0 μs with an enrgy of 180J

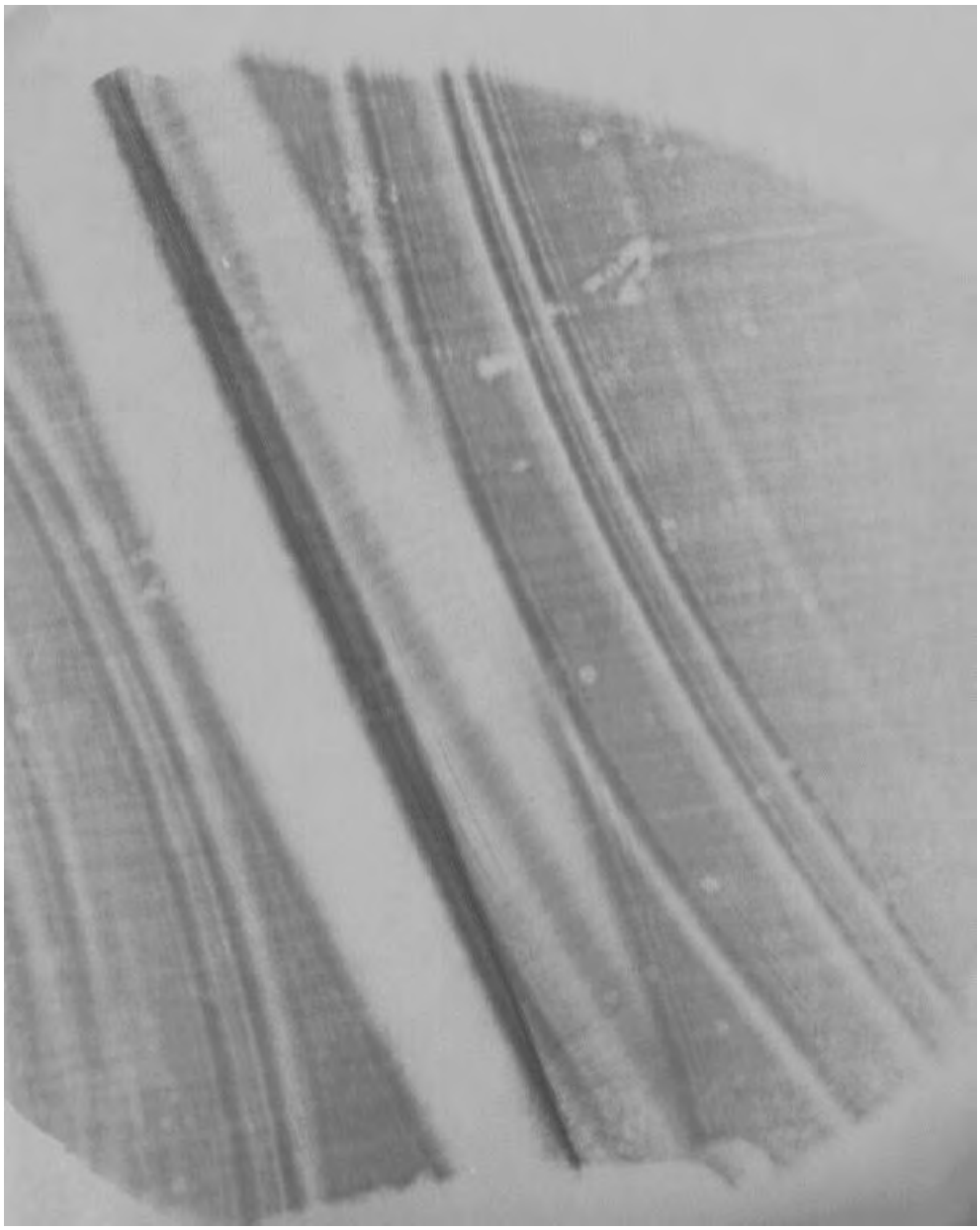

Figure 4.2.1.: The line focus with two shocks. The shocks have already collided in the center. Several secondary shocks are visible.

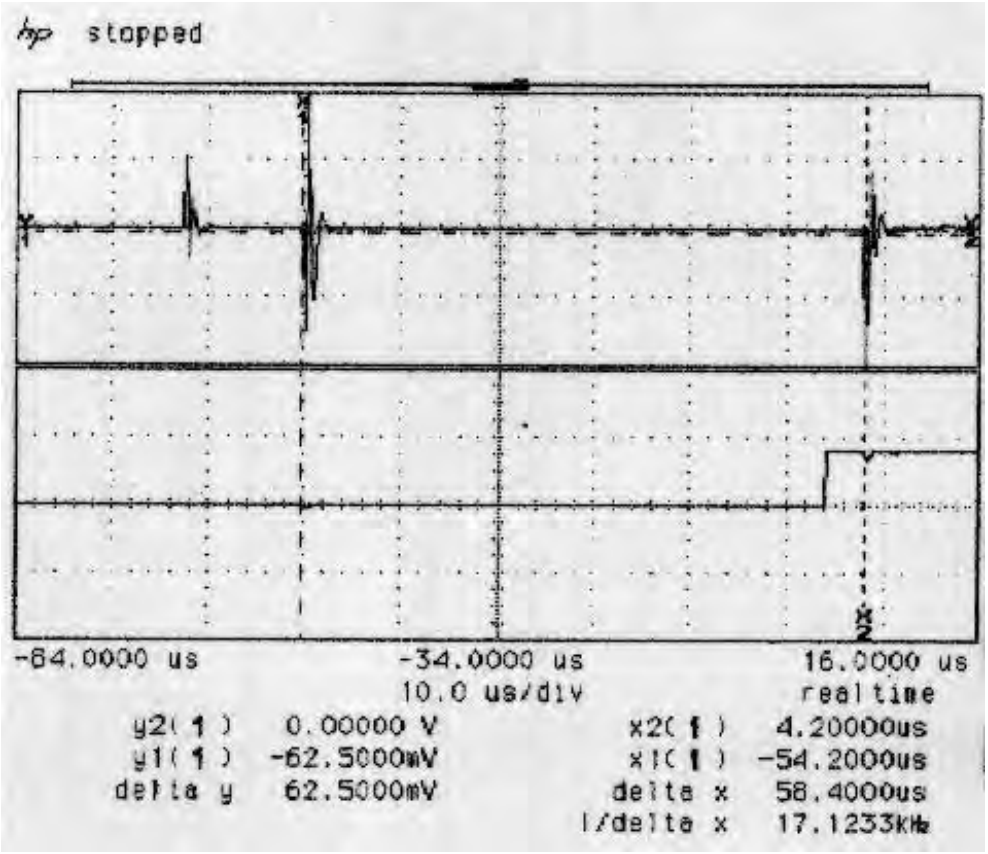

Figure 4.2.2.: An oscilloscope trace of one of the pipe experiments. The actual explosion is the second peak from the left in the top trace.

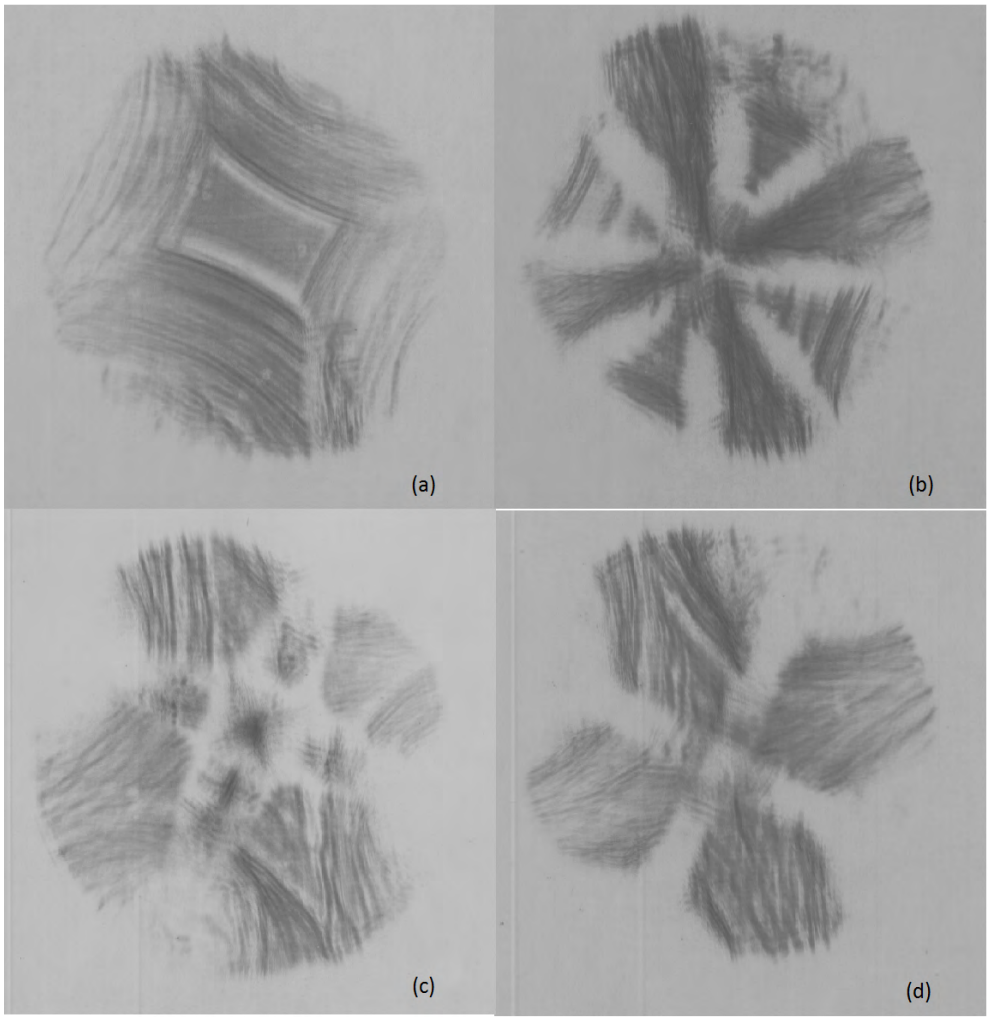

Figure 4.2.3.: Four pictures of the square pipe. From the top left, going clockwise: (a) the four shocks coming to the center; the shortest side of this square pipe is about 5 mm long (b) the moment of the collision; the pipe is not visible, as the shocks collide in the center at the same time (c) the moment immediately after the collision, and (d) the instant square pipe is focusing the light; the light is refracted to the centre of the image, which appears darker. Between the first and the last image, the delay is approximately 6 μs.

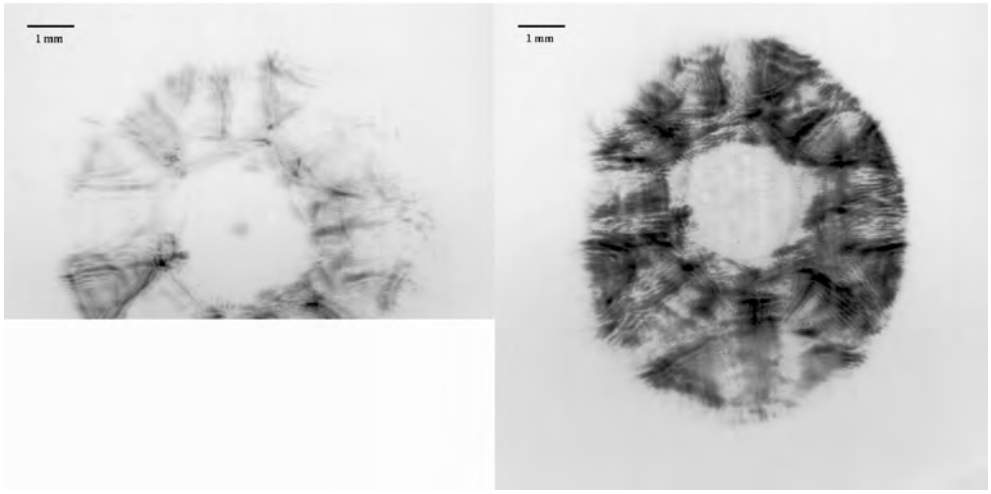

(a)

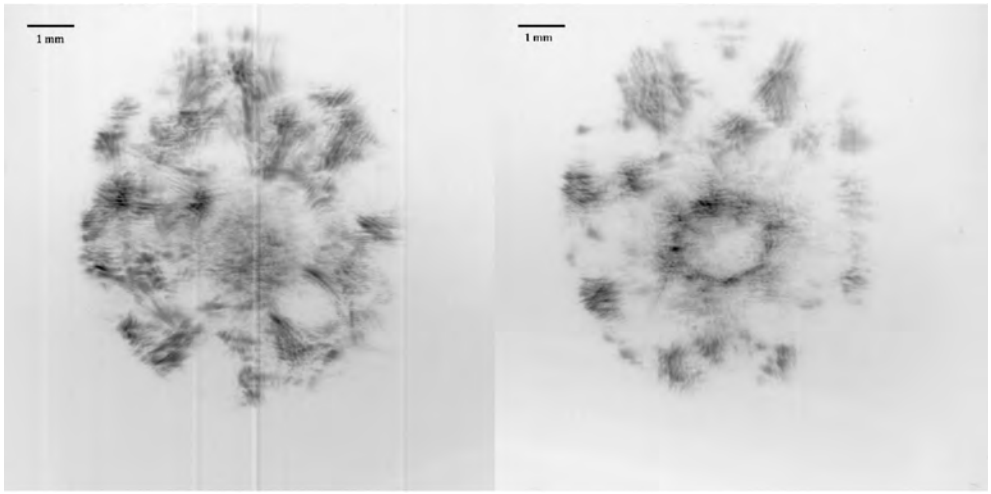

(b)

Figure 4.3.1.: Experiments performed with higher energy than required. The image on the left of (a) was taken just before collision, whilst the other three were taken during or after. It is clear that there is no channel formation after collision, because of the turbulence. The delay between the first and the last image is approximately 5 μs.

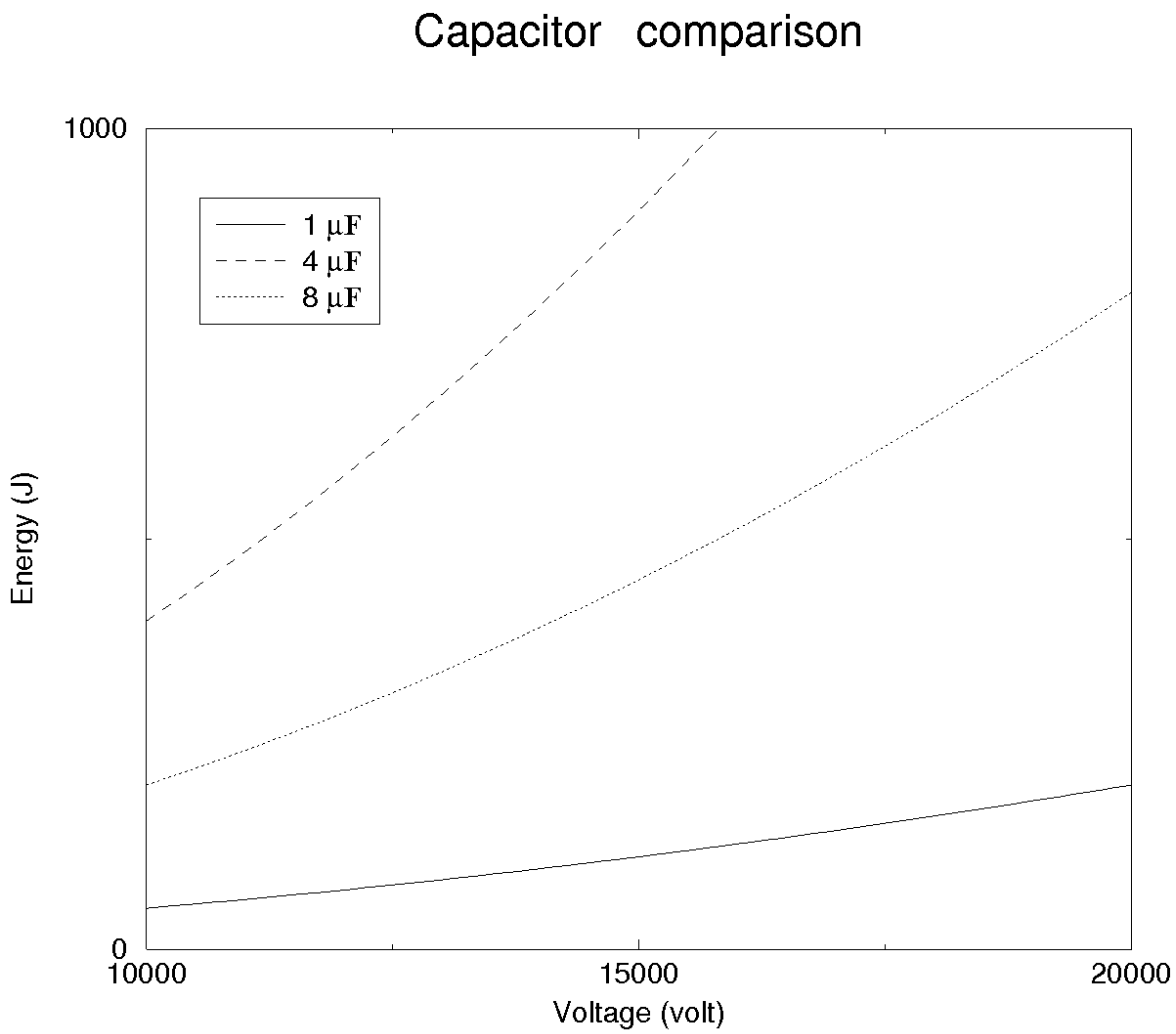

Figure 4.3.2.: This graph shows the energy vs the voltage for the three capacitors used.

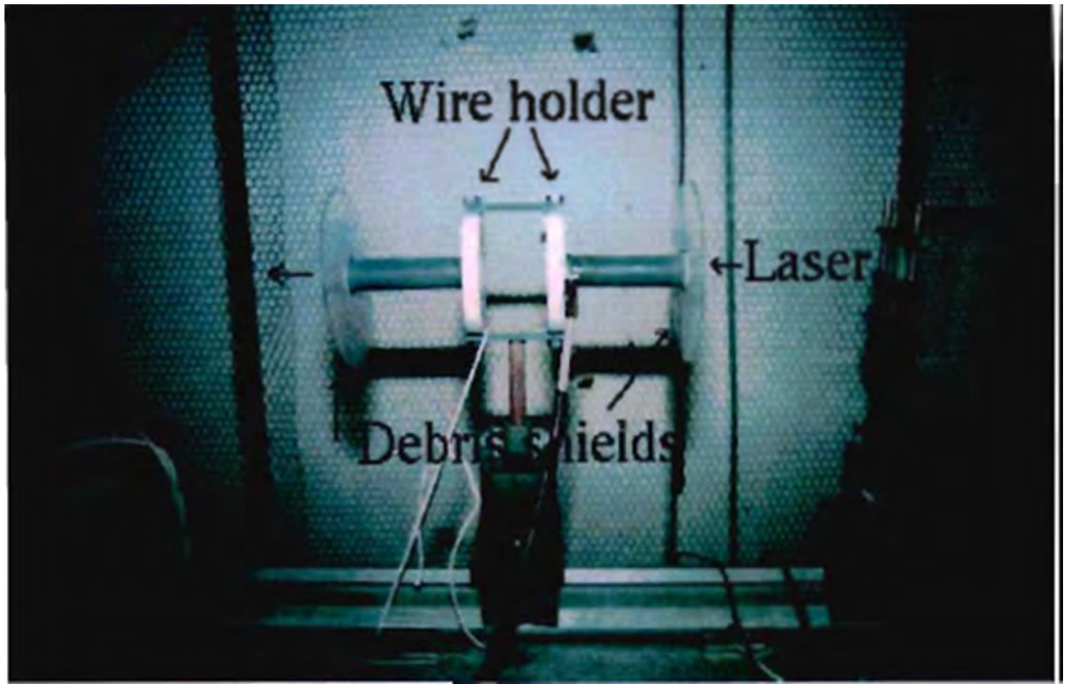

Figure 4.3.3.: The wire holder used for the experiment. The debris shield is used to protect the optics from the debris.

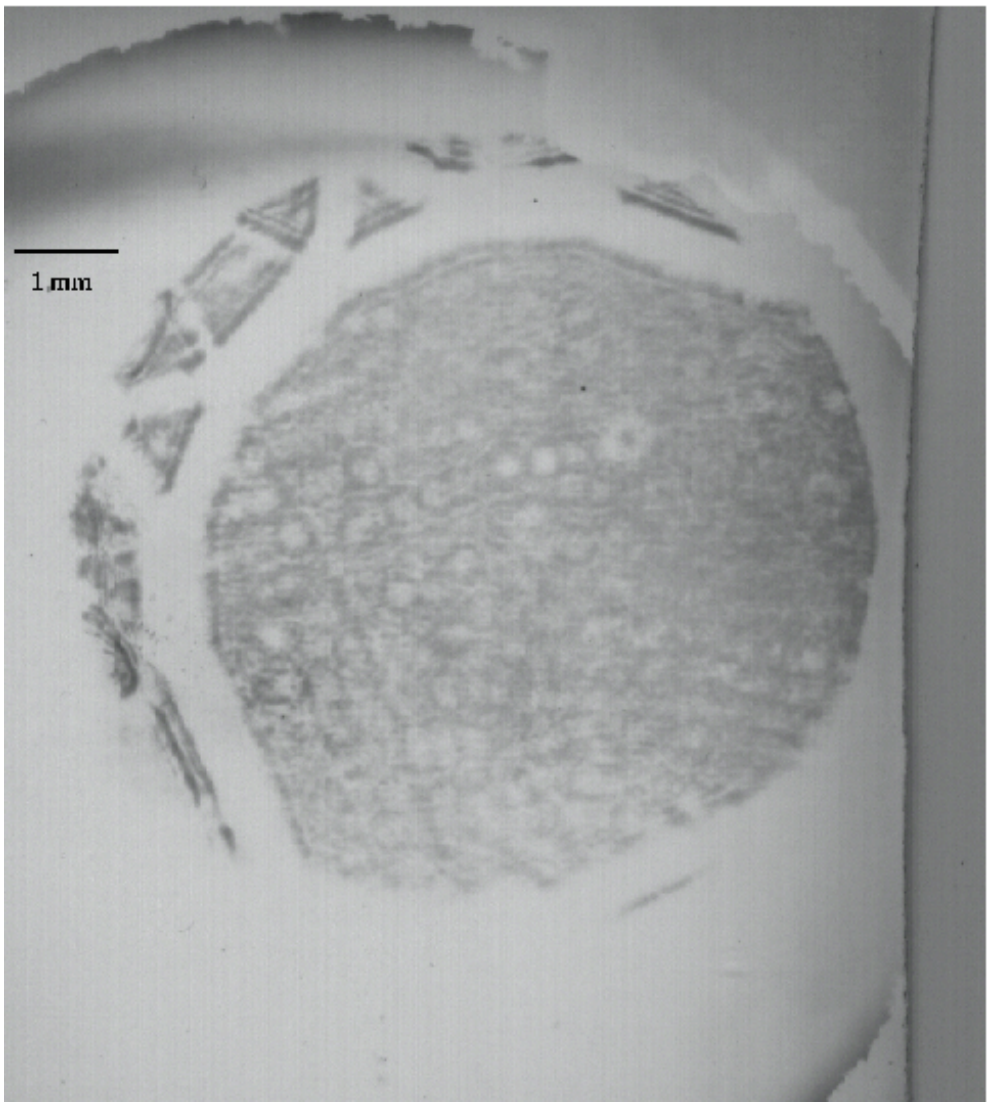

Figure 4.3.4.: A circle of approximately 7 mm well before the collision of the shocks. The delay between the explosion and the diagnostic laser is 49.8 μs. The uneven background is due to gas lens defects.

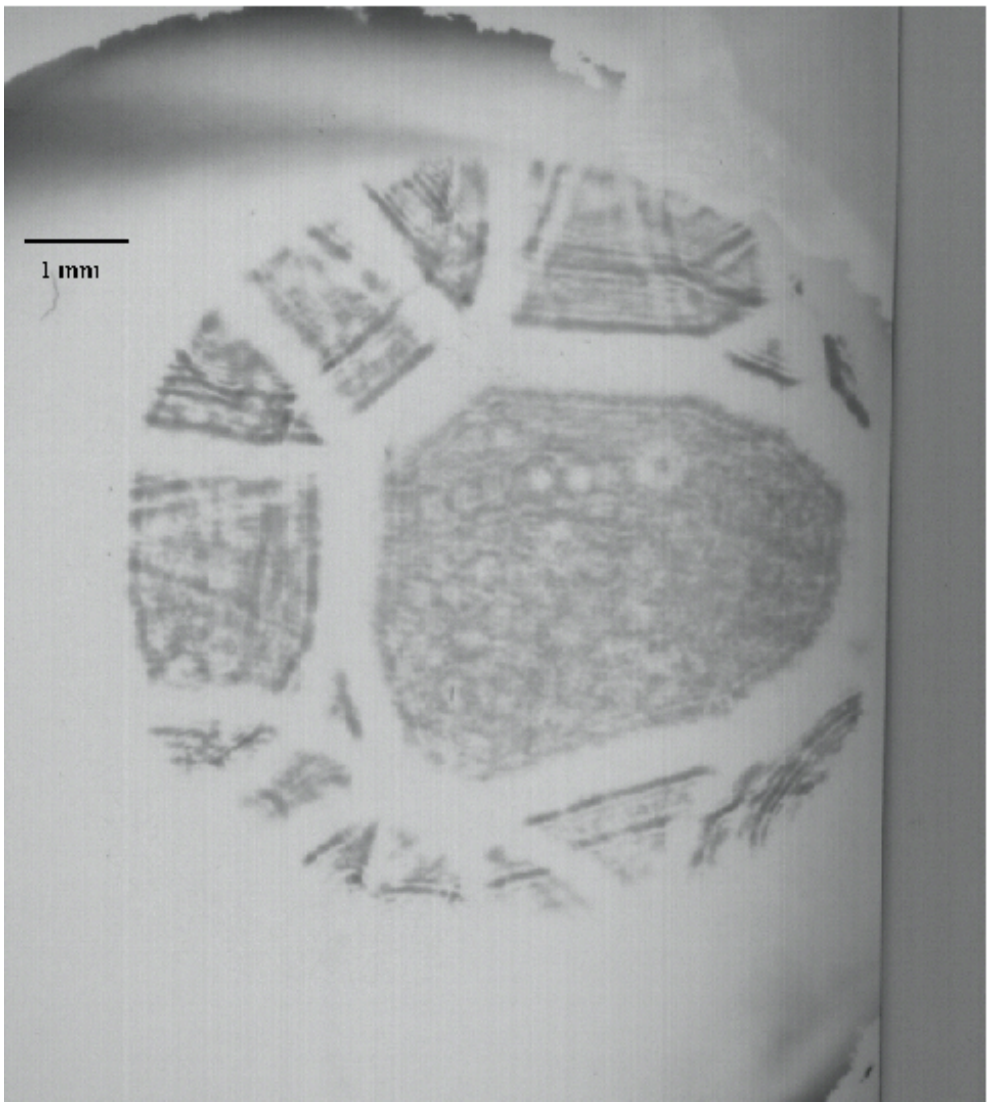

Figure 4.3.5.: Image of an approximately 4.5 mm pipe before the collision of the shocks. The delay between the shocks and the diagnostic laser is 52.8 μs.

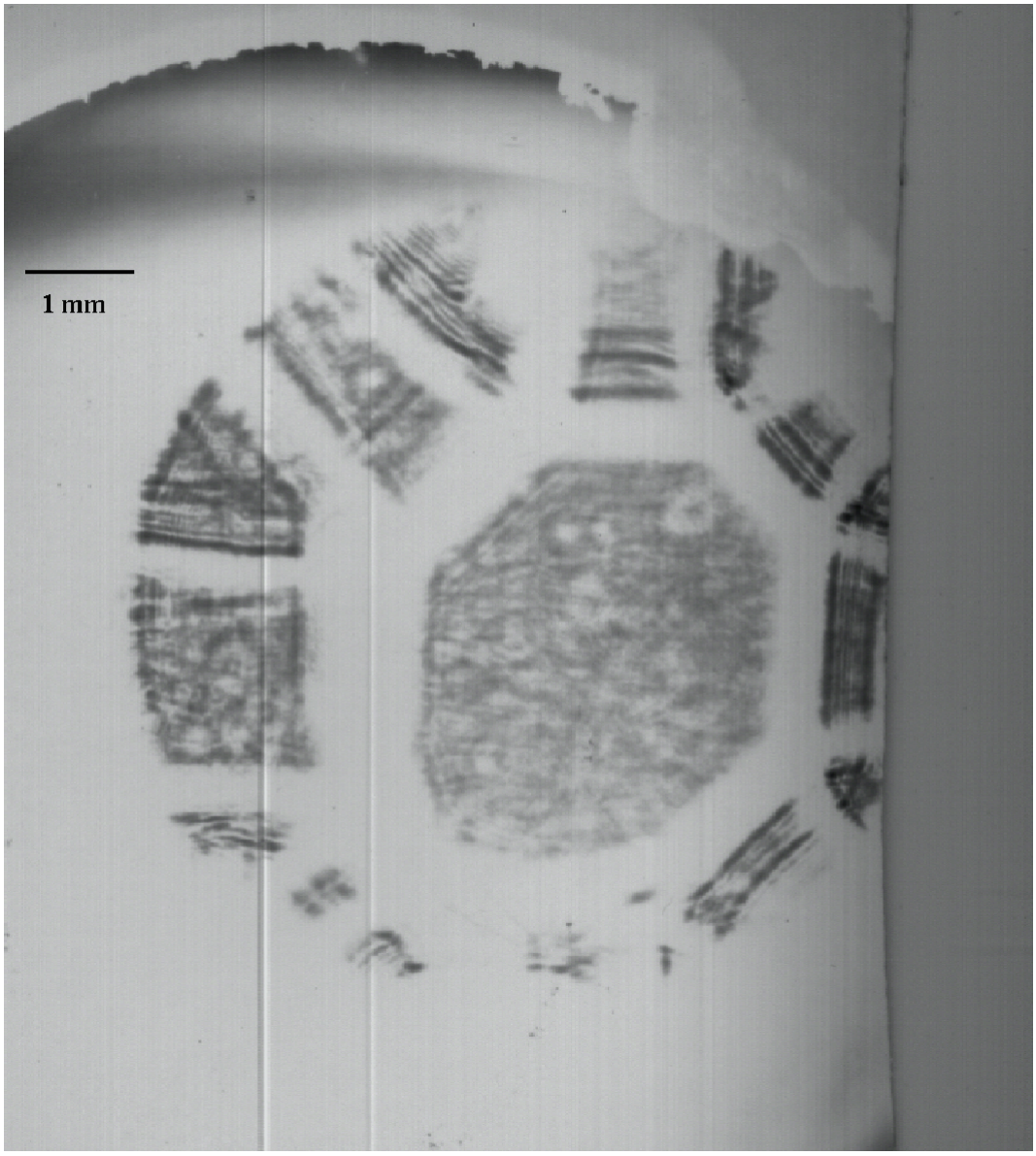

Figure 4.3.6.: Image of a big pipe before the collision of the shocks. The delay between the shocks and the diagnostic laser is 56.6 μs. The pipe has a horizontal diameter of approximately 3 mm.

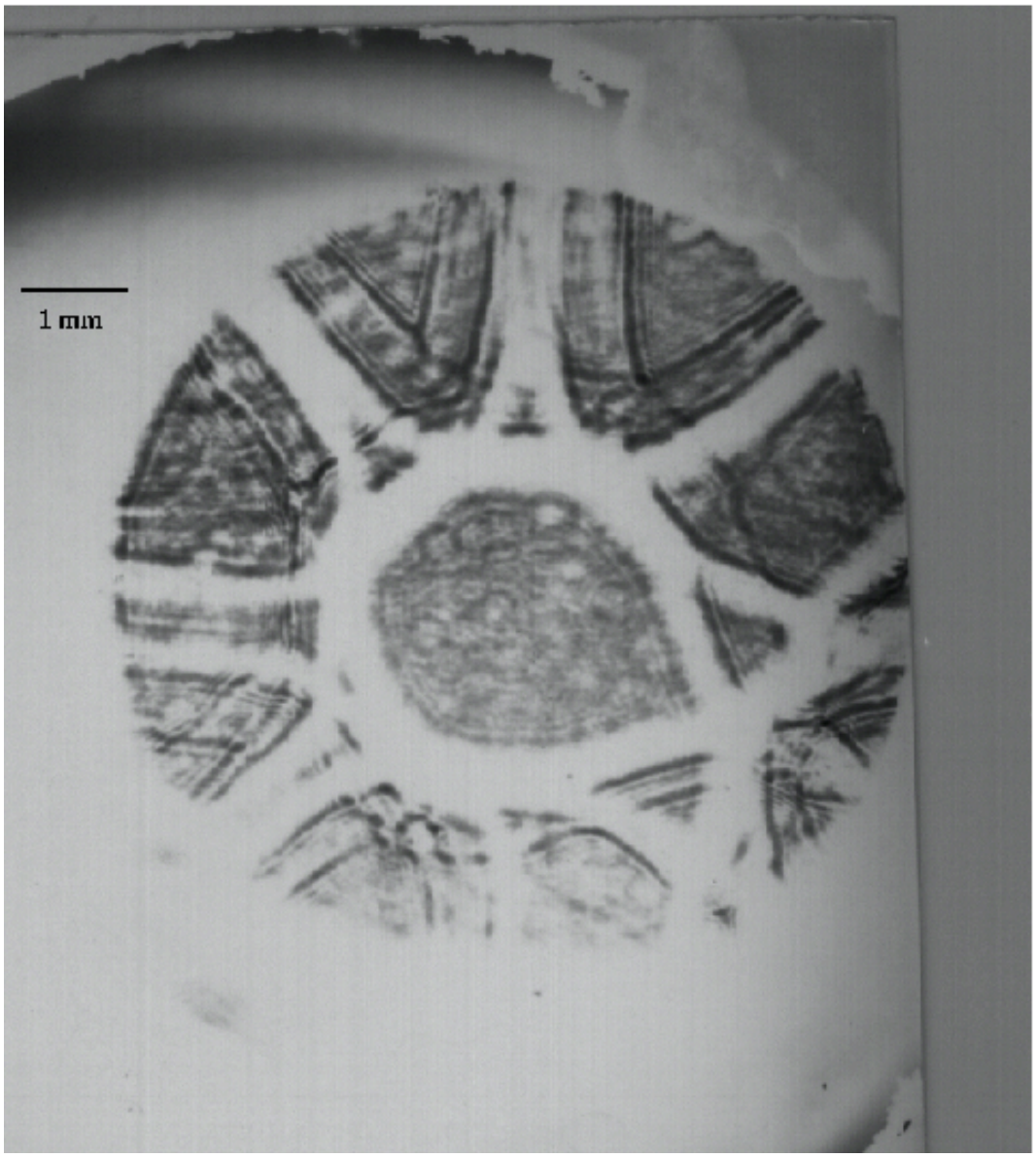

Figure 4.3.7.: An example of a very good pipe obtained, with a delay of 61.2 μs. Only one shock wave is arriving later.

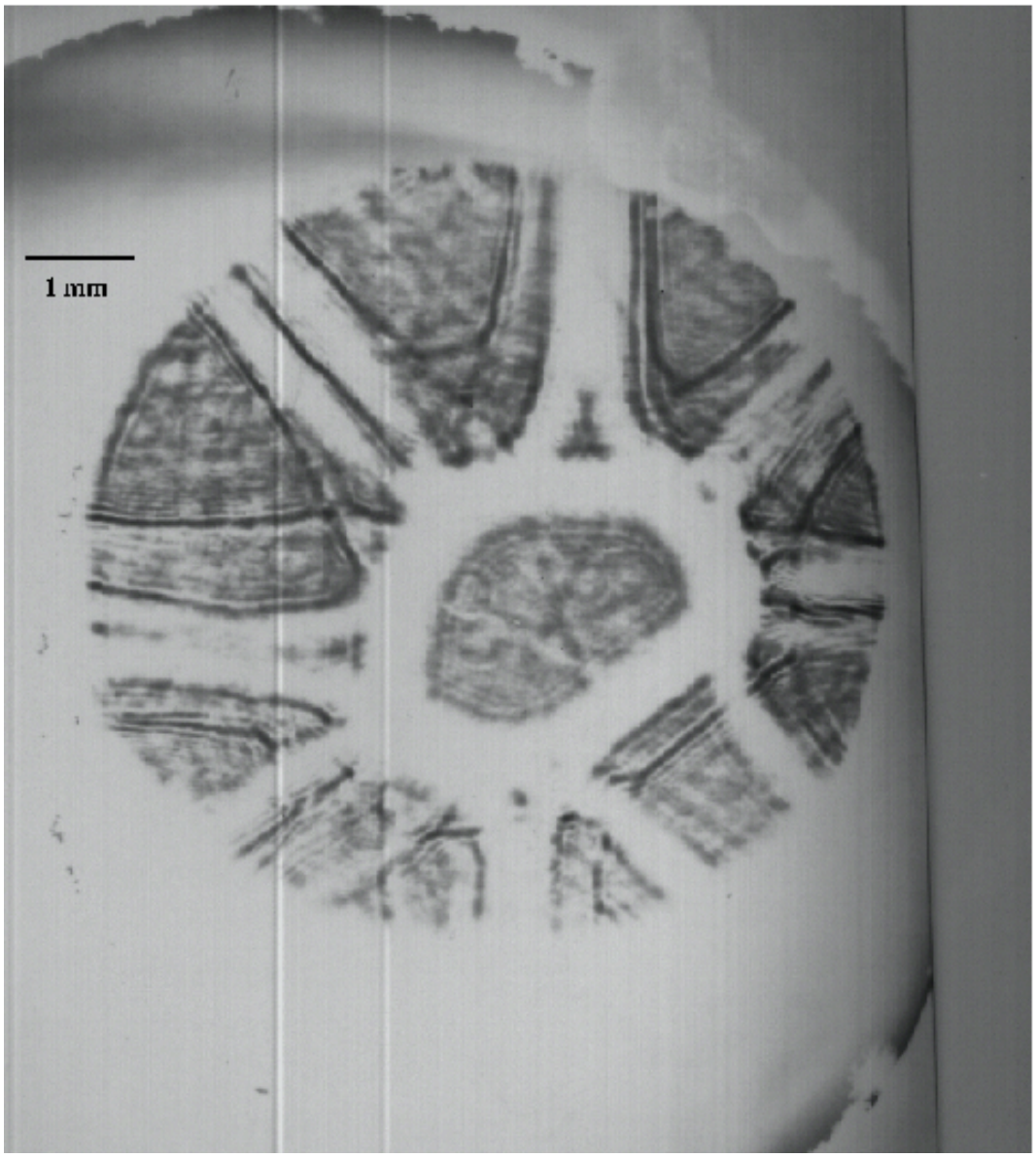

Figure 4.3.8.: Image with shocks travelling at a higher speed. Despite the delay of 57.4 μs the inner diameter of the pipe is smaller.

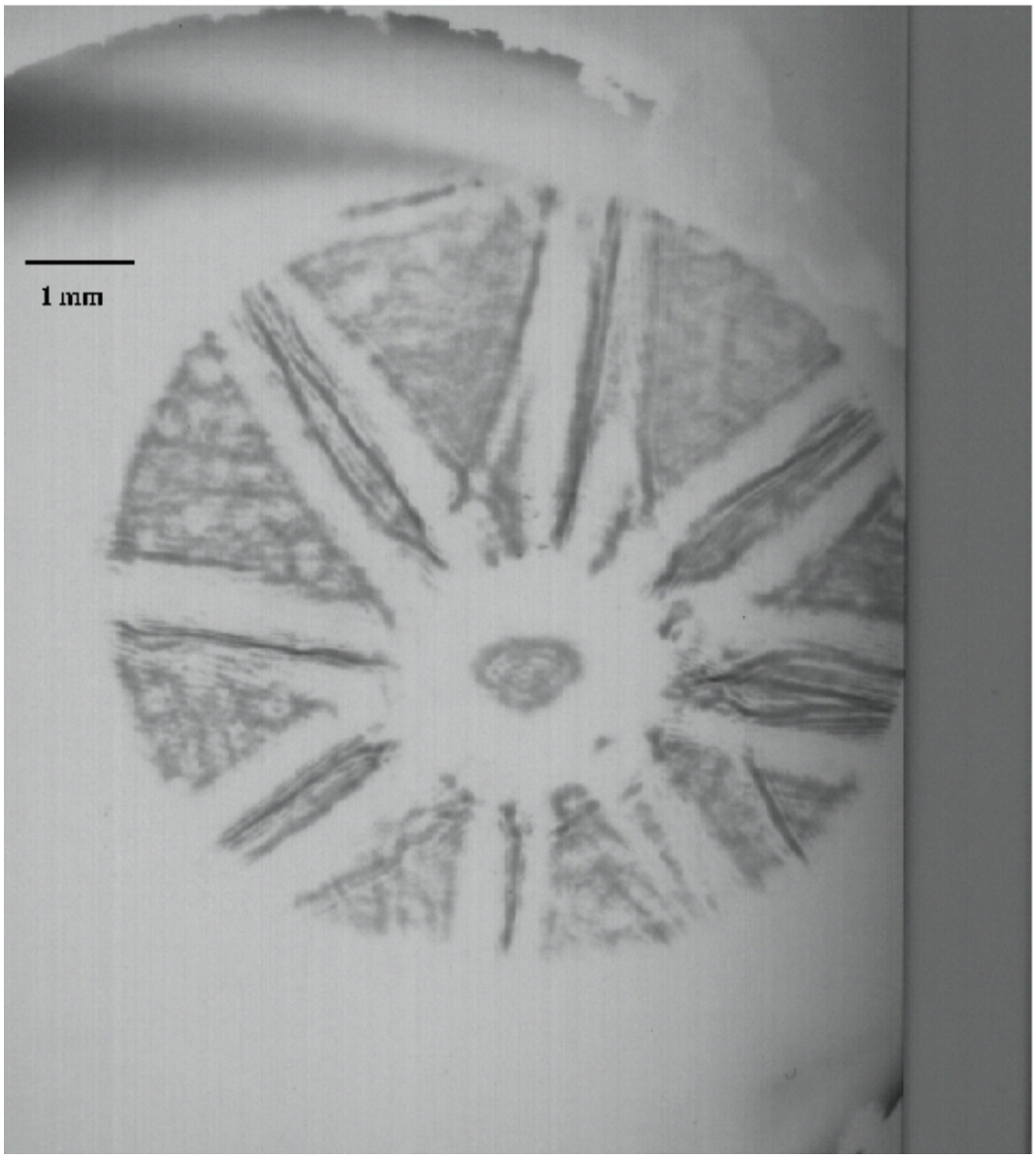

Figure 4.3.9.: After 55.8 μs the shocks have already merged through Mach addition. The centre of the picture resembles a circle and individual shocks cannot be recognized.

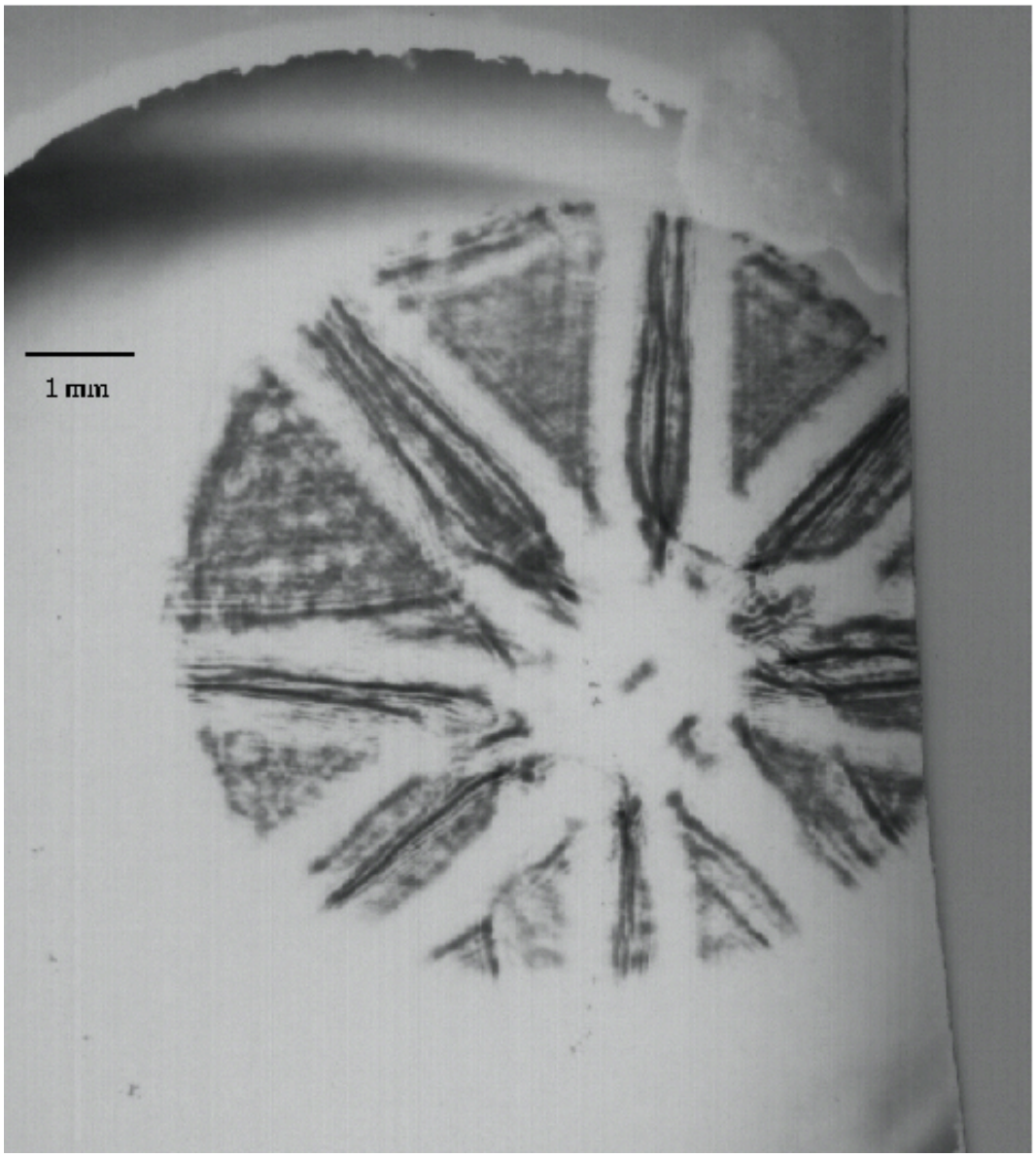

Figure 4.3.10.: Picture with a delay of 57.0 μs shows the smallest pipe observed before collision. The pipe has an elongated shape.

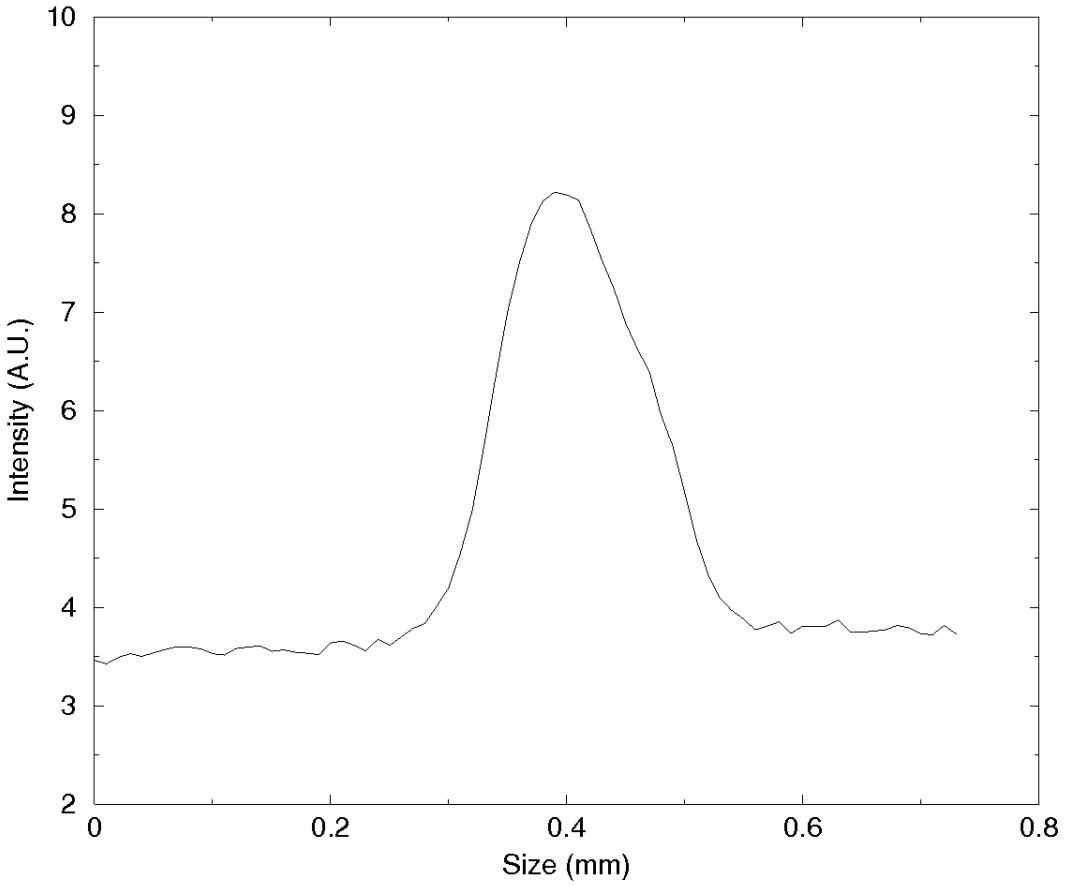

Figure 4.3.11.: Densitometry of Figure 4.3.10 on the previous page.

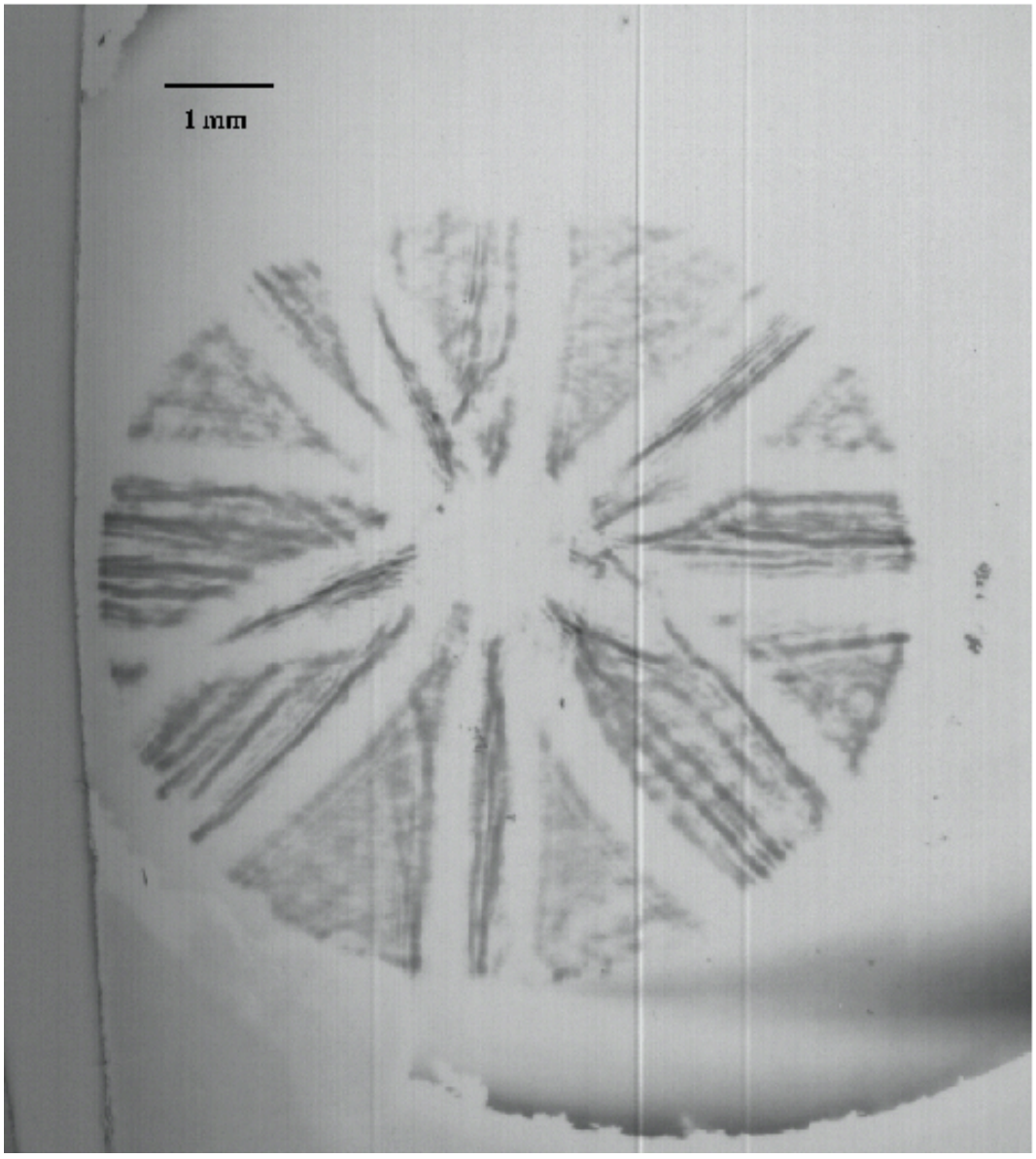

Figure 4.3.12.: Picture with a delay of 62.2 μs, the shock waves are colliding in the center. The pipe is very small and slightly misaligned, so there is very little light getting through.

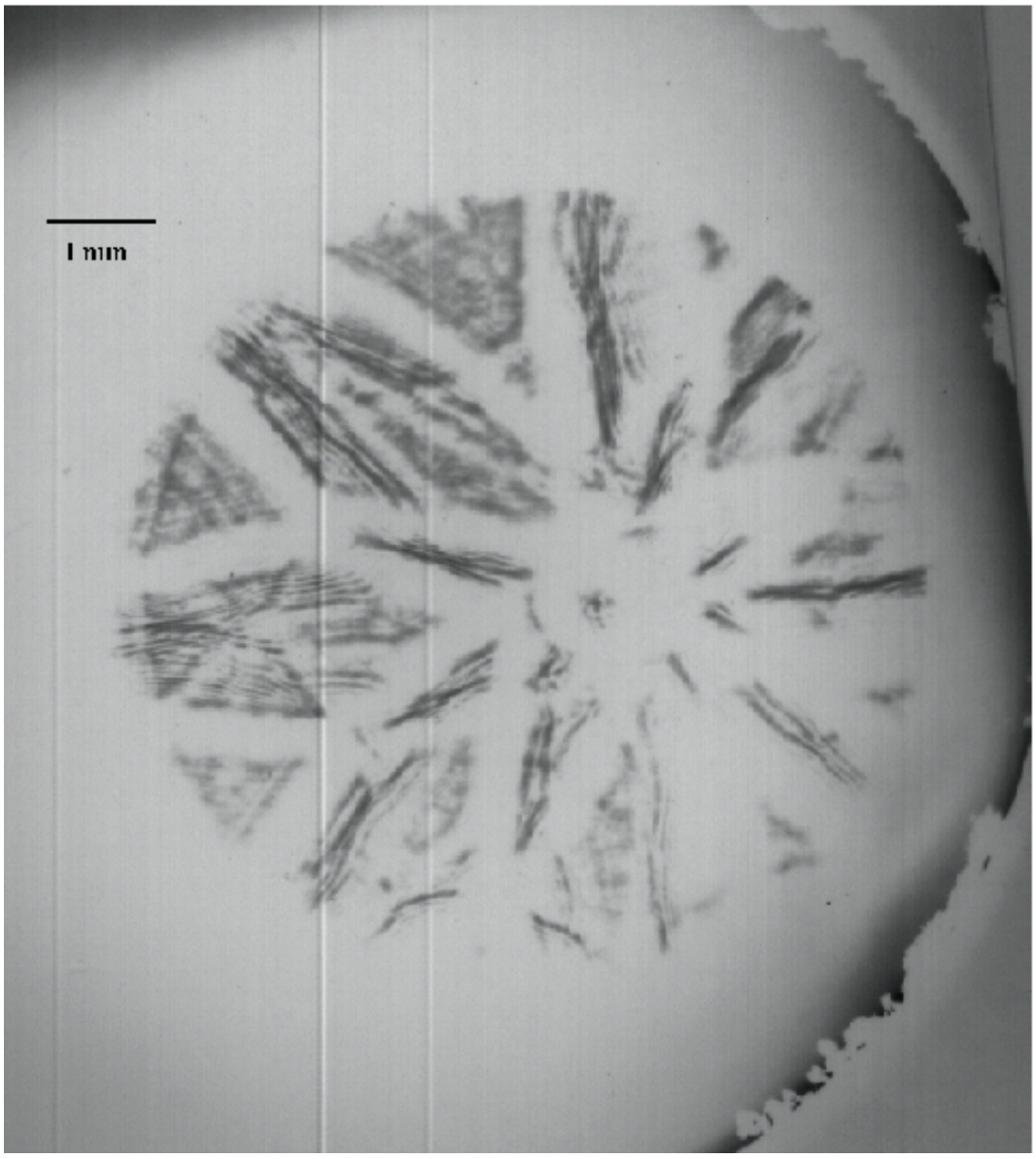

Figure 4.3.13.: Picture obtained with a delay of 54.6 μs showing the smallest pipe obtained after collision. The pipe is not a perfect circle because of some turbulence, but the size was the smallest observed.

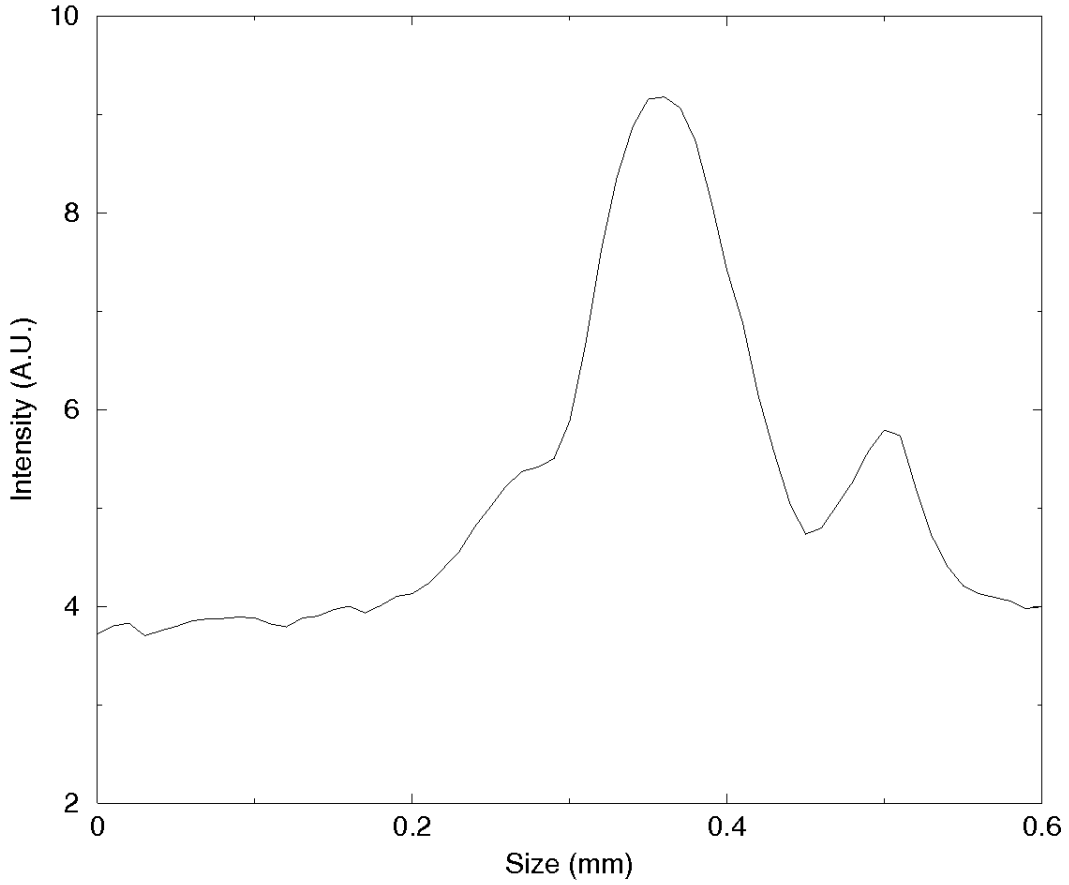

Figure 4.3.14.: Densitometry of Figure 4.3.13 on the previous page. The bright spot in the center has a size of approximately 1.5 *mm*. The diffraction limit for the focus is smaller than in the case of the parallel beam, because of the shortened optical path.

4.4. Problems

This section covers the drawbacks of CSL operation. The first one is the fact that the wire must be changed after every shock. The holder also has to be manually changed and takes a few minutes. This problem may be solved in two different ways. The holder is a very inexpensive device, so many of them may be prepared already pre-loaded with the wire, ready to be inserted into the experiment. A better way is the use of a row of small sparks to replace the wire, aligned longitudinally [2].

4.5. Debris

An exploding wire produces a substantial amount of debris, which may jeopardize the experiment to be performed using the gas structure. The quality of the gas lens used to focus the laser beam was being damaged by the debris from the wires, which posed a problem to the experimental setup. The Scanning Electron Microscope (SEM) pictures shown in Figures 4.5.1 on the following page and 4.5.2 on page 88 show the tiny droplets, with diameter ≤ 100 μm, on the lens.

A possible application of high power lasers in the future is in particle accelerators [21]. In this case, since the debris is traveling more slowly than the shock wave, it should not have a bearing on particle acceleration experiments, in which the center of the interaction chamber is empty.

Figure 4.5.1.: SEM pictures of droplets of melted wire on the lens.

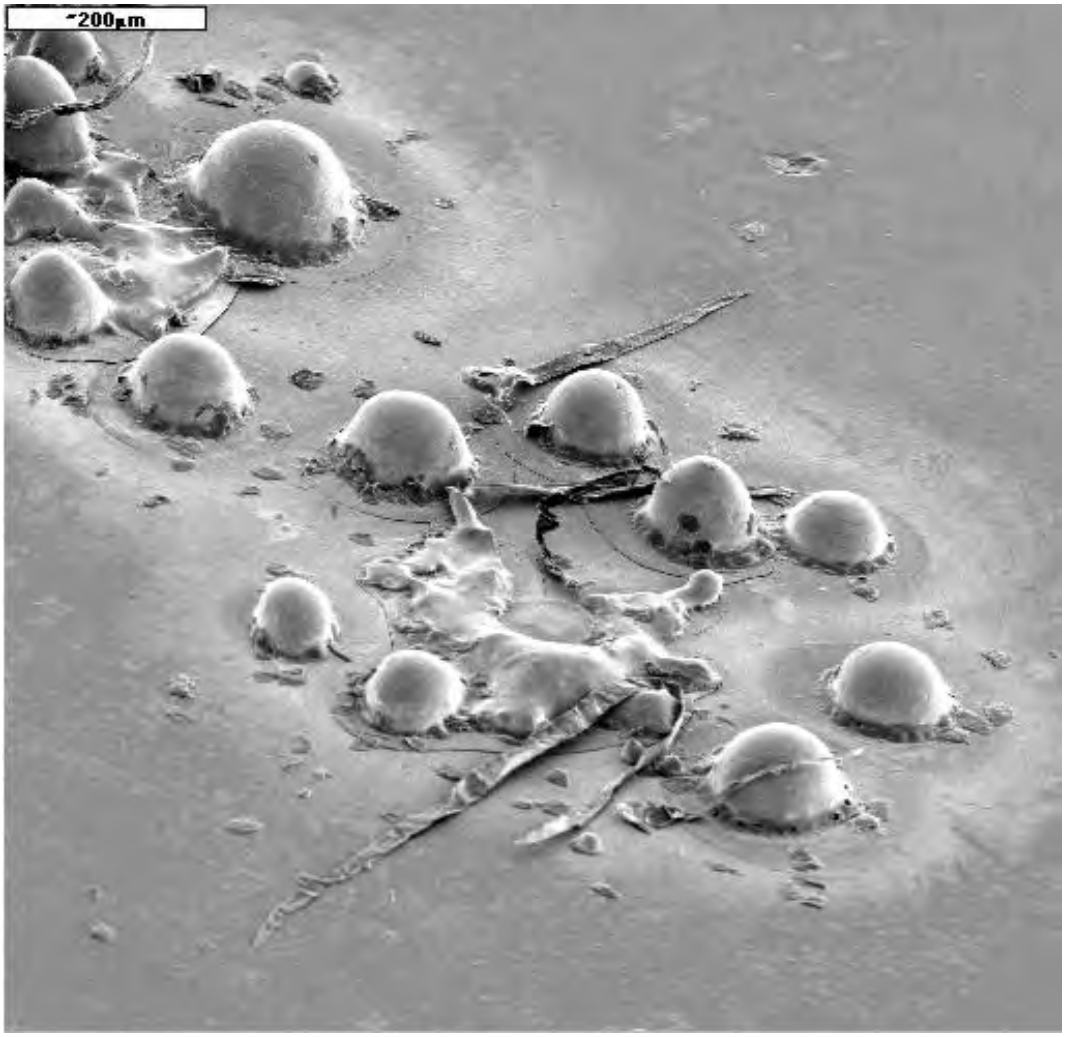

Figure 4.5.2.: SEM pictures of droplets of melted wire on the lens.

4.6. Concluding comments

It has been shown that cylindrical shocks interact in a similar way to the spherical shocks generated by the spark gap CSL. This is useful since a cylindrical system can be modelled in 2D by CFD if end effects are neglected.

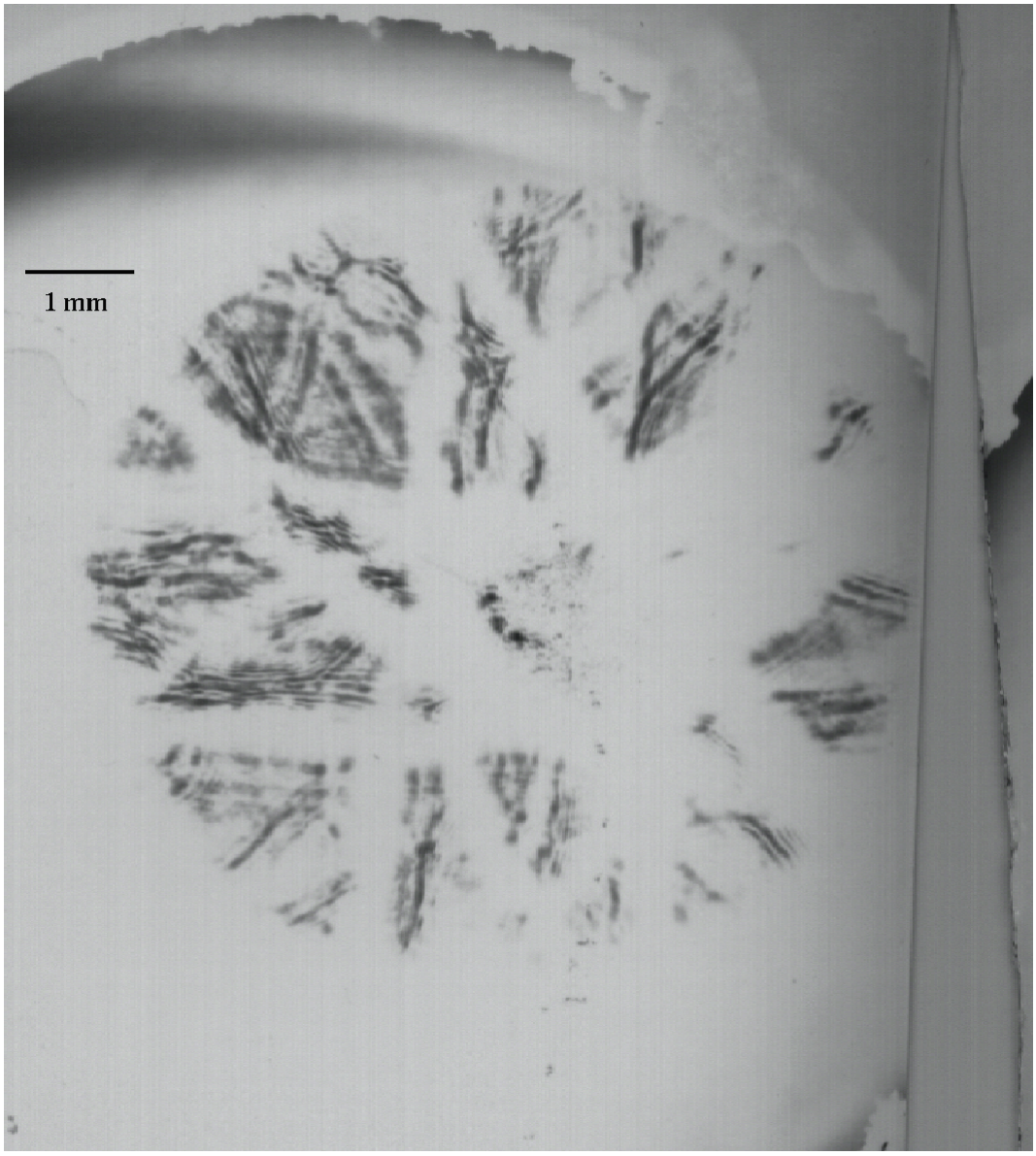

Figure 4.3.15.: A result immediately after the collision of the shocks in the center. The small dark spots are probably multiple foci due to turbulence. The centre has a diameter of about 5 mm.

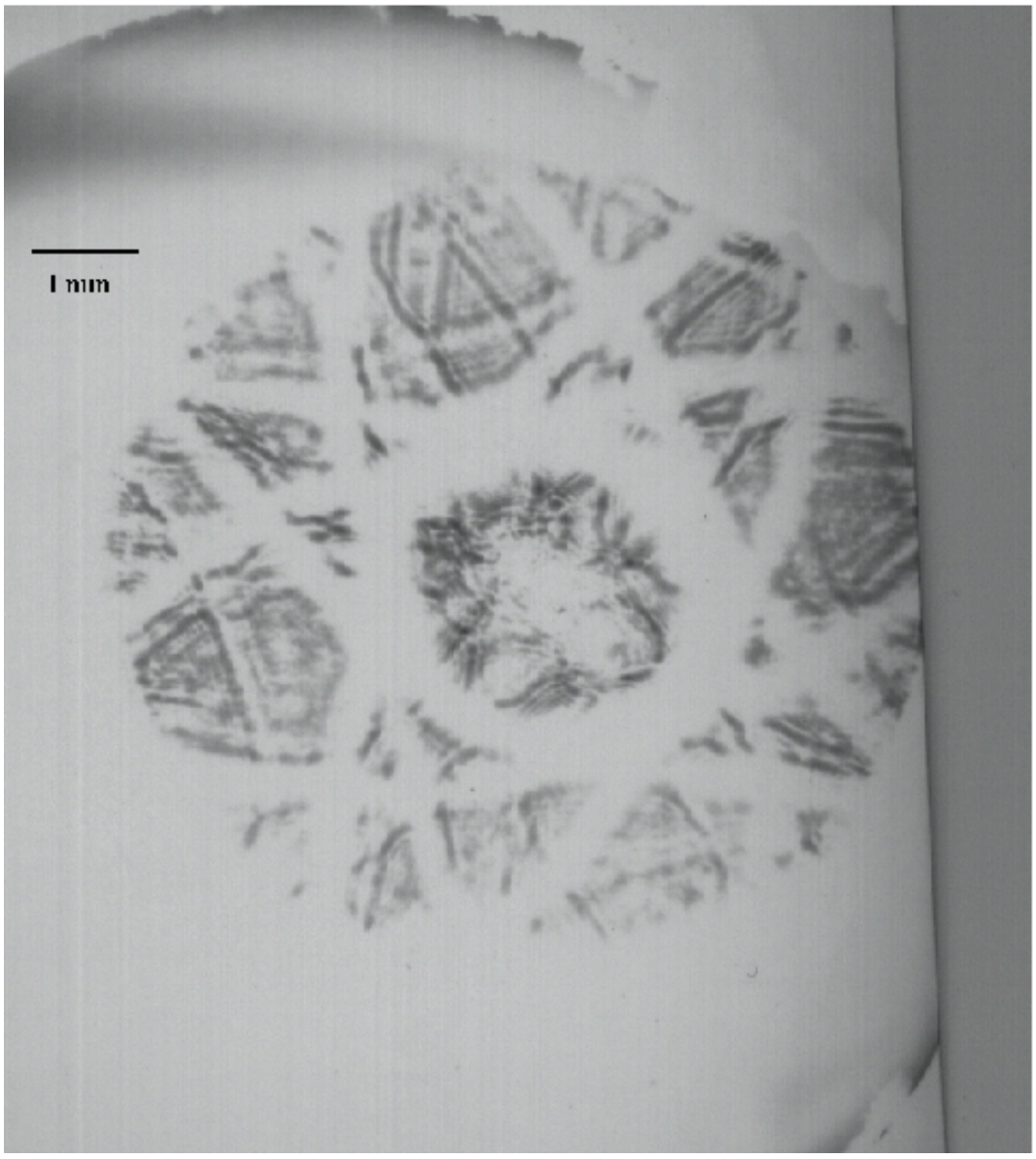

Figure 4.3.16.: The VC breakdown with a delay of 65.2 μs, and the centre has expanded more than 4.3.15. Now the circle has expanded up to more than 1 cm in diameter and no focus is observed in the center.

5. Computational Fluid Dynamics of Shock Waves

5.1. Introduction

Fluid dynamics is a field of science in which the physical laws governing the flow of fluids under various conditions is studied. Computational Fluid Dynamics (CFD) is used to generate flow simulations with the help of computers and it involves solving the governing laws of fluid dynamics numerically.

The profile of the shock waves as they interact towards the middle of the CSL is difficult to determine experimentally. This would, among other things, include the interference of the physical probes with the actual shock waves. CFD was exploited to investigate the physics of the shock waves, and to understand their behaviour better.

CFD complements experimental and theoretical fluid dynamics by providing an alternative cost-effective means of simulating real flows. As such it offers the means of testing advances for conditions unavailable experimentally. CFD also provides the convenience of being able to switch off specific terms in the governing equations. This permits testing theoretical models and, inverting the connections, suggests new paths for experimental exploration. Fletcher [33] has suggested advantages of CFD as compared to experimental fluid dynamics, these are :

1. Lead time in design and development is significantly reduced

2. CFD can simulate flow conditions not reproducible in experimental model tests

3. CFD provides more detailed and comprehensive information, and

4. CFD produces a lower energy consumption.

In the previous chapter it has been shown that cylindrical shocks in the exploding wire experiment can be used to form a CSL. These shocks can be simulated in a plane normal to the CSL axis.

This 2D simulation was performed using Computational Fluid Dynamics Fastran (CFD-Fastran). CFD-Fastran is a 3D, compressible, density-based finite volume flow solver with higher order differencing and flux splitting methods [34]. It can handle a full range of flow conditions including incompressible/compressible, steady/unsteady, inviscid/laminar/turbulent and can import various types of grids and hybrid grids. The governing equations are discretized and numerically integrated based on a finite volume approach. This method divides the flow domain into discrete points from which control volumes are built. Flow information is stored at each cell center and the flow from one cell to the next cell is determined by evaluating the fluxes across the common face between the adjacent cells.

5.2. Theory of CFD-Fastran

The governing equations for the problem are [34]

- Conservation of Mass

$$\frac{\partial \rho}{\partial t} + \frac{\partial}{\partial x_j}\left(\rho u_j\right) = 0 \tag{5.2.1}$$

where ρ is the density and u_j is the mass averaged velocity in the j^{th} direction.

- Conservation of Momentum

$$\frac{\partial}{\partial t}\left(\rho u_j\right) + \frac{\partial}{\partial x_j}\left(\rho u_i u_j\right) = \frac{\partial}{\partial x_j}\left[-\left(p + \frac{2}{3}\rho k\right)\delta_i + \tau_{ij}\right] \tag{5.2.2}$$

where p is the pressure, k is the turbulent kinetic energy, δ_{ij} is the Kronecker delta and τ_{ij} is the shear stress tensor, which is

$$\tau_{ij} = (\mu + \mu_t)\left(\frac{\partial u_i}{\partial x_i} + \frac{\partial u_j}{\partial x_i}\right) - \frac{2}{3}\left(\frac{\partial u_k}{\partial x_k}\right)\delta_{ij} \tag{5.2.3}$$

where μ is the dynamic viscosity of the mixture, and μ_t is the turbulent viscosity.

- Conservation of Total Energy

$$\frac{\partial E_t}{\partial t} + \frac{\partial}{\partial x_j}\left[\left(E_t + p\right)u_j\right] = -\frac{\partial q_j}{\partial x_j} + \frac{\partial}{\partial x_j}\left(u_i \tau_{ij}\right) \tag{5.2.4}$$

where E_t is the total energy per volume and q_j is the heat flux in the j^{th} direction. The closure models are

- Thermal Equations of State

$$p = \frac{\rho R_u T}{M_w} \tag{5.2.5}$$

where p is the static pressure, ρ is the gas density, R_u is the universal gas constant (8314.4 J kmole^{-1} K^{-1}), T is the static temperature and M_w is the molecular weight of the gas.

- Caloric Equation of State

$$E = \rho c_v T \tag{5.2.6}$$

where c_v is the heat capacity of the gas mixture at constant volume.

- Definition of Total Energy

$$E_t = E + \frac{1}{2}\rho u_i u_j \tag{5.2.7}$$

5.3. Assumptions

- A 2D model of the flow is to be investigated to compare with the experimental profiles, as these are images of a vertical plane within the CSL which is located centrally between the electrodes (see Chapter 2 on page 18)
- The wire is to be simulated initially as a circular region of high pressure and the surrounding medium at Standard Temperature and Pressure (STP).
- The walls that hold the wires are not included as they are outside the region of interest.
- The simulation is to be inviscid since compressible effects will dominate. Viscous effects are expected to be comparatively small because there are no wall boundaries in the shock region that is imaged; and although shear layers may be present, their effect is also expected to be small in comparison to the shocks.
- At the far field boundary, conditions at infinity are modeled.

5.3.1. Simulation Outline

The outline for the setup of the simulation has been broken down into the following tasks:

- Single wire simulation
- Four wire simulation
- Eight wire simulation, and
- Scaling the geometry.

The single wire simulation had a degenerate point in the CSL centre, which may cause the 8 wire simulation numerical anomalies. The 8 wire simulations allows the removal of this point (see Figure 5.3.5).

For a 2D structured grid a 2D surface is generated by 4 connected lines (as in a rectangle) with opposite sides having the same number of grid points. If the surface has 3 connected lines (as in a triangle) then a degenerate point is created on one of the vertices of the triangle. In CFD-Fastran the vertex with the degenerate point is determined by the order in which the lines are chosen to create the face [34]. The CFD-Fastran solver treats degenerate points and lines as a boundary condition, at which values of adjacent points are averaged. This is less general than solving across the point.

5.3.2. Geometry and Grid

A circle was envisaged to simulate the cross section of the wire in the two dimensional simulation plane. The circle was placed at the same distance from the centre as that of one of the wires used in the experiment. A quadrant was used as the surrounding grid to the circle. The quadrant also serves to simulate the air medium that the CSL is in. The walls of the CSL were not modeled, as only the effects of the colliding shocks, and not wall reflections, are modeled. The far field boundaries were modeled as conditions at infinity so as not to interfere with the interaction in the near field.

The quadrant geometry of Figure 5.3.1 on the next page was modified to one of an octant as shown below on Figure 5.3.2 on page 97. It also created a degenerate cell at the apex which might introduce some interpolation errors. It was therefore made as a step towards designing the 8 wire grid.

5.3.3. Single Wire

A simulation of a two dimensional single wire constrained in a octant grid was set up as in Figure 5.3.2 on page 97. The experimental results obtained were 2D pictures of the shocks as shown in Figure 2.2.2 on page 23 of chapter 2. This 2D simulation would provide an adequate comparison with the experimental results.

The circle that represents the wire has a radius (r = 0.13 mm) measured from

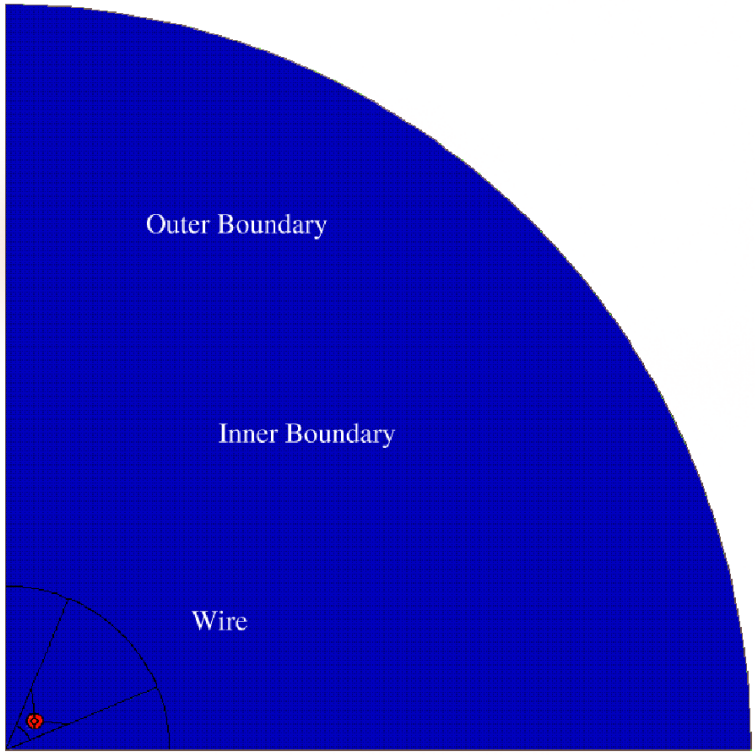

Figure 5.3.1.: Single Wire Geometry showing the far field.

the SEM picture of Figure 4.1.3 on page 62 and the length between the centre of the wire to the centre of the CSL is shown as $L = 5.5$ mm in Figure 5.3.2 on the following page. The dimensions of the CSL device are the same as that used by Bucellato *et al.* [1].

The outer boundary was created at about $10L$ from the actual wire so that it minimizes boundary interference with the shock waves traversing towards the apex. This geometry was also used to find the right initial conditions to produce a cylindrical shock. The initial conditions of the geometry are uniform (temperature is 288.16 ^{0}C, pressure is 10^5 N/m^2) except that within the wire boundary, where the initial pressure is 10^{10} N/m^2. This is analogous to the situation that, at time $t = 0$ s, a membrane around the higher pressure region is removed and a shock wave starts propagating cylindrically outwards. It is still uncertain as to whether the shock wave would travel at the experimentally determined value of Mach 1.5 from Bucellato *et al.* [1] . However this was sufficient to demonstrate the principle behind

the propagation and interaction of the shock waves.

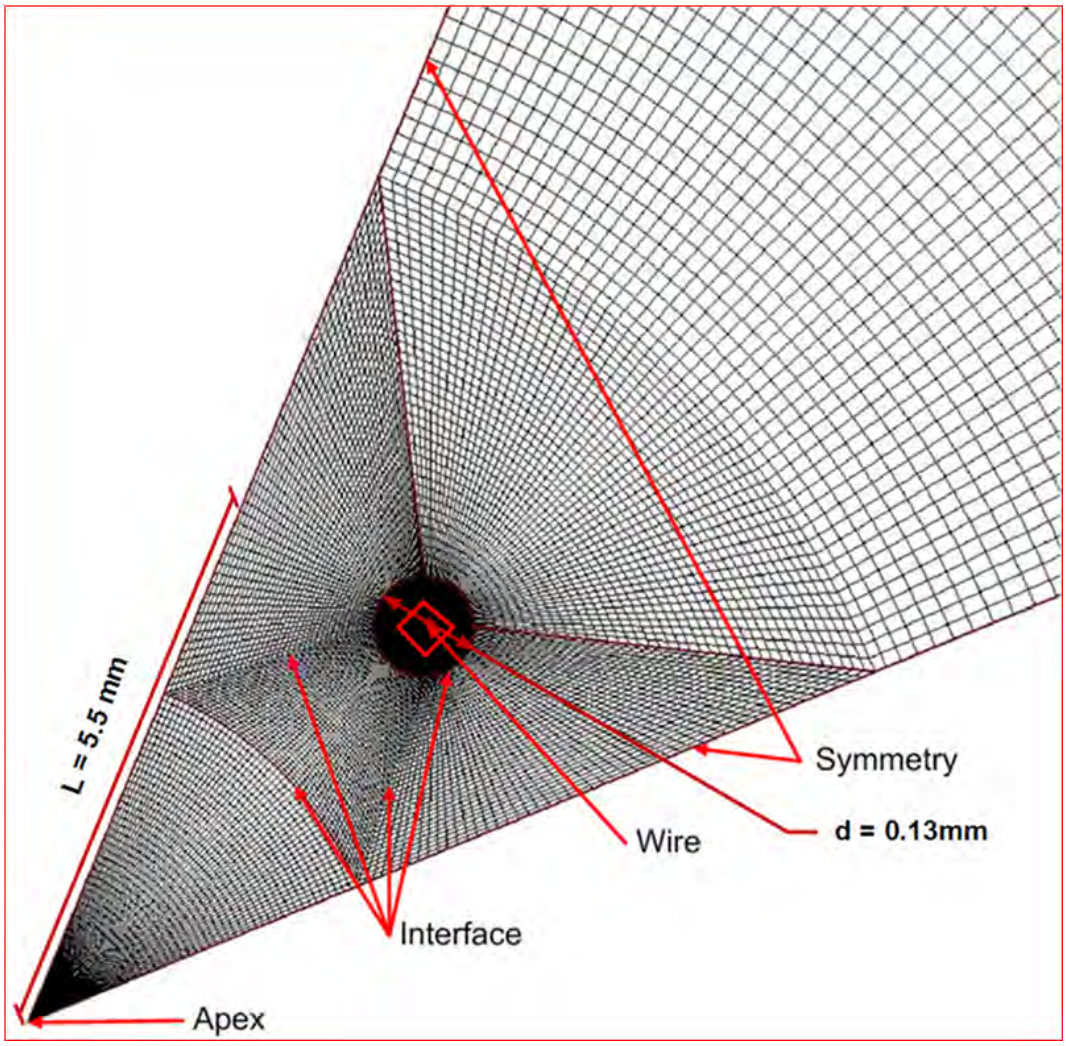

Figure 5.3.2.: 2D magnified single wire geometry.

The black circle in the centre of Figure 5.3.2 is a representation of the fine cells in the wire. The apex or tip of the triangle on the picture is at the centre axis of the device. The far field boundary conditions are extrapolated outlets. The sides are symmetry boundary conditions and the wire boundaries are interfaces.

5.3.4. Four Wires

The above geometry was rotated 4 times orthogonal to the plane of the paper to give half of the wires required to make up a complete geometry, and the degenerate point was replaced by a rectangle, as shown in Figure 5.3.3.

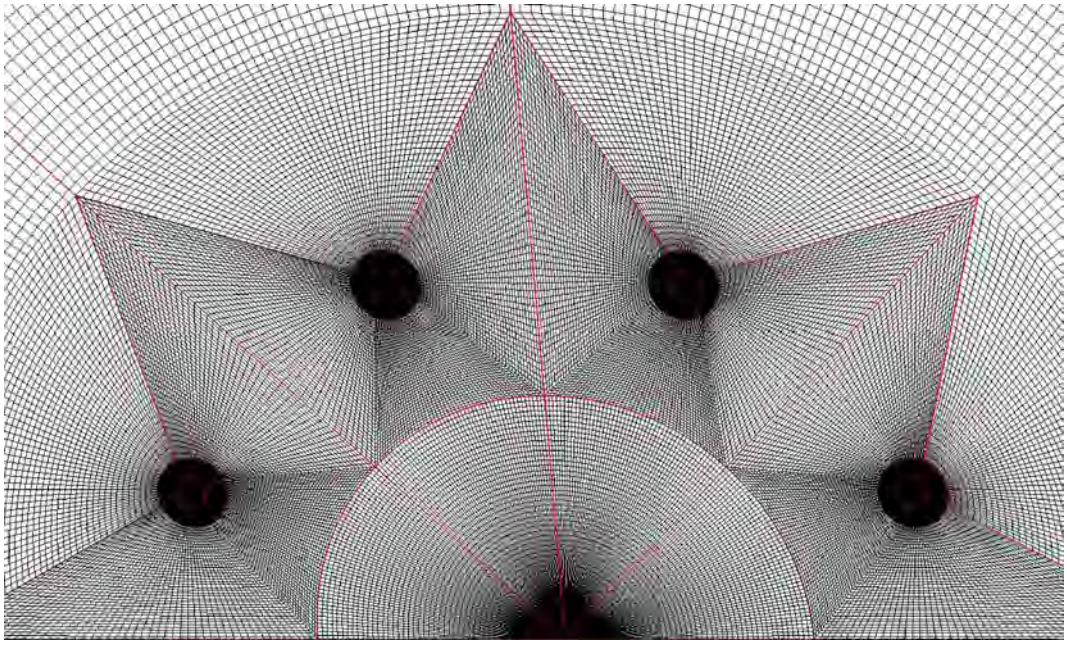

Figure 5.3.3.: 2D four wire geometry

Figure 5.3.3 shows the near field around the wires. The outer boundaries are not shown as they are far away from the wires ($10d$). The boundary where the pressure is greater initially is shown as the wire boundary. The rectangle inside the circle is only there to enable correct geometry settings and also to set up the required grid. The initial pressure inside the rectangle is the same as that of the circle.

5.3.5. Eight Wires

Although the very first CSL designed consisted of four electrodes, experimental data for it was minimal. More data had been taken on the eight electrode CSL. Therefore the computational simulation was based on eight electrodes and eight shocks.

The single wire geometry was rotated seven times around the axis orthogonal to the simulation plane to give 8 wires around a circumference to model the whole CSL device.

Because this created a degenerate point at the centre of the device, a modification was made to the geometry. A grid box was made around the centre of the device, similar to the butterfly geometry mentioned above in Sub-section 5.3.4.The grid was

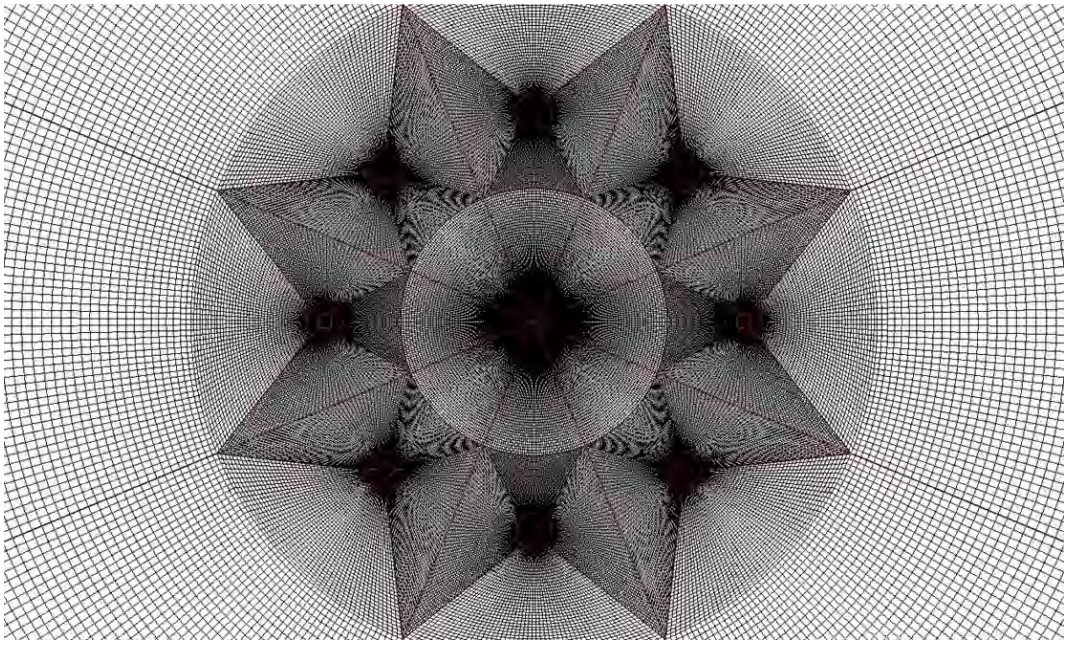

Figure 5.3.4.: 2D eight wire geometry magnified at the centre of the CSL.

smoothed, resulting in the final geometry shown in Figure 5.3.5.

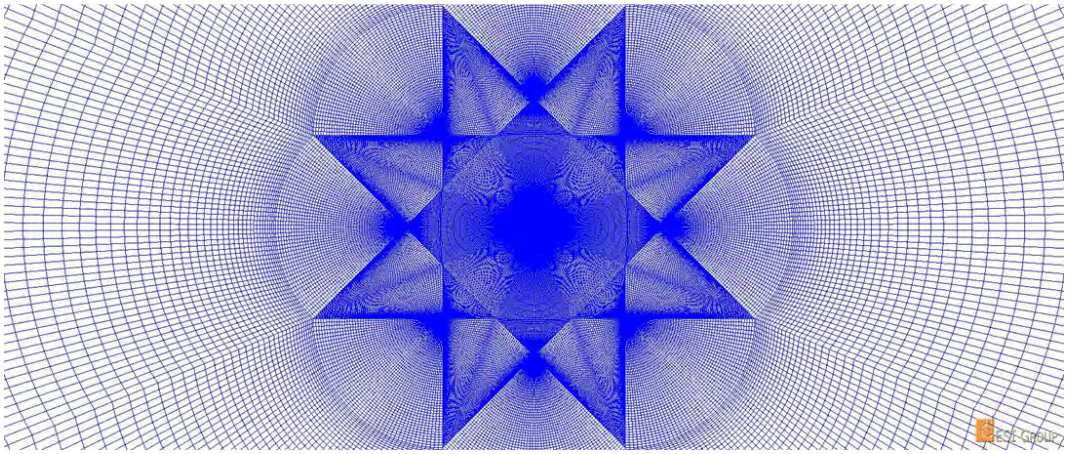

Figure 5.3.5.: Final mesh geometry.

This removed the problems associated with degenerate points and also aided in the mesh geometry creation. The shock waves as they traverse towards the centre also travel through a more uniform grid, and the effects of the inter-block interfaces are removed.

5.3.6. Scaling The Entire Geometry

The initial geometry was designed for a CSL on the scale of metres. To capture the shocks, a grid size that is the same as the experimental setup was required, and the big-scale CSL would have required a very large number of grid points. The entire geometry structure was therefore scaled to a millimetre range with the help of the dimensions obtained from the CSL from Bucellato *et al* [1].

The distances from the centre of the wires that form the circumference to the entire structure (radius of the circumference) is 5.5 mm. Hence from the centre of one wire to the opposite wire is 11 mm. The outer boundaries of the structure are so far away that they can be thought of as at infinity and this enables the outer boundaries to be ignored.

5.4. Simulation Setup

The model properties were as shown in Table 5.4.1 on the next page.

The flow is compressible, for shock propagation.

The mesh geometry is axi-symmetric in cases of less than eight wires.

The ideal gas law was chosen with air properties being simulated. CFD-Fastran has the capability to model other gases, which might be interesting for any further work that can be done to investigate the operation of the CSL in other gaseous media, or mixtures of gases.

The momentum transport model is chosen as Euler. The Euler equations are the Navier-Stokes equations without viscosity and heat conduction.

The mesh is multi-block, and all the zones are fluid as there were no walls or blocked zones.

There were three boundary conditions:

- Far field boundary, that was at the circumference of the mesh and all flow variables are extrapolated to the exit from the domain interior for supersonic

Number of Zones/Areas	89
Problem type	Compressible
Geometry	Axi-symmetric
Gas Model	Calorifically Perfect(ideal) gas
Transport Model	Euler/Inviscid
$\gamma\left(\frac{C_p}{C_v}\right)$	1.4
Molecular Weight	28.97 kg/kmole
Area Conditions	Fluid
Wire Zones Initial Pressure	10^{10} N/m^2
Surrounding Zones Pressure	10^5 N/m^2
Spatial discretization	Roe's Flux Differencing Scheme higher-order
Limiter	Osher-Chakravarthy (L)
Solver-Time Integration	Implicit Non-Iterative
Flow Discretization	Backward Euler
Implicit scheme	Point Jacobi (Fully Implicit)
Sub-iterations	20
Tolerance	0.0001
Solution Files saved every	50 iterations
Total number of iterations	6000
Spatial Differencing Scheme	Van Leer

Table 5.4.1.: Details of FASTRAN input file.

flow.

- Inflow/Outflow for the regions that simulated the wire, this boundary condition is used by CFD-Fastran similarly as the extrapolated exit boundary condition where all variables are extrapolated from the interior to the exit face, and

- Interfaces for the rest of the mesh, as shown in Figure 5.3.2 on page 97. This boundary condition does not have to be set in CFD-Fastran, these are automatically found between zones that are abut.

As mentioned above there were two initial conditions set, as is a requirement for each fluid volume in the model:

- inside each of the eight wires and

- the surrounding medium in which these wires reside.

The number of time steps was set to 6000 which were enough to observe the propagation of the shock waves towards and away from the centre of the device.

The flux terms in the flow equations are the spatial derivatives. In numerical models, these terms are approximated. The first order upwind Van Leer scheme was chosen because it provides continuity in the solution variables at sonic points [35]. The Van Leer scheme is monotone which means that dispersion is unlikely to occur within a flow near a strong gradient, such as a shock. This scheme has also been tailored for transonic flows and should provide better transonic shock structure. The Van Leer flux limiter was also chosen. This increases the local spatial order of accuracy to second and third order spatial accuracy. The slope limiter is defined as

$$\psi(r) = \frac{r + |r|}{1 + r} \tag{5.4.1}$$

where r is the ratio of flow variables in adjoining cells.

A transient simulation was performed with files written every 50 iterations to enable visualization of the shock waves as they interacted and traversed to the centre of the CSL device. The time step size is automatically calculated, i.e. determined by the grid cell with the most restrictive stability requirement. The time step size Δt is calculated for all grid cells according to the calculation described in equation 5.4.2. Then the smallest Δt among all the values in all the domains is identified and every grid cell marches the solution using the smallest value Δt_{min}.

$$\Delta t = \frac{CFL.V}{\lambda_{max}} \tag{5.4.2}$$

where CFL is the Courant-Friedrichs-Lewy number, and is related to the numerical stability and accuracy of the numerical time-integration procedure. Smaller

CFL numbers are required for strongly nonlinear behavior and highly time-accurate calculations. Larger *CFL* numbers are taken (when the flow will allow), when the goal is to reach the steady-state quickly but not necessarily through a time-accurate process. The CFL number was ramped from 0.1 to 1.0 over the first 100 iterations. The spectral radius λ_{max} is a local stability parameter and is defined by Hirsch [35].

5.5. Results and Discussion

The eight-wire geometry simulation was run to 6000 time steps. An animation of the shock waves as they traverse and interfere towards the centre was also obtained. The animations are scaled to the maximum values of each frame. Each frame is taken in steps of 50 iterations as it would have taken too much hard drive space to capture every iteration.

The figures to be shown are for the

- initial iteration, showing the initial input conditions for the simulation.
- 950^{th} iteration, just before the adjacent shock waves interact with each other.
- 1000^{th} iteration, after the adjacent shocks have interacted.
- 1150^{th} iteration, the line focus of adjacent shocks form.
- 1450^{th} iteration, the shock waves converge at the centre of the device
- 1500^{th}iteration, the eight shock waves interfere at the centre of the device
- 1550^{th} iteration, the shocks waves have collided and are commencing to diverge, and the figure is enlarged towards the centre of the device
- 1850^{th} iteration, the shocks have diverged away from the centre of the device.

Figure 5.5.1 on page 105 shows the initial conditions of the simulation. The highest density is 1.209×10^5 kg/m^3 which is on the side of the centre of the CSL. The

value is high because of the pressure in the region. This is due to the mesh as shown in Figure 5.3.4, where towards the centre of the CSL the mesh is denser than the opposite sides which was made coarser because the far field boundary was not of interest to this investigation and also to decrease computational time by reducing the number of cells in the simulation. The surrounding density is at the lowest value of 0.6063 kg/m^3.

The highest pressure is 10^{10} N/m^2 and is similarly shown to be towards the center of the CSL with reasons similar to the ones given above. N/m^2 instead of Pa is to be used as a unit of pressure to be consistent with the units on the legend of the pictures to be shown.

The temperature is at the set value of 288.2 K which was set initially in the boundary and initial conditions for the respective zones.

The Mach number is at 0 which shows that the shock waves have not started to propagate.

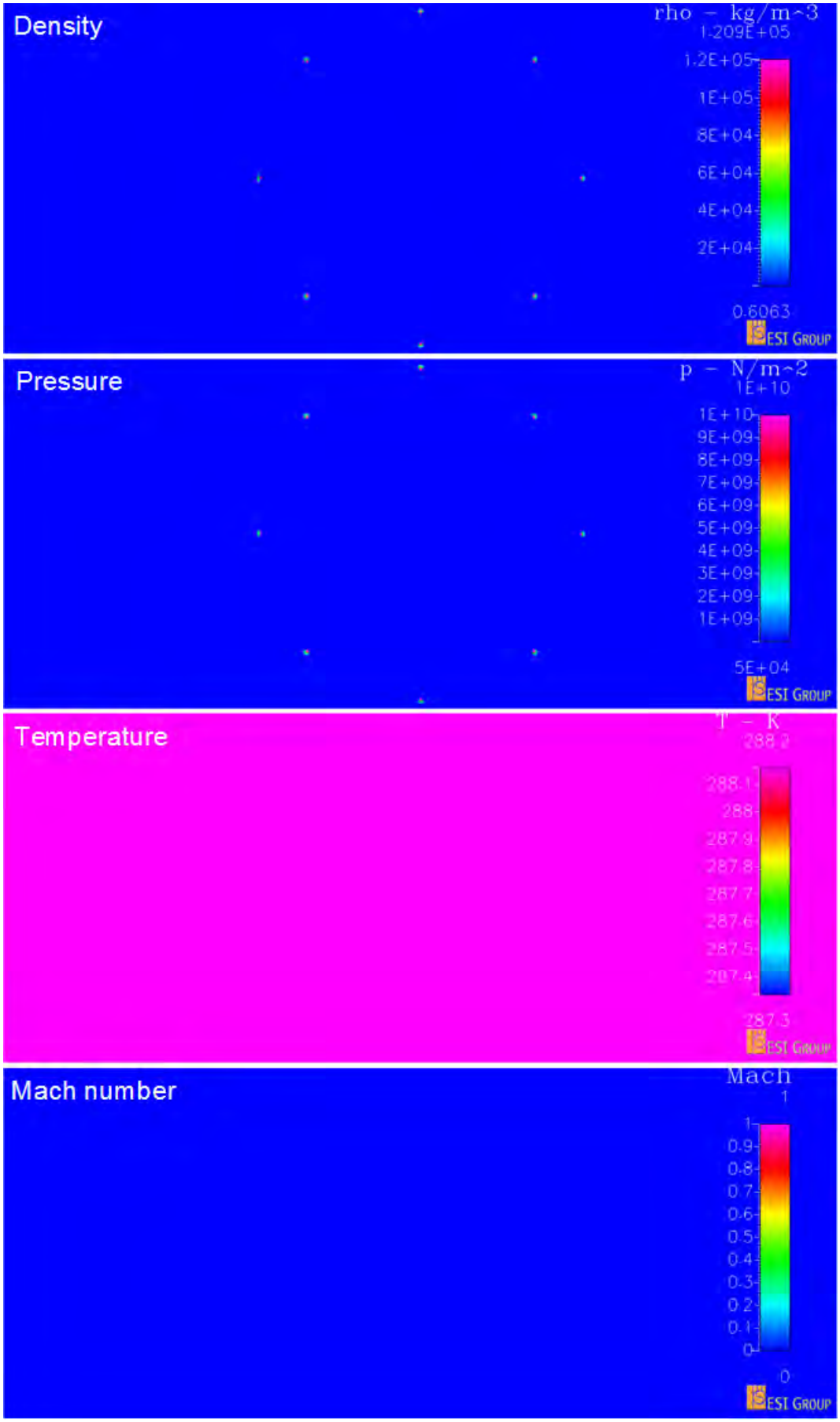

Figure 5.5.1.: Images at the initial iteration.

At the 950^{th} iteration the line focus is forming, as shown in Figure 5.5.2 on the next page. The density in between adjacent wires is approximately 125 kg/m^3 and forming an ellipse of greater density. At the tips of the major axes the density drops to approximately 85 kg/m^3. Surrounding this structure the density is lower at approximately 60 kg/m^3.

Midway between adjacent wires the pressure is highest at approximately 2.5×10^7 N/m^2. Surrounding the ellipse the pressure is at approximately 10^5 N/m^2 which was the pressure that was initially set. This shows that the pressure at the wires has dissipated from approximately 10^{10} N/m^2 to approximately 2.5×10^7 N/m^2.

The temperature is highest at the tips of the major axes of the ellipse, with a temperature of approximately 1000 K from approximately 228 K that was initially set. The wave that is propagating to the centre has a temperature of approximately 700 K.

The cylindrical shock waves are moving at approximately Mach 2 towards the centre of the wires as shown by the Mach number picture of Figure 5.5.2 on the following page. The figure also shows that the shock wave moving away from the centre of the CSL is propagating at a lower Mach number of less than 2. This is due to the fact that the post processor (i.e. CFD-VIEW) averages the values and since the mesh as shown in Figure 5.3.5 on page 99 is coarser towards the far field boundary than towards the centre, it seems as if the shocks are propagating slower towards the far field.

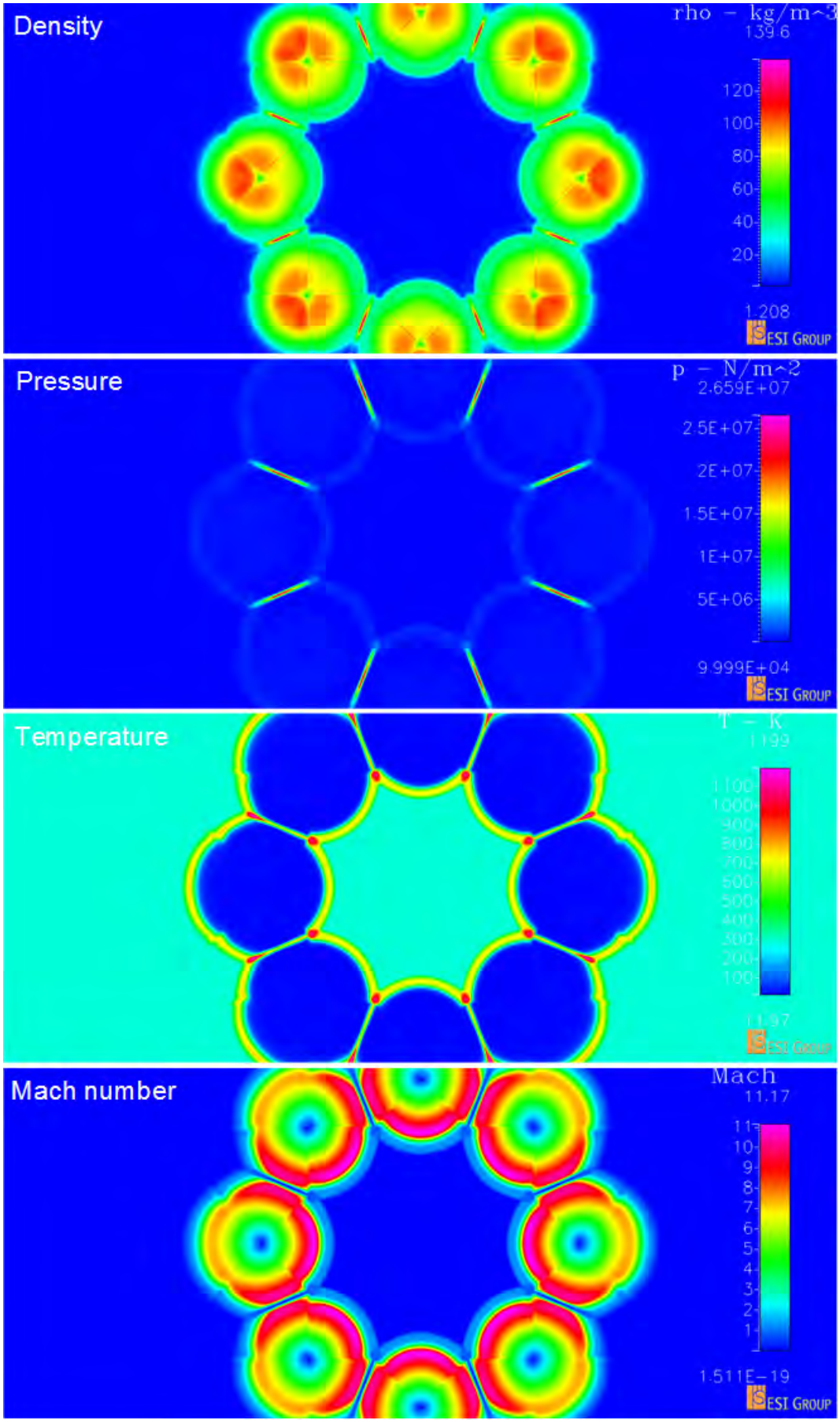

Figure 5.5.2.: Images at the 950^{th}iteration.

At the 1000^{th} iteration, as shown in Figure 5.5.3 on the following page, the line focus has formed between two adjacent wires. The density at the line focus is approximately 250 kg/m^3. The line focus region is more dense than the surrounding. The density has increased from the previously shown iteration in Figure 5.5.2 on the previous page indicating that when the waves interact they enhance each other and increase the density.

The pressure is also higher at the line focus region, with value of 4.7×10^7 N/m^2. From iteration 950^{th} the pressure was 2.5×10^7 N/m^2. This is physically possible as it would be expected that when the pressure increases the density should also increase indicating that more mass is contained by the high pressure region.

The temperature does not change significantly over the 50 iterations from the last one with the temperature values remaining at approximately 1100 K.

The shock front is still propagating at Mach 2 towards the centre of the CSL, as shown by the Mach number picture of Figure 5.5.3 on the following page.

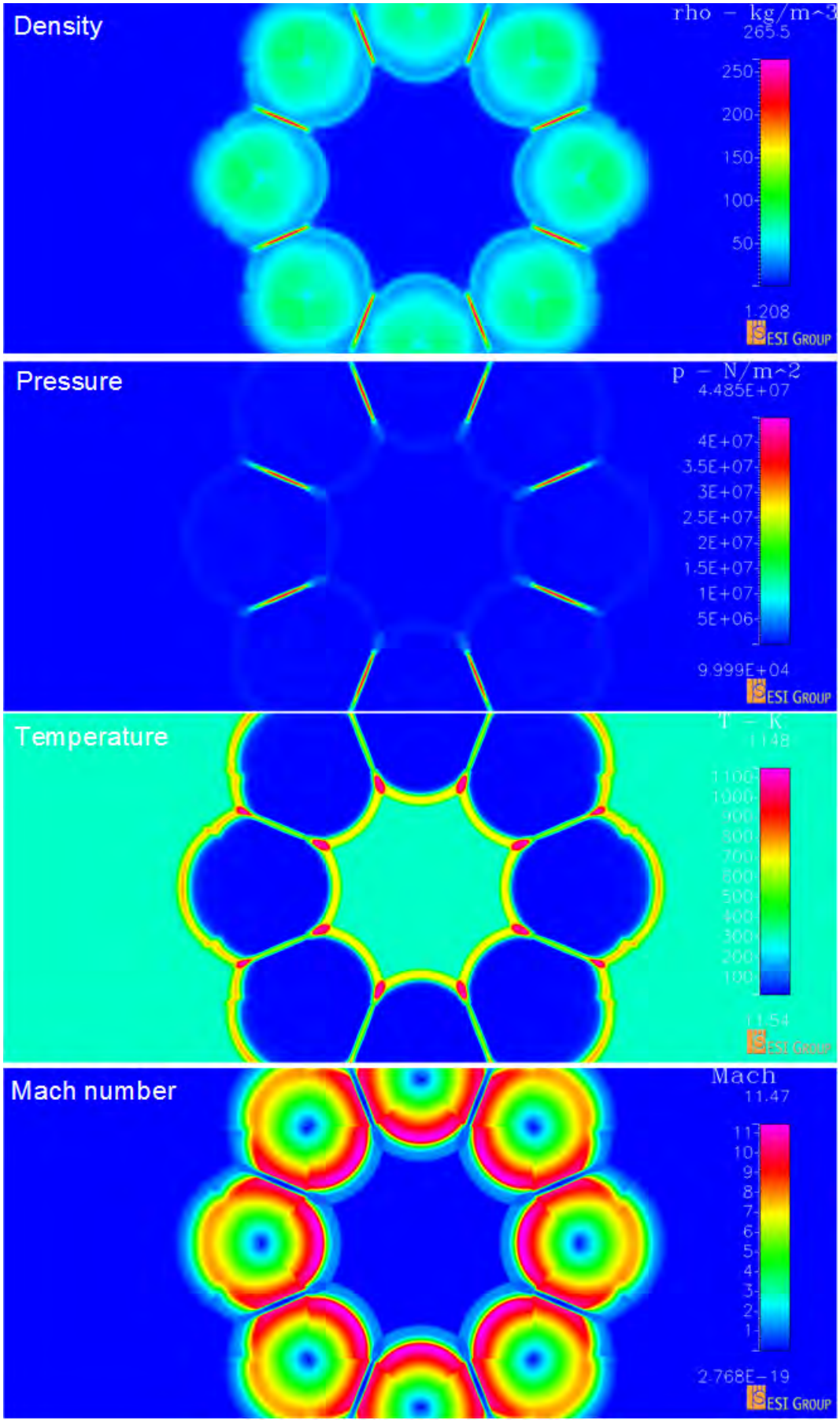

Figure 5.5.3.: Images at the 1000^{th}iteration.

Figure 5.5.4 on the next page shows the waves propagating further from the line focus, at the 1150^{th} iteration. The density is lower at approximately 140 kg/m^3 than the density at 50 iterations before, shown on Figure 5.5.3 on the preceding page. This is because the line focus is now expanding.

The pressure is also lower at approximately 1.6×10^7 N/m^2, at the line focus region.

The highest temperature is still at approximately 1100 K as in the previous 100 iterations, but the higher temperature is at the major axes of the ellipse.

The shock front is still propagating at Mach 2 towards the centre of the CSL.

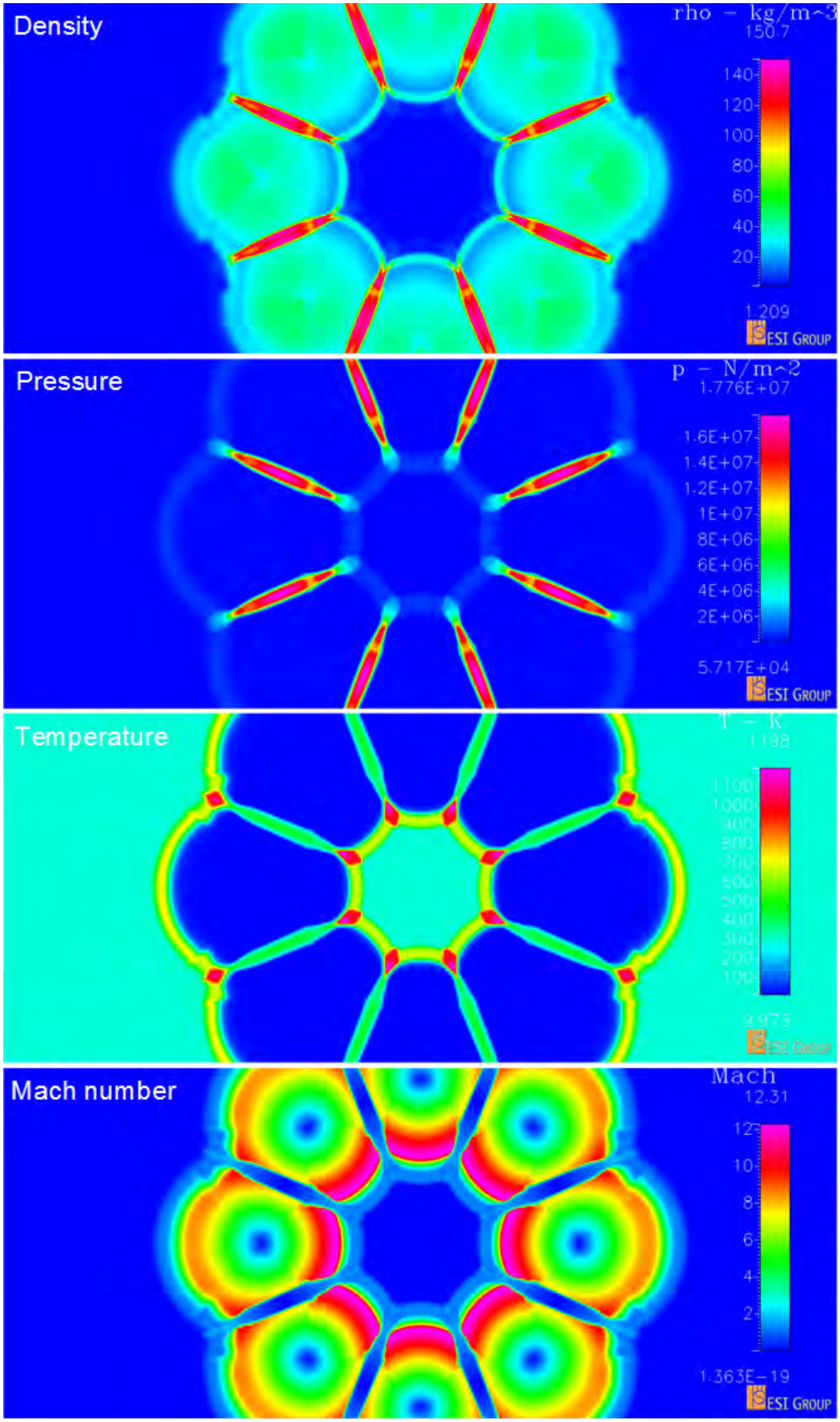

Figure 5.5.4.: Images at the 1150^{th}iteration.

At the 1450^{th} iteration the shock waves are approaching the centre of the CSL. The density has dissipated considerably and is now at approximately 55 kg/m^3 at the shock front. The pictures on Figure 5.5.5 on the next page also show a plot of the respective parameters with respect to distance along the horizontal line passing through the central points in Figure 5.5.5 on the following page.

The pressure is also lower at the shock front at approximately 10^7 N/m^2.

The temperature is lower at approximately 1000 K but is rising to above 2000 K immediately before the shock front.

The shock front is still propagating at Mach 2.

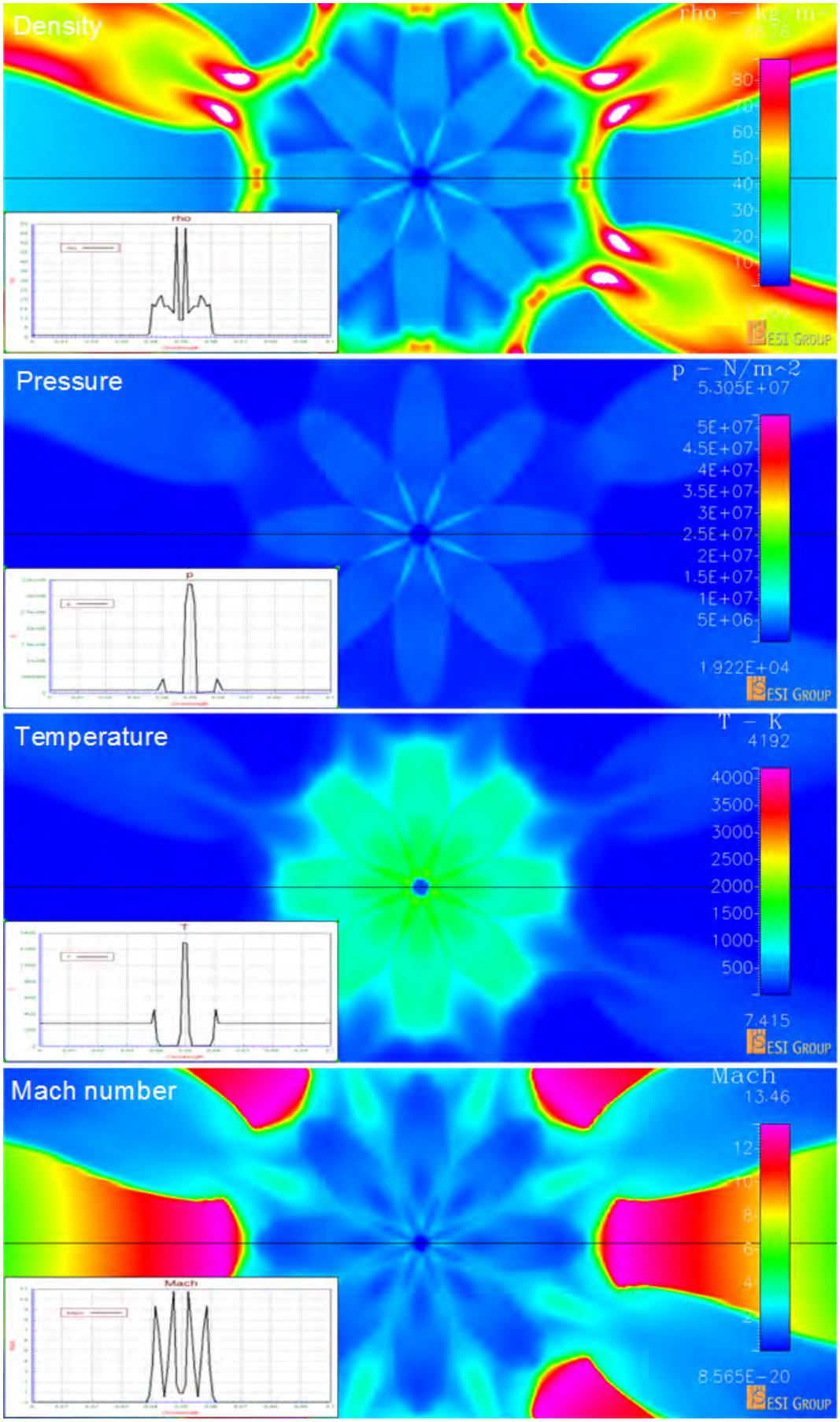

Figure 5.5.5.: Images at the 1450^{th} iteration.

At the 1500^{th} iteration the shock waves have reached the centre of the CSL and are interacting with each other, as is shown in Figure 5.5.6 on the next page. The density has increased from 10 kg/m^3 over the past 50 iterations as shown in Figure 5.5.5 on the preceding page to around 60 kg/m^3. This indicates that when the shock waves converge at the centre of the CSL they enhance each other and create a region of higher density.

The pressure has also increased to approximately 5.3×10^7 N/m^2. A region of higher pressure is formed at the centre of the CSL.

Temperature has increased to above 4000 K, indicating that as the shock waves converge at the centre of the CSL a region of higher temperature is created.

The Mach number picture though shows that the waves have interacted and are now diverging rapidly with the waves propagating at much less than Mach 1.

This is the condition at which the dense air region forms the gas lens.

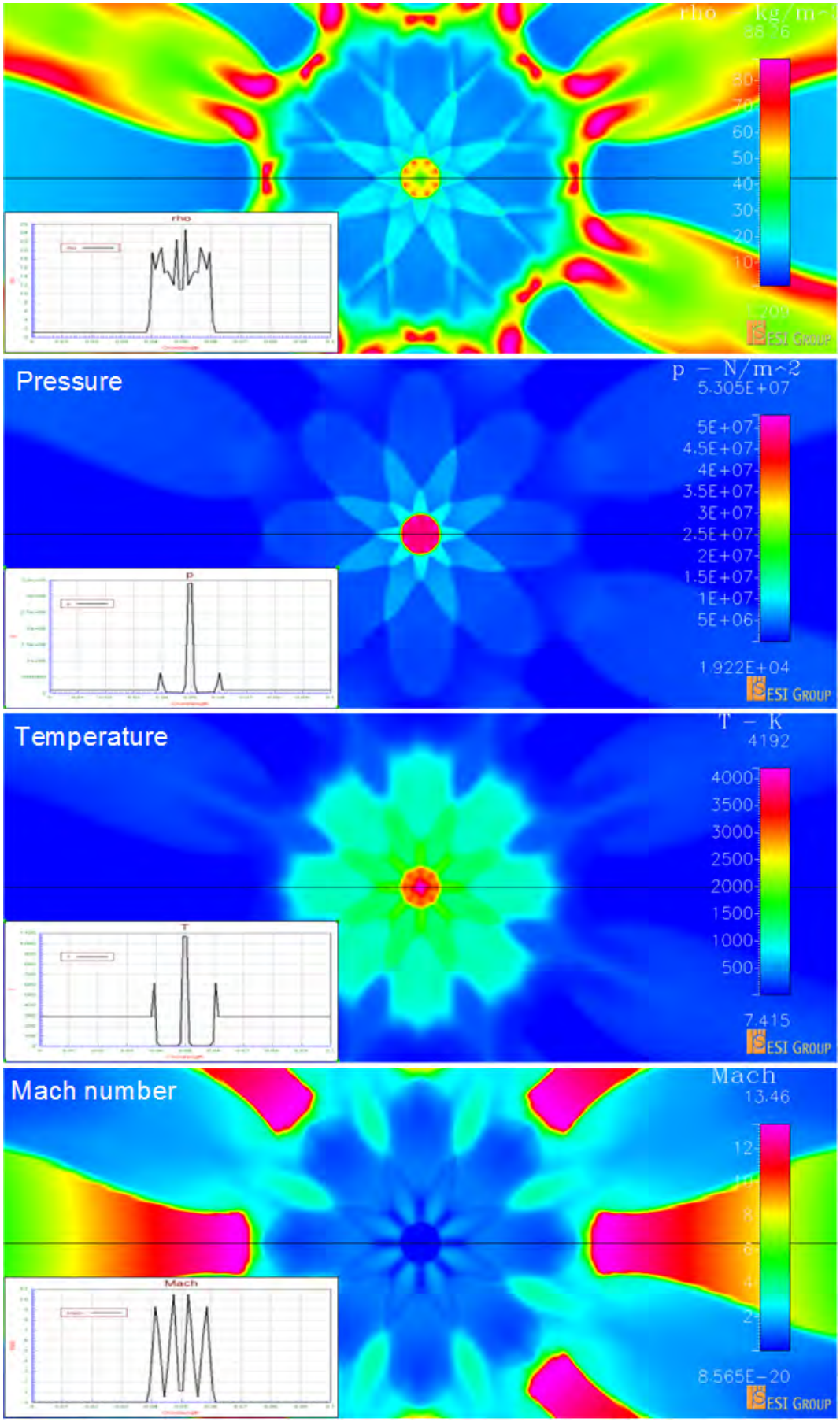

Figure 5.5.6.: Images at the 1500^{th} iteration.

At the 1550^{th} iteration the shock waves have collided and are beginning to diverge from the centre of the device, as shown in picture 5.5.7 on the next page. The density has decreased from 60 kg/m^3 over the past 50 iterations, as shown in the density picture of image 5.5.6 on the preceding page to 30 kg/m^3. Since the shock waves are diverging the amount of particles contained in a cubic metre has decreased.

The pressure has also decreased from 5×10^7 N/m^2, as shown in the pressure picture of image 5.5.6 on the previous page to 3.5×10^7 N/m^2. In this picture the centre high pressure region is circular, confirming the statement by Bucellato *etal.* [1] in connection with Mach addition that the shock waves lose their initial identity after they have collided and created a new expanding wave. The centre of the device is losing pressure and this is in agreement with the decrease of density.

The temperature decreases from 4000 K, as shown in the temperature picture of image 5.5.6 on the preceding page, to 3500 K, indicating that the centre of the device is cooling down after 50 iterations. Because of divergence the particles contained in a unit volume have more space to move in hence loosing energy.

The waves have weakened further and are now propagating in the subsonic regime.

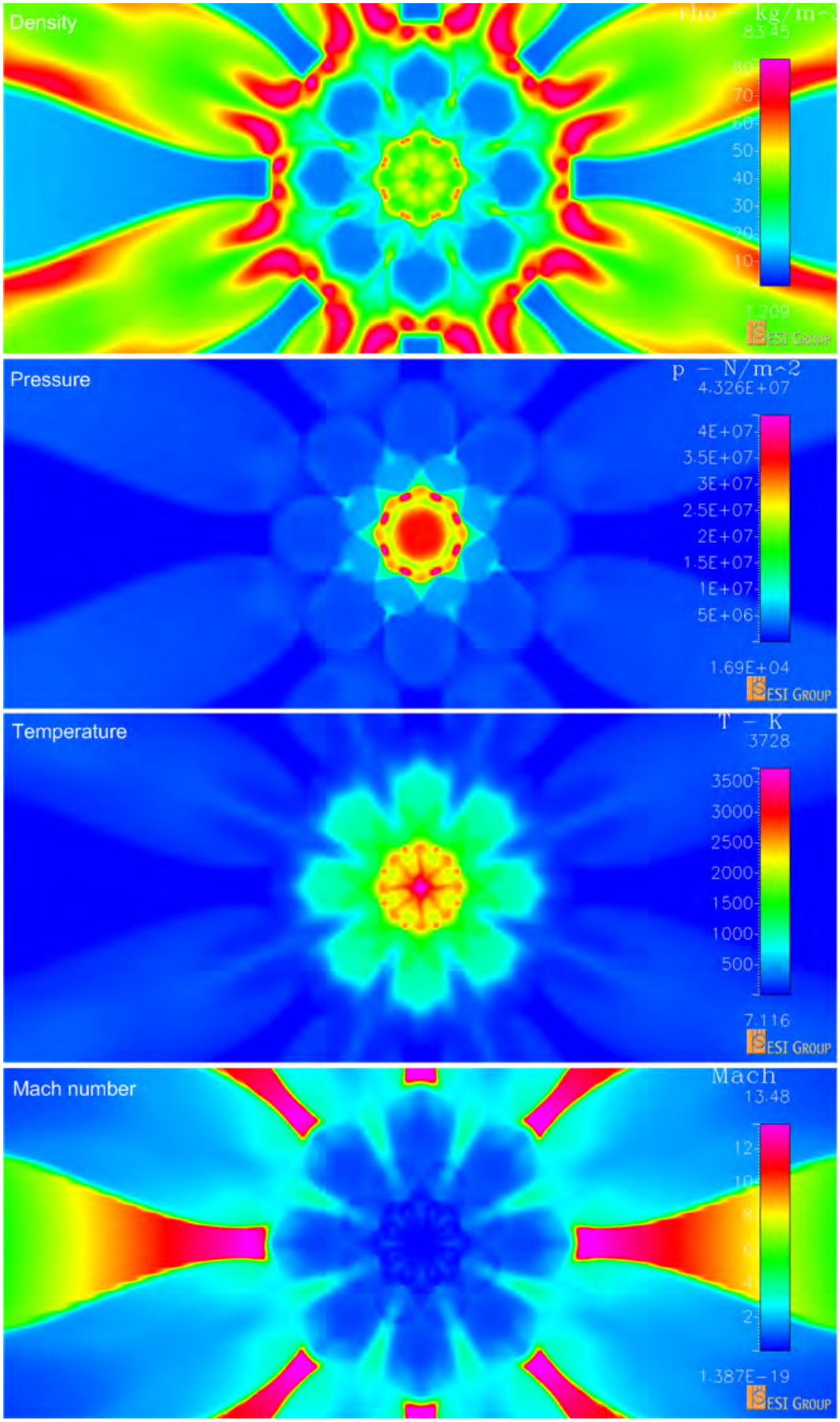

Figure 5.5.7.: Images at the 1550^{th} iteration.

At the 1850^{th} iteration the waves have propagated away from the centre of the circle and are diverging further. The density at the centre is lower than 50 kg/m^3.

The pressure is still high but also decreasing further. Close inspection of the star shape indicates some grid dependance.

The temperature is still at approximately 4000 K.

Strong shock propagation is taking place outside the CSL device. For further work the enclosed CSL should be simulated to investigate how these shocks influence the interaction of the CSL. This is discussed in the recommendations.

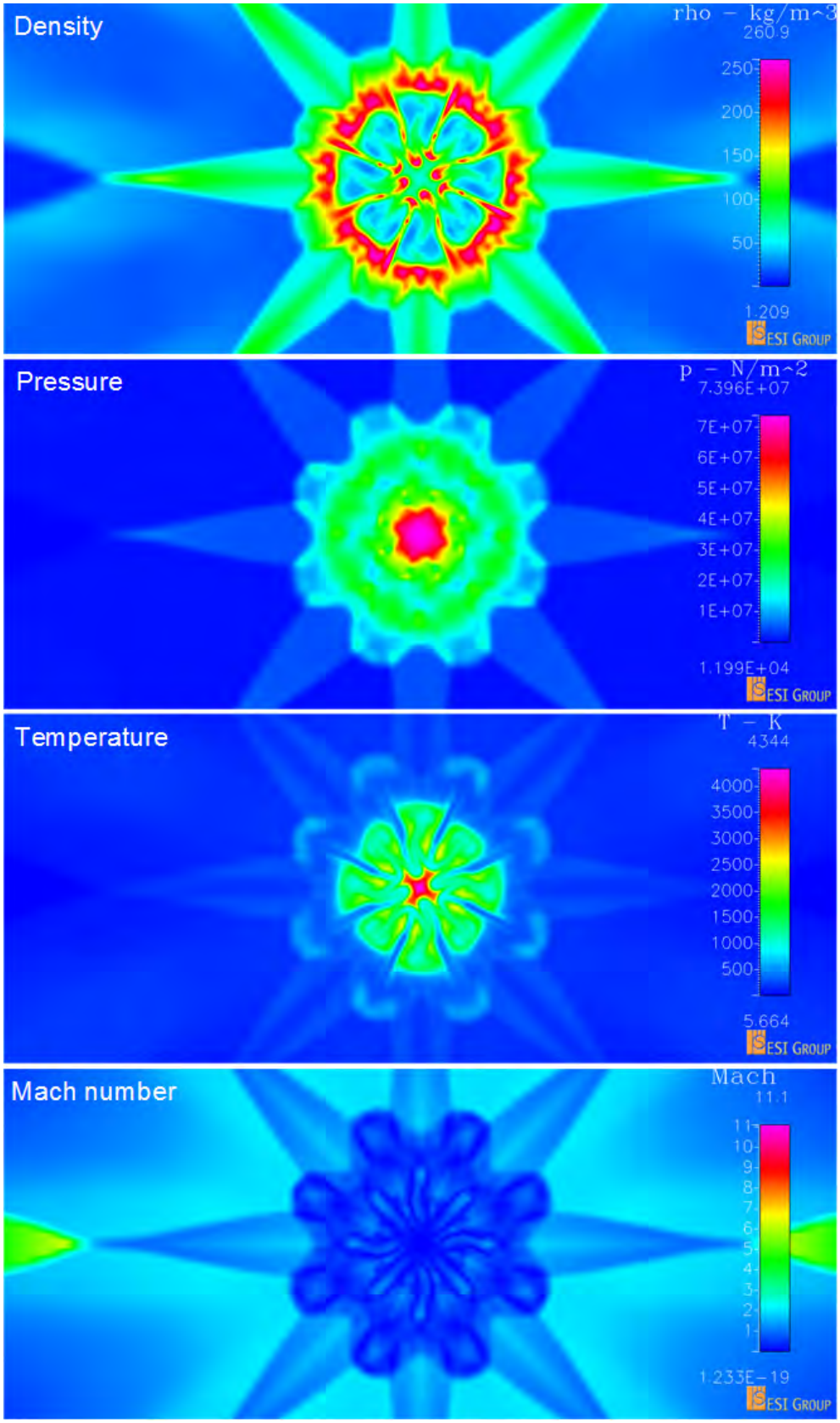

Figure 5.5.8.: Images at the 1850^{th} iteration

6. Conclusions

It is known that colliding shock lenses provide a way of focusing high-powered laser beams without destroying solid optical components. The primary aim of this work was to determine whether existing CSL's can be scaled up from the previous experiments performed in [1]. In the experiments summarized in this thesis, the optical aperture was successfully scaled up to 10 mm from the one that was performed by Bucellato *et al.* As part of the process the trigger circuit reliability was considerably increased and the spark gap redesigned. In addition a virtual capillary (or exploding wire) configuration was built and tested. A CFD simulation of the formation of the lens region in the exploding wire configuration was completed and the results were compared with the results from the experiments.

In the following paragraphs, detailed conclusions are presented. Recommendations follow for future work.

6.0.1. Trigger Modification

The modified trigger circuit, discussed in Section 2.3 on page 24, proved more stable than the ignitron and the pressurized spark gap previously used. There was considerable improvement in the breakdown of the CSL, and the dangers of grounding the capacitors when the ignitron did not work were considerably minimized. The inconvenience of cleaning the pressurized spark gap after only several shots was also not experienced.

However, considerable jitter was still present, and the necessary readjustment of

the separation of the electrodes became the main disadvantage of the new setup.

Clearly, this type of CSL triggering is only acceptable for a research environment when a small number of shots are required to characterize the lens and its power consumption. High power, high repetition rate gas lasers operate with kilowatt/kilovolt power supplies which would require virtually no adaptation to power a CSL.

6.0.2. Scaling the CSL

The electromagnetic noise of the BCSL, as discussed on Section 3.4 on page 33, is significant. The noise can affect, or even damage, computers and sensitive electronic equipment.

The electrodes sometimes do not breakdown, sending all of the energy to the coil, which then acts like an antenna, radiating most of the energy in a large burst of noise as shown in Figure 3.4.1 on page 33. The top trace records the electromagnetic noise in the Faraday cage. It can be seen that the noise has a higher voltage level than that of the trace shown in Figure 3.4.2 on page 34. Note that the sensitivities of the two traces are the same. The noise persists for a longer time in Figure 3.4.1 on page 33 than in Figure 3.4.2 on page 34. The noise also activates the optical trigger after some time as shown on the second trace of Figure 3.4.1 on page 33, even in the absence of a breakdown and hence of no light.

The results show that it is feasible to scale the CSL to bigger apertures so that it can be used in industry. Some further engineering is greatly needed to render the BCSL reliable and free from the above mentioned problems.

6.0.3. Exploding Wire Experiment

From Section 4.3, colliding shock waves generated by exploding wires proved to be a viable way of producing a uniform pre-formed channel for a laser pulse. As shown in the experimental results, there are many factors to be taken into account as follows.

The device still is far from perfect. Firstly, there are not yet any means to tighten

the wire. As a result, there are small kinks in it, which then induce non-uniformities in the VC pipe. In this case the pipe lens needed for an electron acceleration experiment, for example, must be much more uniform. Moreover, the position of the wires in the device cannot be controlled very well. The wire goes through a hole 1 mm wide. Since the goal is to obtain a pipe smaller than a few hundreds of microns (if not less) the attainable precision is not sufficient.

This may be seen in the form of small differences from different VC breakdowns. Nevertheless, small differences are probably going to be compensated after the collision by Mach addition. It is true that the pipe gets usually more uniform after collision. All these problems can be easily overcome by a more precise design of the holder.

6.0.4. Computational Fluid Dynamics

Section 5.5 on page 103 shows that there is a relatively good qualitative comparison between the pictures obtained experimentally on Figure 2.2.2 on page 23 and the CFD. However, the times of the frames shown are not the same as those in Figure 2.2.2 on page 23 and the arrival times of the waves are therefore expected not to correspond.

CFD shows that the waves create a region of high temperature, pressure and density at the centre when they collide. A maximum density of approximately 60 kg/m^3 and temperature of approximately 4000 K at the 1500^{th} iteration was found. The CFD enables us to make a comparison of the propagation speed of the waves as they move towards and away from the centre. Experimental timing of the frames was based on a starting time deduced from the electromagnetic disturbance of the Rogowski coil, but this is not necessarily the time at which the spark gap breaks down. The use of high speed cameras to resolve the experimental issues of timing is discussed in the recommendations below.

6.1. Recommendations

The pipes described in chapter 4 approached the requirements for wall-less micro-capillaries or "virtual capillaries". These structures can become interesting for lasers generating soft X-rays. In the Rocca scheme [9], an electrical discharge is sent through a capillary, containing the appropriate gas e.g. argon. But after a number of shots the capillary deteriorates and has to be replaced. In another scheme, a laser beam is sent through the capillary and, in this case, after a while the capillary mouth melts. In order to be of interest for these experiments, a gas capillary must be as small as 100 μm. In the laboratory, we have produced capillaries with an internal diameter of 500 μm, which is not very far from this limit.

Another special application is that it is also possible to bend the VC. In our system this could not be done, because the wire is not stiff enough to hold itself in position and we did not have enough energy to explode a thicker wire.

The walls that hold the wires should be modeled. The walls have an influence on the propagation of the shock waves. They, amongst other things, will reflect the shock waves back into the region of interest and possibly cause a secondary CSL. This might be interesting as it might produce a better CSL.

The simulation should be extended to a 3D scenario. This will give insight into the 3D variables of pressure, temperature, Mach number and density, which are difficult to measure experimentally without interfering with the shock waves path. The structure of the of the lens formed can be approximated by the CFD simulations and hence this could be simulated with a ray tracing code to investigate how the laser beam would propagate though such a structure.

The scaling of the geometry still needs to be done to demonstrate the possibility of enlarging the optical diameter of the lens by increasing the size of the lens.

The CFD data should be further considered to ascertain if the shock interactions resemble Regular or Mach reflections as described in Courant and Friedrichs [32].

A quantitative comparison has been hampered by the fact that the delay times

from the experiment do not correspond to those obtained from the CFD. It is recommended that a detailed quantitative investigation and experimental timing should be done, preferably with the use of a high speed camera. This would decrease the uncertainty of the breakdown time of the wires of the CSL. It will also alleviate the uncertainty in the repeatability of different shots and delay times, and give a more precise measure of the propagation speed of the shock waves.

It is recommended that future computational studies should include a simulation of the optical properties of the CSL. Given the density, the refractive index through the lens volume is obtainable, and ray tracing would be possible. The laser focus could then be studied as a function of time.

Bibliography

[1] Buccellato, R, Lisi, N & Michaelis, MM 1993, "Colliding shock lenses", *Optics Communication*, vol. 101, pp. 350 - 355

[2] Kuppen, M 1996, "On the Interaction of Laser with Air", PhD. thesis, University of KwaZulu-Natal, South Africa.

[3] Collier, D & Pantley, W 2006, "Deep UV Applications Challenge Optical Fabrication", *Alpine Research Optics.*

[4] Doty, J 2000, "A Practical Guide to avoiding Laser Damage to Optics", *Photonics Spectra,* 113 - 116

[5] Michaelis, MM, Nottcut, M & Cunningham, PF 1986, "Drilling by gas lens focused laser", *Optics Communication*, vol. 59, no. 5-6, pp. 369 - 374

[6] Michaelis, MM, Cunningham, PF, Cazalet, RS, Waltham, JA & Notcutt, M 1991, "Gas lens applications", *Laser and Particle Beams*, vol. 9, no. 2, pp. 641 - 651

[7] Michaelis, MM, Bhagwandin, N & Cunningham, P 1985, "Flame focussing of laser beams and refractive fringe formation", *Optics Communication*, vol. 52, no. 6, pp. 371 - 376

[8] Michaelis, MM 1980, "Laser beam guidance by flames", *American Journal of Physics*, vol. 48, no. 11, pp. 990-991

[9] Michaelis, MM 1997, Gas lens, US Patent 5682268

[10] Bucellato, R 1994, "Refractive Effects in Phase Objects and Associated Phenomena", PhD thesis, University of KwaZulu-Natal, South Africa

[11] Waltham, JA, Cunningham, PF, Michaelis, MM, Campbell, M & Notcutt, M 1987, "The application of the refractive fringe diagnostic to shocks in air", *Optics & Laser Technology*, vol. 19, no. 4, pp. 203 - 208

[12] Michaelis, MM, Waltham, JA & Cunningham, PF 1991, "Refractive fringe diagnostic of spherical shocks", *Optics & Laser Technology*, vol. 23, no. 5, pp. 283 - 288

[13] Michaelis, MM, Dempers, CA, Kosch, M, Prause, A, Notcutt, M, Cunningham, PF & Waltham, JA 1991, "A gas-lens telescope", *Nature*, vol. 353, pp. 547 - 548

[14] Lisi, N 1995, "Laser applications and refractive properties of non-homogeneous gas distributions", PhD. thesis, University of KwaZulu-Natal, South Africa

[15] Michaelis, MM, Kuppen, M, Prause, A, Forbes, A, Viranna, N & Lisi, N 1996, "Progress with gas lenses", *Laser and Particle Beams*, vol. 14, no. 3, pp. 473 - 485

[16] Kuppen, M, Michaelis, MM, Bucellato, R & Lisi, N 1995, "Scaling up the colliding shock lens", *Review of Scientific Instruments*, vol. 66, no. 10, pp. 5037-5044

[17] Lisi, N, Michaelis, MM, Buccellato, R, Kuppen, M & Prause, A 1995, "Colliding shock Lens as an intracavity Q-switch element", *Applied Optics*, vol. 34, no. 6, pp. 942-945

[18] Forbes, A 1997, "Photothermal Refraction and Focussing", PhD. thesis, University of KwaZulu-Natal, South Africa

[19] Conti, A, 2004, "Gas and Plasma Structures", PhD thesis, University of KwaZulu-Natal, South Africa.

[20] Turner, GR 2001, "Novel Pulsed Power Applications", MSc thesis, University of KwaZulu-Natal, South Africa

[21] Michaelis, MM, Forbes, A, Conti, A, Nativel, N, Bencherif, H, Bingham, R, Kellet, B & Govender, K 2006, "Non-solid, non-rigid optics for high power laser systems", High-Power Laser Ablation 2006, vol 6261, *International Society for Optics and Photonics*

[22] Lisi, N, Buccellato, R & Michaelis, MM 1994, "Optical quality and temperature profile of a spinning pipe gas lens", *Optics & Laser Technology*, vol. 26, no. 1, pp. 25 - 27

[23] Mafusire, C, Forbes, A, Snedden, G & Michaelis MM 2007, "Characterisation of a spinning pipe gas lens using a Shack-Hartmann wavefront sensor", *Proc. SPIE 6663*, Laser Beam Shaping VIII

[24] Mafusire, C, Forbes, A, Michaelis, MM & Snedden, G 2008. "Optical aberrations in a spinning pipe gas lens", *Optical Express*, vol. 16, no. 13, pp. 9850 - 9856

[25] Mafusire, C, Forbes, A, Snedden, G & Michaelis, MM 2008, "The spinning pipe gas lens revisited", *South African Journal of Science*, vol.104, no.7-8, pp. 260-264

[26] Notcutt, M, Michaelis, MM, Cunningham, PF & Waltham, JA 1988, "Spinning pipe gas lens", *Optics & Laser Technology*, vol. 20, no. 5, pp. 243 - 250

[27] Waltham, JA, Notcutt, M, Cunningham, PF & Michaelis MM 1990, "Evaluation of gas lens laser-produced plasmas", *Laser and Particle Beams*, vol. 8, no. 1-2, pp. 361-367

[28] Buccellato, R, Michaelis, MM, Dempers, C, Prause, A & Cunningham, PF 1993, "Pulsed gas lens", *Optics & Laser Technology*, vol. 25, no. 4, pp. 247 - 250

[29] Cazalet, RS, Cunningham, PF, Michaelis, MM, Notcutt, M & Waltham, JA 1990, "Demonstration of optical phase conjugation by stimulated Brillouin scattering using a gas lens", *Measurement Science and Technology*, vol. 1, no. 2, pp. 147

[30] Michaelis, MM, Kuppen, M, Turner, G, Mahlase, ACK, Prause, A, Conti, A & Lisi, N 1998, "Limitations and applications of the colliding shock lens", Proc. SPIE Vol. 3343, pp. 228-241, *High Power Laser Ablation*

[31] Hasson, V & von Bergman, HM 1979, "Ultraminiature high-power gas discharge lasers", *Review of Scientific Instruments*, vol. 50, no. 1, pp. 59 -63

[32] Courant, R & Friedrichs, O 1948, *Supersonic Flow of Shock Waves*, vol 1, pp 320 - 335, Interscience Publishers, New York

[33] Fletcher, CAJ 1991, *Computational Techniques of Fluid Dynamics*, 2nd ed., New York, Springer-Verlag

[34] ESI CFD Inc. 2004, *CFD-FASTRAN Theory manual,* Huntsville, Alabama, USA

[35] Hirsch, C 1990, *Numerical computation of internal and external flows*, vols. 1 and 2, Wiley, New York.

A. Appendix

A.1. Regular reflection and Mach reflection

In the present work, the experimental resolution has not been high enough, in most cases, to warrant an investigation of regular or Mach interaction of shock waves. The extensive theory supporting the description of shock reflection phenomena is not within the scope of this thesis. However, for later reference, a brief note is necessary. A wedge in steady two-dimensional supersonic flow generates an oblique shock. In Figure A.1.1, double wedges are illustrated. Supersonic flow is incident from the left. When this shock encounters a horizontal wall (or a symmetry plane), two types of reflections occur, depending on the shock angle, and whether the flow behind the shock is subsonic or supersonic.

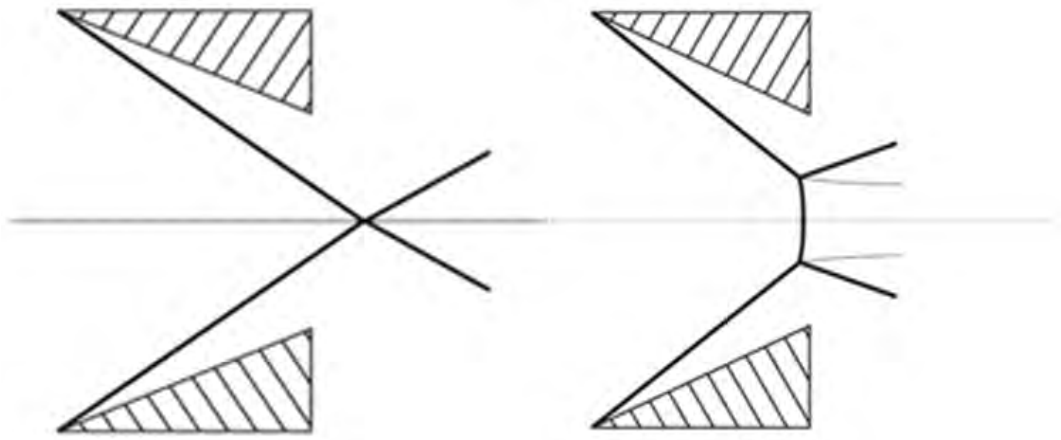

Figure A.1.1.: Reflection of an oblique shock from a horizontal plane: (left) regular reflection and (right) Mach reflection (figure adapted from reference [1])

In Figure A.1.1, regular reflection from the symmetry plane is illustrated on the left. This case occurs for lower angles between the incident shock and the symmetry plane. On the right, the formation of a Mach stem across the symmetry plane between the shocks is shown. (The grey lines to the right are slip surfaces, across which the fluid velocity differs.) This case occurs for larger angles between the incident shock and the symmetry plane. The occurrence of Mach or regular reflection depends on the angles at which colliding shocks meet. The interaction has been observed in colliding blast waves and the theory appears in Courant and Friedrichs [32].

Bibliography

[1] Mouton, CA 2007, "Transition between Regular Reflection and Mach Reflection in the Dual-Solution Domain", PhD Thesis, California Institute of Technology